Multi-Dimensional Characterization of Soil Surface Roughness for Microwave Remote Sensing Applications

Philip Marzahn

Dissertation
an der Fakultät für Geowissenschaften
der Ludwig-Maximilians-Universität
München

vorgelegt von
Philip Marzahn
Hamburg

06. November 2012

Supervisor: Prof. Dr. Ralf Ludwig, Department of Geography, LMU Munich
2nd Supervisor: Prof. Dr. Irena Hajnsek, ETH-Zürich, Switzerland and DLR-HR

External Reviewers: Dr. Dirk Rieke-Zapp, University of Bern, Switzerland
Dr. Urs Wegmüller, Gamma Remote Sensing, Switzerland
Dr. Francesco Mattia, ISSIA-CNR, Italy

Tag der Disputation: 13.02.2013

Preface

This work is the synthesis of several projects that have taken place the past five years working together with Prof. Dr. Ralf Ludwig at LMU Munich. It was an exciting journey, where I had the chance to meet many interesting people, travel around the globe and observe a lot of different roughness conditions. It all started with an initial plan to derive soil surface roughness more accurately than done to date and to assimilate the output in a physically based eco-hydrological model. However it resulted in going back and refine the *in-situ* measurement techniques which was a crucial issue back then - solving the uncertainties in the derivation of soil surface from remote sensing data.
Thus, I want to sincerely thank **Prof. Dr. Ralf Ludwig** for supervising this thesis and giving me the freedom to "go my way". Without his passion for science and his understanding this project would not have taken place. I hope I have met your expectations.
A special thanks to **Prof. Dr. Irena Hajnsek**, ETH-Zürich and DLR-HR, for taking over the co-supervision of my Ph.D. and being an inspiring source through out.

I also want to thank people, who were part of this journey:
Dr. Dirk Rieke-Zapp, formerly at the Institute of Geological Science Bern, now with the Institute of Geoinformation at the University of Applied Science, Mainz. Without his knowledge in Photogrammetry and his overall interest in measuring micro-topography for geomorphological studies, this work would not have been completed. He provided the first metric camera we used in this study and also provided the new camera system, the fixed Canon EOS 5d.
Dr. Francesco Mattia, who is with ISSIA-CNR, Italy, for his fruitful and constructive discussions on soil surface roughness characteristics as well as his always helpful hand when it came down to the physics behind microwave remote sensing and soil surface roughness.
Dr. Urs Wegmüller, Gamma Remote Sensing, Switzerland, for allowing me to join the *Flashing Fields* project and bringing me closer to the physics behind it. It was his passion in directional scattering that enabled me to carry out another campaign with a focus on the impact of soil surface roughness on the directional scattering problem. He also provided the Wallerfing ERS-2 dataset, which was one of the last acquired before ERS-2 was switched of.
The SMOS Cal/Val Team, especially **Dr. Florian Schlenz** and **Dr. Alexander Löw**, for seeing the importance of soil surface roughness in (passive) microwave remote sensing and "ordering" some roughness measurements during their campaign.
Stephanie Chalmers, Joanne Foster and **Geoff Poulton** for reviewing and editing all my papers as well as this thesis. I hope you learned a lot about soil surface rough-

ness. All my colleagues here at the Department of Geography, especially Swen Meyer for moving with me from the good old north to Munich and having always a chair in his office for me to hassle him. Josef "*Seppo*" Schmid for sharing the office with me during the last days of this thesis. Vera Erfurt and Gudrun Lampart for keeping the business running and managing all the things a Ph.D. student could not.
All the student-assistants, *Hiwis*, who were forced to process the huge amount of images to accurate digital surface models, especially Theresa Brandlhuber, Georg Fischer and Moritz Seidel.

Last but not least I have to thank my beloved family, **Eva**, **Marta** and **Mattes** who supported me with their endless love.

Summary

In the environmental system, soil surface roughness is a critical parameter in a wide range of eco-hydrological processes. In the context of a high resolution process-based eco-hydrological modeling approach, the knowledge about soil surface roughness conditions at field scale is essential due to the importance for runoff generation. With regard to a rougher surface, the time to the point where surface runoff starts is more delayed compared to a smoother surface. Also the surface runoff pattern is dependent on soil surface roughness conditions. For a smooth surface the generated surface runoff is more uniformly distributed, indeed the generated surface runoff over a rough surface follows more preferential pathways, thus more concentrated along the highest relief gradient. This information is essential for a physically-based modeling of soil erosion. In addition, due to soil crusting, the infiltration rate of soil can be significantly reduced, thus increasing the potential of river floods. Crusts can also reduce the plant development over agricultural fields due to a lack of available oxygen for the plants. However, the measurement of soil surface roughness is limited to small plots, thereby increasing the uncertainties of such models to predict the above mentioned processes. As shown in the first part of this thesis, microwave remote sensing offers the possibility to map soil surface roughness conditions over bare and sparsely vegetated agricultural fields. Using polarimetric SAR datasets, the polarimetric *RRLL* coherence shows a dependency on the roughness conditions of agricultural fields. However, the uncertainty of the in-field roughness measurements hamper the retrieval approach due to the scale dependency of soil surface roughness. In addition to the above mentioned impacts, soil surface roughness has also a strong influence on microwave remote sensing. As shown in Paper II of this thesis, the directional scattering phenomena, which is characterized by a strong backscatter over several agricultural fields, can be related to the roughness conditions - especially the horizontal periodical component - of the imaged fields. Thus a robust roughness measurement technique is needed to measure in-field soil surface roughness over large sample plots and to characterize the full spectrum of soil surface roughness on an agricultural field. In Part II of this thesis, a measurement device based on photogrammetric image acquisitions is developed, which allows to measure soil surface roughness highly accurate over large sample plots efficiently. In an extensive analysis, the performance of the device in terms of representativeness was carried out, indicating that the developed system is statistically more robust in the determination of soil surface roughness compared to classical profile measurements. This was also indicated by a developed algorithm, the *representative elementary area*, which tests the measurement's sample size to its representativeness, as the determined roughness values are depended from the sample size over which they are estimated. In addition it was found that soil surface roughness has a strong non-isotropic, multi-scale appearance, revising the previous

assumptions of an isotropic and stationary surface. Finally in Part III, the developed system was used to measure soil surface roughness for the modeling of SAR backscatter values in the presence of directional scattering over agricultural fields using a backscatter model, which was developed in the framework of this thesis. The *modified Shin and Kong* model which accounts for different roughness scales as well as anisotropy, was able to predict the backscatter values in the case of directional scattering quite accurately. In this context it could be shown that a certain roughness condition alters the directional scattering significantly for different sample points with the same row orientation to the sensors look vector.

In summary, the major scientific achievements of this thesis can be summarized as in the following:

- A better understanding of soil surface roughness and its quantification in terms of roughness scales and non-isotropic appearance for an improved parametrization of backscatter models was achieved.
- An improved and enhanced understanding of the directional scattering phenomena, occurring in SAR imagery acquired over agricultural landscapes, which could be related to soil surface roughness conditions.
- An approach was proposed to derive soil surface roughness from polarimetric SAR data which could be further assimilated in process-based eco-hydrological models in the future.

Zusammenfassung

Im Umweltsystem spielt die landwirtschaftliche Bodenrauigkeit eine zentrale Rolle in einer Spannweite von ökologischen und hydrologischen Prozessen. In räumlich und zeitlich hochaufgelösten, prozessbasierten öko-hydrologischen Modellansätzen ist das Wissen von dem Zustand der Bodenoberfläche hinsichtlich der Rauigkeit von essentieller Bedeutung. Infiltration, oberflächen Abflussbildung und schliesslich Bodenerosion sind Prozesse die direkt von der Bodenrauigkeit abhängig sind. So ist der Zeitpunkt an dem Oberflächenabfluss ensteht massgeblich von der Rauigkeit abhängig. Für eine raue landwirtschaftliche Bodenoberfläche, im Vergleich zu einer glatteren/ebeneren Fläche, kann eine Verzögerung dieses Punktes festgestellt werden. Ebenso ist die Ausprägung des Oberflächenabflusses für beide Oberflächen unterschiedlich. Während Abfluss auf einer glatten Fläche eher schichtförmig über die gesamte Fläche fließt, folgt der Abfluss auf rauen Flächen eher dem höchsten Reliefgradient und damit eher konzentriert entlang von preferenziellen Pfaden. Das Wissen dieser Ausprägung ist wichtig für eine akkurate prognose des Bodenabtrags durch physikalisch basierte Erosionsmodelle. Durch den Einfluss von Niederschlag können sich Regenschlag- oder Verschlämmungskrusten ausbilden, die die Infiltrationsleistung einer Bodensäule signifikant reduzieren. Dies kann die Gefahr von Hochwasser erhöhen und das Wachstum landwirtschaftlicher Pflanzen reduzieren. Allerdings ist die Möglichkeit der Messung von Bodenrauigkeit in der Regel nur auf kurze Profile oder kleine Messfelder begrenzt. Eine erhöhte Unsicherheit in der Vorhersage der oben genannten Prozesse ist die Folge. Wie im ersten Teil dieser Dissertation gezeigt werden konnte, eignet sich der Einsatz von Fernerkundungssensoren, operierend im Wellenlängenbereich der Mikrowellen, für die Ableitung der mikroskaligen Bodenrauigkeit von unbewachsen und gering bewachsen landwirtschaftlichen Feldern. So lässt sich unter Einsatz voll-polarimetrischer Radardaten (SAR) eine Abhängigkeit der $RRLL$ Kohärenz von der Bodenrauigkeit feststellen. Allerdings wird diese Korrelation durch Unsicherheiten, aufgrund der skalenabhängigen Messung der Bodenrauigkeit sowie der anisotropen Erscheinung im Feld, verzerrt. Neben den oben genannten Effekten hat die Bodenrauigkeit einen bedeutenden Einfluss auf das Rückstreuverhalten von Mikrowellen in der Radarfernerkundung. Wie in Paper II dieser Dissertation gezeigt, leistet die Bodenrauigkeit, speziell die periodische horizontale Komponente, einen signifikanten Beitrag zur Entstehung von direktionaler Rückstreuung von landwirtschaftlichen Nutzflächen. Diese Form der Rückstreuung ist charakterisiert durch eine untypisch hohe Rückstreuung über unbewachsenen und gering bewachsenen Flächen. Demnach ist eine adäquate Beschreibung der Bodenrauigkeit notwending für ein verbessertes Verständnis und beeinhaltet die Erfassung der Rauigkeit über grosse Messplots, um die verscheidenen Skalen und Komponenten der Rauigkeit zu charakterisieren. Im zweiten Teil der vorliegenden Dissertation wird dazu ein Messsystem entwickelt, das auf Basis photogram-

metrischer Messungen Bodenrauigkeit über große Messplots sehr genau ($RMSE_Z = < 2$ mm) und effizient messen kann. In statistischen Tests wurde die Effizienz des Messsystems analysisiert und ein deutlicher Vorteil der Apparatur gegenüber den üblichen Messtechniken (Laser, Nadelbrett) hinsichtlich der Robustheit und Geschwindigkeit ausgemacht. Ein Testverfahren um die Abhängigkeit der berechneten Rauigkeitswerte von der Größe des Messplots zu untersuchen wurde im Rahmen dieser Dissertation entwickelt und vorgestellt. In Anlehnung an das *representive elementary volume* Verfahren, wurde eine Schätzstatistik zur *representive elementary area* vorgestellt und auf den Datensatz angewendet. Ergebnisse dieser Schätzstatistik unterstreichen die statistische Robustheit des entwickelten Verfahrens zur Bestimmung der Rauigkeit. Weiterhin konnte aufgrund der Datenlage belegt werden, dass die Bodenrauigkeit landwirtschaftlich genutzter Flächen eine starke anisotrope und multiskalige Ausprägung besitzt. Somit kann die bisherige vorherrschende Annahme der isotropie und stationarität landwirtschaftlicher Bodenrauigkeit widerlegt werden. Abschliessend wurden in Teil III der vorliegenden Dissertation die erfassten Daten zur Modellierung von Rückstreuwerten verschiederner Radarsensoren herangezogen. In einer Studie zur Analyse gerichteter Rückstreuung von landwirtschaftlichen Flächen, konnte unter Einsatz des *modified Shin and Kong* Modells, welches Anisotropie sowie die verschiedenen Skalen der Rauigkeit berücksichtigt, die Rückstreuung modelliert werden. In diesem Zusammenhang konnte erstmals gezeigt werden, dass die unterschiedlichen Skalen der Rauigkeit neben der Saatreihenorientierung einen erheblichen Einfluss auf die gemessen Rückstreuwerte solcher Flächen hat.

Abschließend kann der wissenschaftliche Beitrag dieser Dissertation folgendermaßen Zusammengefasst werden:

- Es konnte ein besseres Verständnis der Bodenrauigkeit landwirtschaftlich genutzer Flächen in Hinblick auf die Parametrisierung von Radarrückstreumodellen im Kontext der Skalenabhängigkeit sowie einer anisotropen Erscheinung erreicht werden.
- Es konnte das Verständnis von gerichteter Rückstreuung innerhalb der aktiven Mikrowellen Fernerkundung deutlich verbessert und auf die Ausprägung der Bodenrauigkeit zurückgeführt werden.
- Es konnte das Potential polarimetrischer SAR-Daten zur Ableitung der flächenhaften Bodenrauigkeit als mögliche Eingangsgröße für öko-hydrologische Simulationsmodelle demonstriert werden.

Contents

List of Figures

1 Introduction

Micro-topography - or soil surface roughness - is a key parameter in a wide range of environmental applications. As investigated in this thesis, soil surface roughness in an agricultural environment originates from the superimposition of tillage activities of the farmers and the local field characteristics such as general and in-field slope. Changes in soil surface roughness conditions are related to, besides agricultural practice, precipitation, soil water and wind erosion as well as sedimentation. While precipitation and erosion processes cause a smoothing of the soil surface, agricultural practice produces different roughness states depending on the applied tillage tool and strategy. Römkens and Wang (1986) defined different scale-dependent roughness classes in the context of an agricultural landscape (see Table 1.1). While the defined roughness classes cover a wide roughness spectra, the submitted thesis focuses on the roughness classes random roughness and orientated roughness. Since Römkens and Wang (1986) address in their approach only the scale dependency, Allmaras et al. (1966) classified soil surface roughness into two terms in dependency of their geometrical appearance: Orientated and random roughness. While orientated roughness is dependent on the tillage tool or general slope effects, random roughness is result of the fortuitous occurrence of peaks and depressions resulting from soil clods and organization of aggregates which cannot be addressed to orientated roughness. Thus, in an agricultural environment, tilled surfaces can be described as a superimposition of several roughness scales, the periodical appearance of the orientated roughness (seedbed rows, wheel tracks) imposed by the random roughness, component which is characterized by a random distribution of soil clods and aggregates in several sizes (see Fig. 1.1). Marzahn et al. (2012b) and Blaes and Defourny (2008) showed a directional dependency of soil surface roughness due to the tillage operations, especially to the seedbed rows.

Roughness Class	**Scale** [mm]	**Topographic Elements**
micro roughness	≤ 2	texture dependent roughness
random roughness	$2 - 200$	soil aggregates and clods
orientated roughness	$200 - 400$	rows, tillage patterns
higher order roughness	≥ 400	slope, field borders

Table 1.1: Roughness classification after Römkens and Wang (1986).

In classical approaches, soil surface roughness is described as a single-scale random stationary process, which can be characterized by a vertical and a horizontal component. To describe soil surface roughness numerically, it is common to use statistical indices,

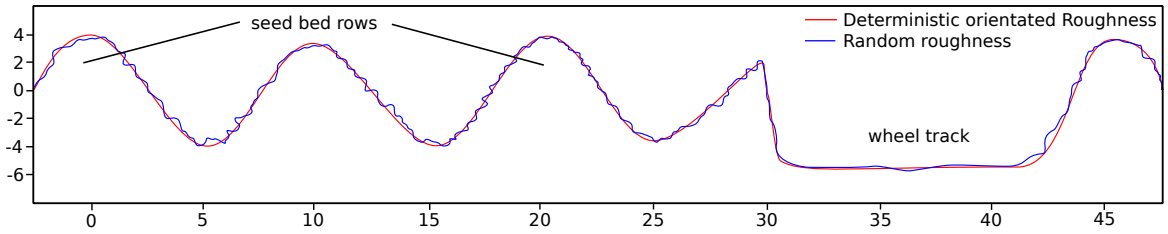

Figure 1.1: Composition of an agricultural quasi-periodic roughness profile with deterministic orientated roughness (red line), random roughness component (blue line) and a wheel track of a tillage machine. Units in [cm]

which differ in their complexity significantly. A simple approach to numerically characterize soil surface roughness is the Random Roughness Index (RR) - or more common the RMS-height s - (Allmaras et al., 1966), which is defined as the standard deviation of the heights Z to a reference height (e.g. the mean height $\bar{Z}$):

$$s = \sqrt{\frac{\sum_{i=1}^{n} \left(Z_i - \overline{Z}\right)^2}{n-1}} \tag{1.1}$$

Helming (1992) introduced the Tortuosity Index T_B for three-dimensional surfaces. It is defined as the ratio between the true (3D) surface and the projected (2D) surface:

$$T_B = \frac{A_{3D}}{A_{2D}} \tag{1.2}$$

Using T_B as a roughness index is especially suggested in soil erosion-related research topics, due to the possibility of calculating the true kinetic impact of the rain drops on the soil surface. With an increase in roughness, s and T_B increase as well. Several authors (Allmaras et al., 1966; Currence and Lovely, 1970; Sommer, 1997), have criticized these indices for not maintaining the spatial distribution for a physical interpretation. Thus, introducing higher order roughness indices, ranging from geostatistics over fractals to spectral analysis. It is common to use the autocorrelation length l for characterization of the horizontal roughness component which can be derived from a autocorrelation function ACF where l is usually defined as the distance where the ACF drops under $1/e$ (Blaes and Defourny, 2008; Davidson et al., 2003; Taconet and Ciarletti, 2007). Davidson et al. (2000) as well as Manninen (2003) showed a strong dependency on the derived autocorrelation length and RMS-height from the profile length over which they are estimated. With an increase in profile length the RMS-height and the autocorrelation length increase as well. With respect to this scale dependency of the proposed roughness values, several studies utilized complex roughness values comprising a fractal description of the soil surface (Zribi et al., 2000; Verhoest et al., 2008). Fractals are based on the formulations of Mandelbrot (1995) and describe a self-affinity at different scales of irregular and fragmented structures. In addition to the before mentioned approaches, Blaes and Defourny (2008) and Marzahn et al. (2012c) decomposed the several roughness

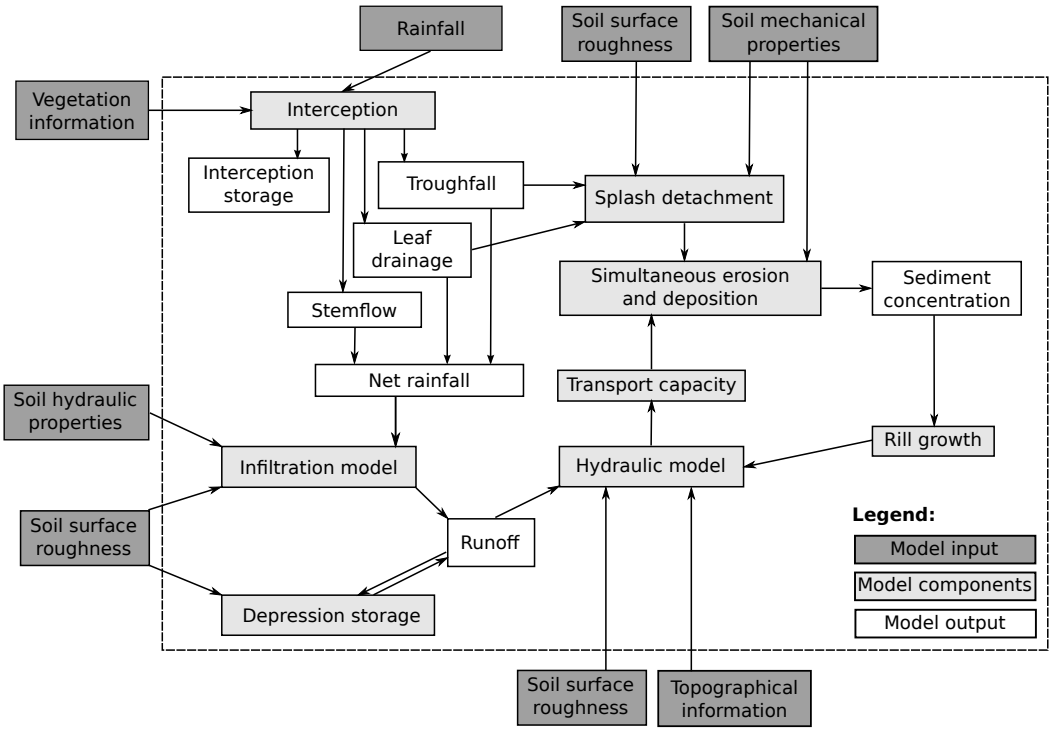

Figure 1.2: Flowchart of the EUROSEM soil erosion model, altered after Morgan et al. (1998)

scales obtained on single roughness measurements into its sub-scales and characterized them by means of the RMS-height and autocorrelation length.

1.1 The role of soil surface roughness in the environmental system

It is well known and understood that soil surface roughness is a key parameter in large-scale environmental modeling efforts, which control most of the soil physical processes such as runoff generation, infiltration and soil erosion at field scale. Several studies showed the impact of soil surface roughness on runoff generation, which is usually delayed at rougher surfaces compared to smooth surfaces (Cremers et al., 1996; Jester and Klik, 2005; Le Bissonnais et al., 1998). In field studies, Johnson et al. (1979) showed that a rough surface reduces runoff (77%) and soil loss (89%) in comparison to a smoother surface. Same was observed in several laboratory studies by Römkens et al. (2001), Darboux and Huang (2005) and Zeiger (2007), showing a decrease in sediment yield by an increase in soil surface roughness conditions. However, this assumption is only valid for an uniform overland flow - *sheet-flow* -, which in an agricultural environment is mostly not the case. With an increase in roughness the anisotropic pattern of roughness is directing and altering the sheet-flow to a more linear flow, thereby increasing the

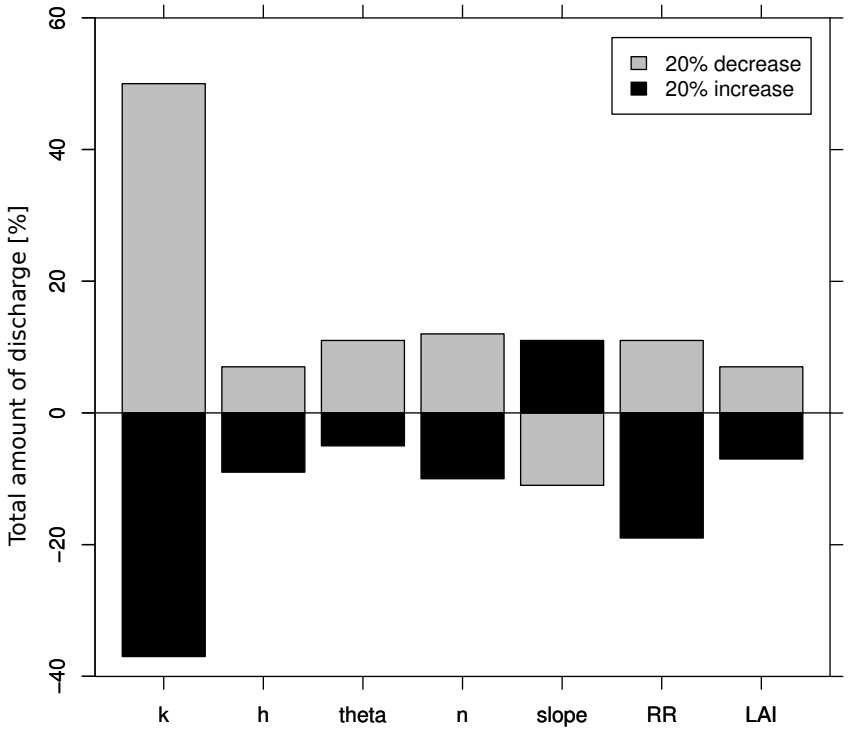

Figure 1.3: Results of a sensitivity analysis of several LISEM input parameters for the total amount of discharge [%]. With k = saturated conductivity, h = matrix potential, theta = soil water content, n = Manning's coefficient, slope = terrain slope, RR = random roughness, LAI = leaf area index. Altered after De Roo et al. (1996)

sediment yield (Darboux and Huang, 2005). In context of an event and physically-based soil erosion model such as *EUROSEM* (Morgan et al., 1998), soil surface roughness is an essential input variable as shown in Figure 1.2. Using the *Limburger Soil Erosion Model* (*LISEM*) for example, De Roo et al. (1996) showed a strong sensitivity of the amount of discharge and sediment yield to a change in soil surface roughness conditions (see Fig. 1.3). Duttman (1999) as well as von Werner (1995) showed similar results for the soil erosion model *Erosion3D* (Schmidt, 1991). Thus, with an increase in roughness, an exponential decrease of sediment yield can be observed. The effect of a reduced soil loss from rough surfaces is related to the fact that a rougher surface has a larger surface to absorb the kinetic energy of the rain drops (Helming, 1992), which preserves the surface from splash. In addition, rougher surfaces show a higher depressional storage capacity (Cremers et al., 1996; Kamphorst et al., 2000), thus showing a higher water retention delaying the point to runoff (Moore and Larson, 1979). Fohrer et al. (1999) mentioned

roughness as one of the future key parameters for an effective spatially distributed flood protection system. Besides soil erosion and surface runoff, soil roughness controls major soil physical processes. As above mentioned, due to crusting and sealing effects resulting from precipitation, the bulk density in the upper few centimetres of the soil column increases, reducing the effective infiltration rate (Farres, 1987; Fohrer et al., 1999; Le Bissonnais et al., 1998) as well as reducing the amount of available oxygen for plants and their development (Hartge and Horn, 1999). In a experimental laboratory study, Sun et al. (2006) established an empirical relationship between soil surface roughness values, namely the RMS-height s and soil bulk density parameters of the upper few centimetres of the soil column. Marzahn and Ludwig (2009a) obtained similar results in their study using field data and showed the potentials of such an approach for hydrological modeling.

1.2 The role of soil surface roughness in microwave remote sensing applications

The backscattering of an illuminated scene is mainly dominated by the geometric and dielectric properties of the imaged media. While the dielectric properties of a natural agricultural bare soil surface are mainly influenced by the soil water content and the soil bulk density as well as soil texture, the geometric properties are formed by soil surface roughness conditions. For a vegetated agricultural surface, the contributors of the backscattering are dependent from the sensor's wavelength. For short wavelengths the backscattering is mainly dominated by the vegetation water content and the geometric appearance of the vegetation layer. For longer wavelengths the backscattering also has contributions from the soil surface (e.g. soil surface roughness and soil water content). Figure 1.4 summarizes the main backscatter contributions for an agricultural scene. In the case of passive microwave remote sensing the radiation measured by a sensor is also composed by the water content (respectively soil- and vegetation water content) as well as by the geometric properties of the focused surface (soil surface roughness and vegetation geometrics) and the optical thickness of the vegetation layer (Woodhouse, 2006). However as this thesis is mainly focused on roughness parametrization for active microwave remote sensing applications, the impact of soil surface roughness on the backscattering of a SAR system is highlighted in more detail.

Soil surface roughness in context of the sensor's wavelength is scale-dependent, thus different authors proposed a wavelength-dependent normalisation of roughness values introducing the wave number k:

$$k = \frac{2\pi}{\lambda} \tag{1.3}$$

which normalizes the RMS-height s and autocorrelation length l to the wavelength λ by:

$$ks = k * s \tag{1.4}$$

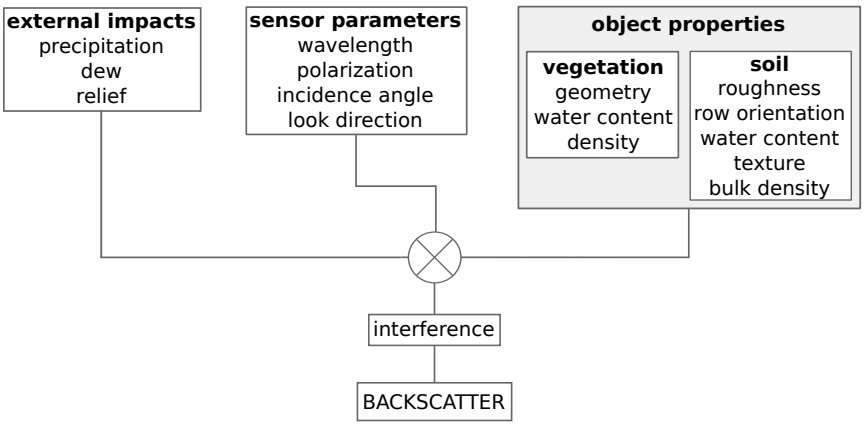

Figure 1.4: Influencing factors of backscattering of a natural agricultural scene of an active microwave remote sensing system

True value [cm]	**X-Band**	**C-Band**	**L-Band**
$s = 2$	4.02	2.22	0.56
$l = 10$	20.12	11.11	2.77

Table 1.2: Dependency of soil surface roughness from the sensors wavelength. X-Band λ= 3.12 cm; C-Band λ= 5.66 cm; L-Band λ= 22.62 cm

$$kl = k * l \tag{1.5}$$

Thus, imaging a surface with a given RMS-height at different frequencies, the surface appears rougher in a X-Band scene and becomes a smoother appearance in a L-Band image. Table 1.2 summarizes the dependency of the roughness values from the sensor's wavelength for three different frequencies. In this context the question arises how to define if a surface is rough or smooth? Therefore two different criteria have been proposed, which account for phase differences in two incident and backscattered waves separated by one standard height deviation h in dependency of the wavelength (λ) and the incidence angle (θ) (Woodhouse, 2006); the Rayleigh and the Fraunhofer criterion. The first one is defined as:

$$h_{smooth} < \frac{\lambda}{8cos\theta_i} \tag{1.6}$$

while the latter one is more stringent:

$$h_{smooth} < \frac{\lambda}{32cos\theta_i} \tag{1.7}$$

This requires a phase difference of $\delta_\phi < \pi/2$ before a surface is considered to be smooth for the Rayleigh criterion and $\delta_\phi < \pi/8$ for the Fraunhoffer criterion (Woodhouse, 2006).

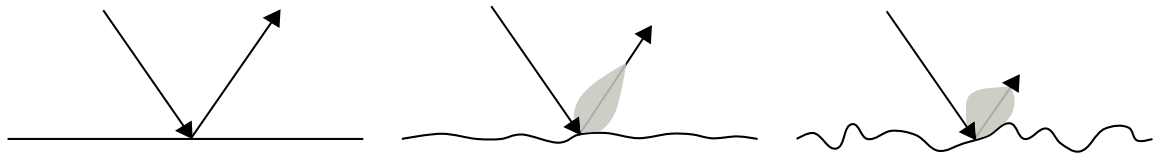

Figure 1.5: Dependency of the scattered field from soil surface roughness. For smooth surface only specular reflection occurs, with an increase in roughness diffuse scattering is also present

Generally there is a dependency of backscattering from soil surface, which shows an increase in backscattering by an increase in roughness. For a defined frequency, incidence angle and dielectric conditions, an increase in soil surface roughness causes an increase in backscattering, due to the more diffuse scattering with a higher fraction scattered to the sensors antenna (see Fig. 1.5). However, the different roughness components (e.g. orientated roughness and random roughness, see Figure 1.1) have a different impact on the backscattering dependent on the orientation of the surface to the sensor's look vector and incidence angle. If orientated quasi-perpendicular to the incident wave, the deterministic orientated roughness component acts like a classical Bragg scatter surface, which is characterized by a large proportion of coherent scattering (Ulaby et al., 1982) and could increase the backscattering up to 10 dB (Beaudoin et al., 1990; Wegmuller et al., 2011). Bragg scattering occurs on surfaces with a clear regular pattern, which is in an agricultural environment defined by the quasi-periodic seedbed rows. However, with an increase of the random roughness fraction superimposed over the deterministic orientated roughness, the coherent backscattering changes to an incoherent scattering. Beaudoin et al. (1990) quantified an influence of the random roughness component over non-periodic surfaces of 2 dB on the backscattered signal. In context of present satellite SAR missions, which operate with an incidence angle of around 20°to 25°, this effect increases up to 3-4 dB. As, for the quasi-parallel orientation of the seedbed rows to the sensor's line of sight, the backscattering is mainly influenced by the random roughness component, while the deterministic periodic roughness component induces polarization orientation angle shifts (Lee et al., 2002, 2000).

Using polarimetric SAR systems (either dual or quad-polarized), soil surface roughness has a significant impact on the backscattering at different polarizations. In earlier studies, Oh et al. (1992) showed a dependency of the different backscatter values (σ_{HH}; σ_{VV}; σ_{HV}) from the roughness conditions on top of soil moisture content, local incidence angle and frequency. Thus for a given frequency (X-Band) and incidence angle (30°) the backscattering increases with an increase in roughness, where the σ_{HH} and σ_{VV} backscatter values are at similar levels (smooth = -10 dB; rough = -7 dB) with a slightly higher backscattering in the σ_{HH} polarization. However, with an increase in s, the σ_{HH}/σ_{VV} ratio becomes one. Indeed, the σ_{HV} backscatter coefficients over the same surface and sensor properties are significantly lower (smooth surface = -20 dB; rough = -15 dB) (Oh et al., 1992). Beaudoin et al. (1990) retrieved similar results for an

airborne C-Band SAR system. In their extensive study on roughness effects on multi-dimensional SAR data, Mattia et al. (1997) observed an increase in the magnitude of the *HHVV* coherence over rougher fields compared to smooth fields, indicating a high similarity of the HH and VV polarization over rough surfaces. Schuler et al. (2002) and Marzahn and Ludwig (2009a) verified the previous findings of Mattia et al. (1997) and extended this approach for the *RRLL* coherence, which decreases by an increase in soil surface roughness. Due to its inherent dependency of the backscattered wave from soil surface roughness contributions and the dielectric properties of an imaged surface, the retrieval of geo and bio-physical parameters such as soil moisture and vegetation characteristics (over sparse vegetated fields) is highly influenced by roughness effects. To account for this inherent dependency, several empirical or semi-empirical backscatter models have been developed for the retrieval of various bio and geo-physical parameters such as soil moisture (Ulaby et al., 1982; Shin and Kong, 1984; Ulaby et al., 1986; Fung et al., 1992; Oh et al., 1992; Zribi et al., 2000). In an early study, Beaudoin et al. (1990) concluded that with an airborne system, the derivation of soil moisture is not possible due to roughness effects at various scales using such a model. However, in recent years good progress was made in the separation of dielectric and roughness contributions on the backscattered wave using polarimetric SAR (PolSAR), polarimetric interferometric SAR (PolInSAR) and differential interferometric SAR (DInSAR) techniques (Hajnsek et al., 2003; Allain et al., 2004; Hajnsek and Prats, 2008; Hajnsek et al., 2009; Jagdhuber, 2012). Indeed, the retrieval of soil moisture with a current RMSE of 5-20 Vol.-% is still not sufficiently solved. Verhoest et al. (2008) concluded that the lack of understanding in roughness parametrization is the main error source in an accurate soil moisture retrieval. Figure 1.6 shows as an example the impact of soil surface roughness on the retrieval of soil moisture using three different approaches over a bare field under seedbed preparation during the AgriSAR2006 campaign. Using the classical empirical model of Oh et al. (1992), only a few pixels could be inverted to soil moisture. This is related to a violation of the boundary conditions of the model by the roughness conditions in the field. However, there is a general bias in the estimation of soil moisture between the already tilled southern part of the field and the still crusted northern part of the field up to 15 Vol.-% which is clearly related to the different roughness conditions. Using the x-Bragg model, introduced by Hajnsek et al. (2003), the amount of invertible pixels increases. However, the bias of 15-20 Vol.-% due to the different roughness conditions is clearly visible (Fig. 1.6b). Choosing a simple hybrid approach (Marzahn and Ludwig, 2009b) by incorporating spatially distributed roughness information derived from the *RRLL* coherence (Marzahn and Ludwig, 2009a) into Oh's model, the roughness effect vanishes and the retrieved soil moisture is homogeneous over the entire field as sampled during the campaign (Field average = 21 Vol.-%; STD= 3.5 Vol.-%). However the RMSE is about 8.4 Vol.-%, which is an improvement compared to other classical soil moisture retrieval algorithms, but not sufficient for hydrological applications, which usually demand a maximum RMSE of approx. 4 Vol.-%.

The effects of soil surface roughness on the backscattered signal are also visible in the presence of directional scattering on bare soil or sparsely vegetated fields, as observed by Ferro-Famil et al. (2003) as well as Wegmuller et al. (2006, 2011). With an orientation

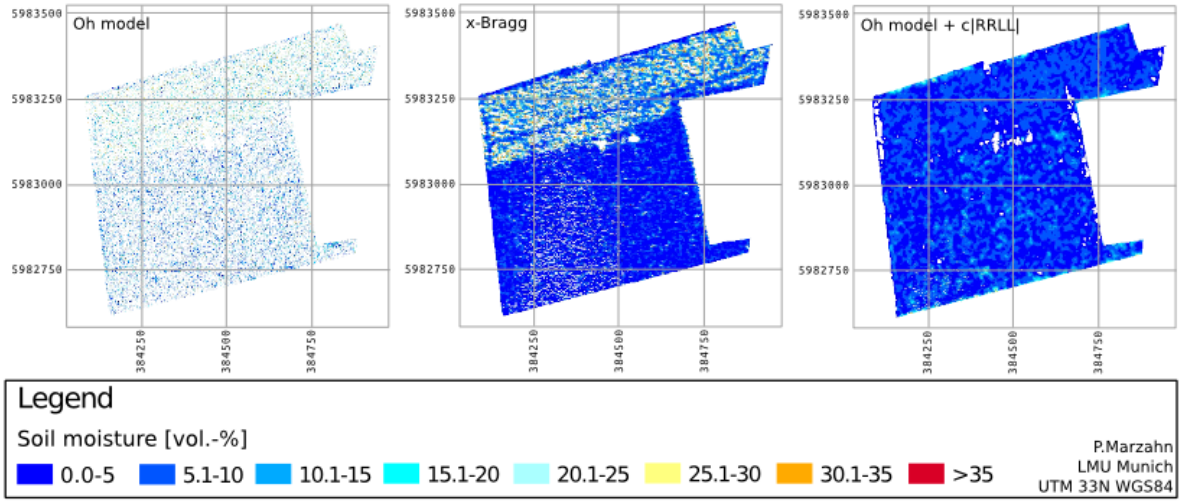

Figure 1.6: Derivation of soil moisture over bare field (AgriSAR2006 @Goermin) with different tillage and roughness conditions using different retrieval algorithms. Southern part of the field already seedbed prepared; northern part of the field still crusted. Measured mean soil moisture = 21 Vol.-%. SAR data acquired with DLR's E-SAR system at L-Band

of the seedbed rows quasi-perpendicular to the sensor's look vector, the backscattering can be significantly increased by a coherent backscattering of the incident wave. Figure 1.7 shows as an example a colour composite of strong directional scattering in close (< 30 min) ERS-2 ASAR Tandem acquisitions over the Flevoland, NL test site. While fully saturated green colours correspond to a 6 dB higher backscattering in the ERS-2 image compared to the ASAR image, fully saturated red colours display a 6 dB higher scattering in the ASAR image. Thus, due to different image geometries with a difference of 1°in the aspect angle (Wegmuller et al., 2011), different fields with slightly different row orientations show this directional effects. Examples of directional scattering could also be found over various test-sites across Europe (e.g. Görmin, Germany; Alling, Germany; Wallerfing/Neusling, Germany; Matera, Italy, Sardinia, Italy) (Ferro-Famil et al., 2003; Wegmuller et al., 2010; Marzahn et al., 2012a). With such a difference in two subsequent and close SAR acquisitions, the confidence of which SAR data is assimilated in land application models (e.g. hydrological models, crop growth models) is not very promising. For example, the change in backscattering related to a change of soil moisture from dry to saturated conditions is in the range of 6 dB for a C-Band system (Mattia et al., 2003), thus the retrieval of soil moisture in presence of directional scattering is highly biased. Marzahn et al. (2012d) showed in an analysis of the roughness contributions to the directional scattering that on top of the strong dependency of the directional scattering from the row orientation a secondary dependency is given from the orientated roughness component.

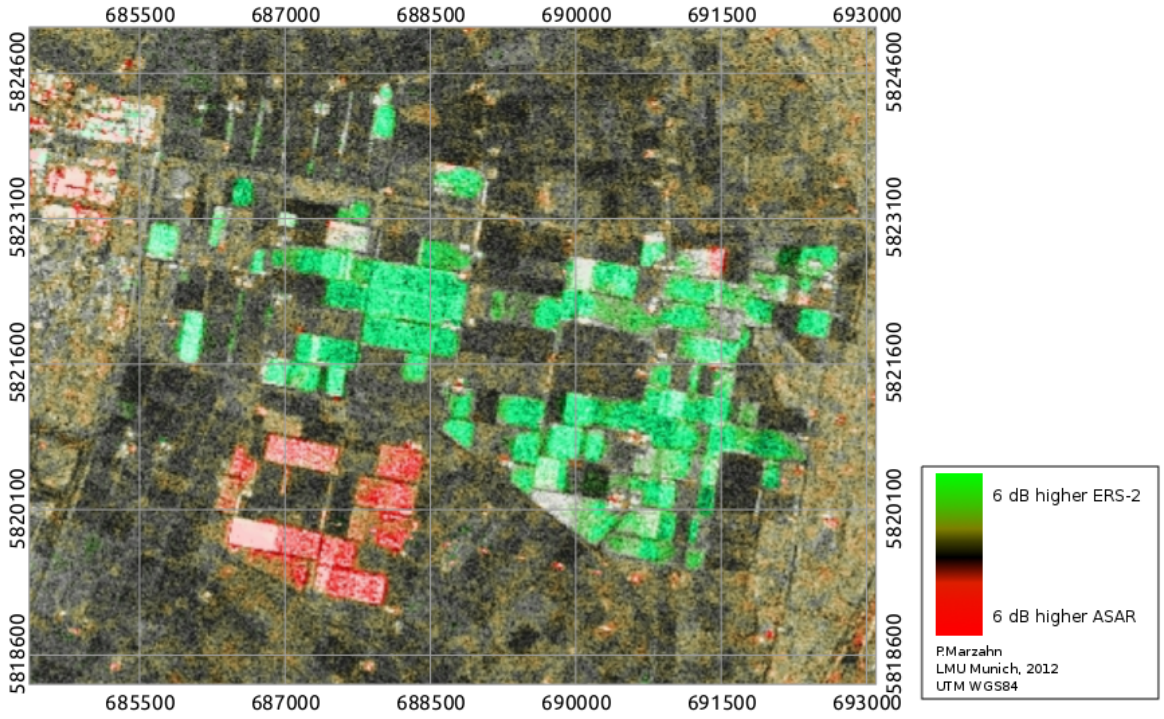

Figure 1.7: Directional scattering in nearly simultaneous Envisat ASAR and ERS-2 acquisitions. Fully saturated green colors represent a 6 dB higher scattering in the ERS-2 imagery, while fully saturated red colors indicate a 6 dB higher backscattering in the ASAR imagery

1.3 State of the art in soil surface roughness measurements

The measurement of soil surface roughness has a long tradition in soil erosion research. And - with a little delay - also in microwave remote sensing research related studies. Once starting with very simple methods, such as the chain method, where the reduction of a chain laid over ground compared to the true length of the chain is a measure of the roughness, the measurement of soil surface roughness has become more sophisticated and physically meaningful. Nowadays the techniques for measuring soil surface roughness can be divided into two groups, contact and non-contact devices, which can be further split in two-dimensional (2D) and three-dimensional (3D) measurements (Jester and Klik, 2005). The common measurement devices of the contact group for the measurement of soil surface roughness are mainly mesh boards or pin/needle profilers, which measure soil surface roughness along a single profile usually at a length of 1-2 meters and a horizontal resolution of 1-5 cm (Hajnsek et al., 2002; Thiel, 2003; Bryant et al., 2007). Both devices could be considered as destructive measurements, especially the mesh board, which is rammed into the upper few centimetres of the soil column. Thus, a multi-temporal measurement over the same sampling area is not possible. For the

non-contact devices, a broad range of methods have been utilized in the past ranging from laser devices (Davidson et al., 2000; Alvarez-Mozos et al., 2009; Darboux and Huang, 2003) and LIDAR devices (Fernandez Diaz et al., 2010) over acoustic backscatter (Oelze et al., 2003) to photogrammetric acquisitions (Helming, 1992; Warner, 1995; Rieke-Zapp and Nearing, 2005; Taconet and Ciarletti, 2007), yielding in two methods commonly applied, laser scanning and photogrammetric measurement of soil surface roughness. While the first one is mainly deployed using 2D devices measuring roughness along single profiles, photogrammetry is able to measure soil surface roughness in 3D giving a more realistic value of the roughness measure (Verhoest et al., 2008). Indeed both measurement techniques have their advantages and disadvantages. Using a 2D laser profiler, one is capable to acquire very long roughness transects in range of 10 m (Davidson et al., 2000) to 75 m permitting the characterization of multi-scale roughness effects of an agricultural field (Manninen, 2003). However, as recent studies have shown, soil surface roughness has to be considered as an anisotropic surface (Blaes and Defourny, 2008; Marzahn et al., 2012c), a 3D representation of the surface is necessary to adequately describe a soil's surface. Indeed, available laser devices capable of measuring soil surface roughness over large sample plots are rare and time-consuming (Rieke-Zapp and Nearing, 2005). However, as shown by Davidson et al. (2000), several proposed roughness indices are scale sensitive and their values increase with an increase in the sampling area or profile length. Thus, the acquisition of soil surface roughness over large areas by a laser scanner is not very suited as they are time-consuming. Jester and Klik (2005) showed in an laboratory experiment the advantage of using a photogrammetric acquisition system for time efficiency reasons. While using a photogrammetric-based system the acquisition time was reduced to 1/6 of the laser's acquisition speed for an sample area of 55x50 cm^2 and a spatial resolution of 2x2 mm^2, thereby outperforming the laser device at same accuracy. However, this is only possible due to the decoupled acquisition and processing steps of the photogrammetric system. Indeed photogrammetric systems have been mainly utilized in the past by photogrammetric experts using special equipment, fitting the demand of an accurate image processing (Lascelles et al., 2002). In recent years, several studies showed the utilization of consumer grade, non-metric cameras for photogrammetric purposes with the same accuracy at reduced cost (Rieke-Zapp and Nearing, 2005; Rieke-Zapp et al., 2009). Therefore the stability of the interior orientation of the camera sufficiently worked out commercial of-the-shelf (Warner, 1995; Lascelles et al., 2002) or could be improved by fixing the lens or sensor by using screws or glue (Rieke-Zapp et al., 2009). The potential error sources of such a system are clearly related to a poorly known or unstable interior and exterior orientation of the deployed system. Wackrow and Chandler (2008) suggested, to minimise the effects of a poorly calibrated lens model, to acquire images in a slightly convergent acquisition geometry.

The basic principle of object reconstruction using a photogrammetric acquisition system will be briefly described in the following. The derivation of object-coordinates of an arbitrary point P could be solved by means of the relations displayed in Figure 1.8 and Equations 1.8 - 1.10. Thus, the object height Z of point P can be directly inverted from the parallax px, the distance between the two camera positions (B) and the focal length (c) (Luhmann, 2003). To find in both images homogeneous points, which are

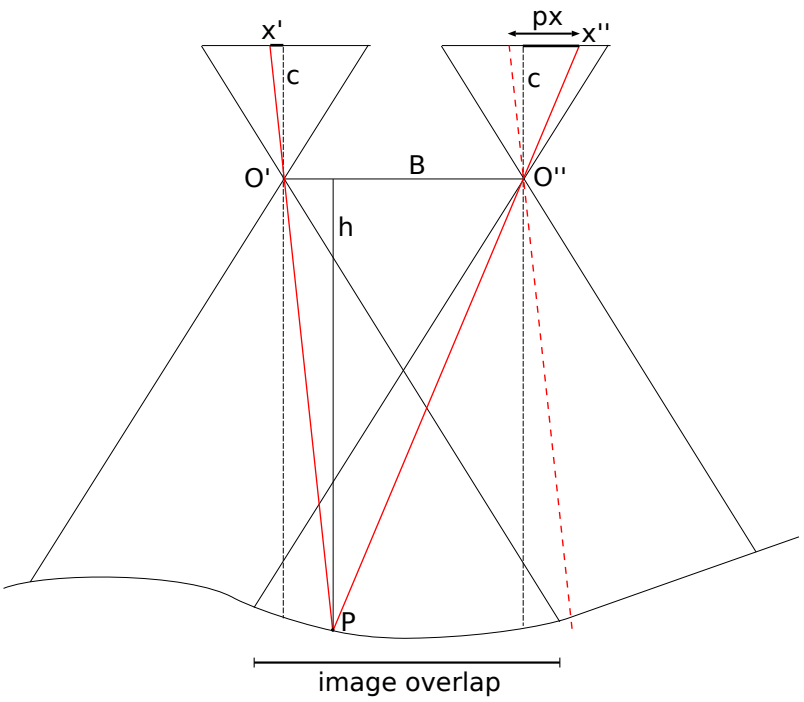

Figure 1.8: Photogrametric object reconstruction with x′ = x-parallax in the left image; x″ = x-parallax in the right image; px = x′-x″; B = Base; h = mean lens height above ground; O = projection center;

obligatory for the derivation of heights, cross-correlation is used where a threshold for the matching algorithm has to be defined by the user. For an efficient computing of the cross-correlation, the two overlapping images have to be perfectly orientated during the pre-processing triangulation step, so the search matrix becomes a one dimensional search matrix (Linder, 2009).

$$X = \frac{h}{c} * x' = mb * x' \tag{1.8}$$

$$Y = \frac{h}{c} * y' = mb * y' \tag{1.9}$$

$$Z = \frac{b * c}{x' * x''} = \frac{b * c}{px} \tag{1.10}$$

In an iterative process the resulting point cloud becomes denser and finally can be interpolated to a regular grid with the desired resolution.

1.4 Aims and goals of this thesis

As shown in the previous sections, soil surface roughness plays a key role in several environmental applications as well as in the utilization of microwave remote sensing systems, at a concurrent fail in the measuring and characterization as well as understanding of soil surface roughness over large areas. Thus, previous proposed methods can be considered as point measurements, with a maximum acquisition size up to a few square meters. As roughness is scale-dependent, large sample sizes need to be measured for an adequate representation of soil surface roughness. In addition, soil surface roughness is highly variable in space and time. As shown in the previous sections, soil surface roughness is continuously altered by weather conditions and strongly correlates to the field conditions (soil moisture, soil texture) and tillage practices, thus showing a large spatial and temporal variance (Römkens and Wang, 1986). To successfully assimilate soil surface roughness in available eco-hydrological models or microwave backscatter models, this spatial and temporal variance has to be considered.
This thesis concentrates on the measurement of soil surface roughness at large scales over large sample plots for an improved characterization of soil surface roughness considering the different scales of soil surface roughness as well as its anisotropic appearance. Therefore, a photogrammetric acquisition system should be developed, which permits the measurement of soil surface roughness over large sampling areas in an adequate spatial resolution at low cost. The potential of this system shall be evaluated in context of robustness and physical meaning and compared to classical approaches such as laser profile measurements. In a further step the derived multi-dimensional soil surface roughness values, where multi-dimensional is considered to account for the anisotropic appearance and multi-scale appearance of soil surface roughness, should be assimilated in available backscatter models to enhance the backscatter modeling and derivation of geophysical variables from available satellite SAR sensors.

2 Scientific Paper

This work is a synthesis of the research done over the past years and published in several papers. It was done to fulfil the aims and goals of this thesis as defined in the previous section. The thesis consists of five papers published in relevant journals. Figure 2.1 illustrates the connection and contribution of each paper to this thesis as well as to the scientific areas. The first two papers describe the potentials and limitations of SAR data utilization in agricultural environments with a special focus on the roughness-induced problems and potentials. In the third paper, a simple photogrammetric acquisition system is developed and roughness statistics were analysed. In the fourth paper, a multi-scale roughness description is introduced. Finally in the fifth paper, the connection to the parametrization of soil surface roughness in recent backscatter models is made.

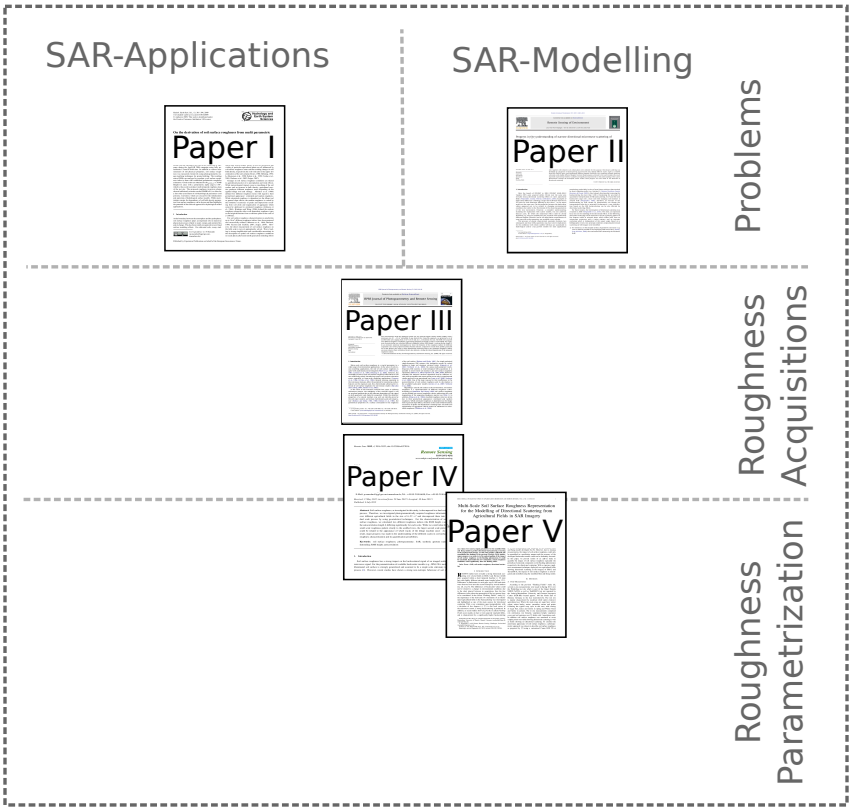

Figure 2.1: Positioning of the papers and topics they are covering within this PhD-thesis

2.1 Paper I: HESS - On the derivation of soil surface roughness from multi-parametric PolSAR data and its potential for hydrological modeling

Paper I describes the potential of deriving soil surface roughness on a landscape scale from multi-polarized SAR data. Using a large data base of photogrammetrically acquired *in-situ* roughness measurements in addition to fully polarimetric airborne SAR data, soil surface roughness was derived spatially distributed by establishing an empirical relationship between three polarimetric roughness estimators and the *in-situ* measurements. In a further analysis, the potential of this approach for the derivation of geo-physical and soil-physical parameters such as soil moisture as well as bulk density parameters for usage in hydrological or soil erosion models was shown.
Thus, Paper I therefore shows the fields of applications, potentials and limitations which occur when deriving soil surface roughness at the landscape scale.

Marzahn, P. and Ludwig, R. On the Derivation of Soil Surface Roughness from Multi-Parametric PolSAR Data and its Potential for Hydrological Modeling. *Hydrol. Earth Syst. Sci.*, **2009**, 13, 381-394

Hydrol. Earth Syst. Sci., 13, 381–394, 2009
www.hydrol-earth-syst-sci.net/13/381/2009/

Hydrology and Earth System Sciences

On the derivation of soil surface roughness from multi parametric PolSAR data and its potential for hydrological modeling

P. Marzahn and R. Ludwig

Department of Geography, Ludwig-Maximilian University Munich, Germany

Received: 26 September 2008 – Published in Hydrol. Earth Syst. Sci. Discuss.: 28 November 2008
Revised: 3 March 2009 – Accepted: 3 March 2009 – Published: 18 March 2009

Abstract. The potential of multi parametric polarimetric SAR (PolSAR) data for soil surface roughness estimation is investigated and its potential for hydrological modeling is evaluated. The study utilizes microwave backscatter collected from the DEMMIN test site in the North East of Germany during the AgriSAR 2006 campaign using fully polarimetric L-band E-SAR data. In addition to various measurements of soil physical properties, soil surface roughness was measured extensively using photogrammetric image matching techniques for ground truthing. The resulting micro-DSMs are analyzed to correlate a soil surface roughness index to three well established polarimetric roughness estimators. Good results are obtained for $Re_{[\rho RRLL]}$ vs. RMS Height for areas with a polarimetric alpha angel $\alpha<40°$, which is thus used to produce multi temporal roughness data of the test site. The proposed roughness inversion scheme showed sufficiently accurate results (RMSE=0.1) to allow for a first order assessment of soil-hydrological parameters (soil porosity, void ratio), which are crucial for the initialization and operation of hydrological surface models. While uncertainties remain, the dependency of soil bulk density parameters from surface roughness can be shown and thus highlights the potential of the retrieval approach for hydrological model applications.

1 Introduction

At the boundary between the atmosphere and the pedosphere, soil surface roughness plays an important role in numerous physical processes related to water, energy and nutrient flux and exchange. This has been widely recognized in novel land surface modeling efforts. On cultivated soils, many studies have demonstrated that different roughness states influence runoff generation and formation due to soil sealing and crusting effects (Fohrer et al., 1999). Furthermore, processes like infiltration, evaporation, soil erosion by wind and water, lateral and vertical matter fluxes, as well as the growth and vitality of particular agricultural plants are all influenced by soil surface roughness states and the resulting changes in soil bulk density, respectively the soil void ratio in the upper few centimetres of the soil column (Farres, 1980; Helming, 1992; Le Bissionais et al., 1998; Fohrer et al., 1999; Cerdan et al., 2001; Darboux et al., 2002; Zeiger, 2007).

Changes in soil surface roughness conditions are related to agricultural practice or to precipitation and wind effects. While meteorological impacts cause a smoothing of the soil surface and an increase in bulk density, agricultural practice produces different roughness states depending on the applied tillage tool and strategy. Allmaras et al. (1966) defined two different roughness terms with regard to their geometrical appearance: orientated and random roughness. While orientated roughness is dependent on the tillage tool or general slope effects, the random roughness is caused by the fortuitous occurrence of peaks and depressions resulting from soil clods and organization of aggregates which cannot be addressed to orientated roughness (Allmaras et al., 1966). Römkens and Wang (1986) defined the random roughness alongside other scale dependent roughness types as the height deviations from a reference plain in the scale of 2–200 mm.

For soil surface roughness characterization on small plots up to 16 m^2, different roughness indices have been proposed and successfully utilized (Allmaras et al., 1966; Bertuzzi, 1990; Taconet and Ciarletti, 2007; Zeiger, 2007). However, the direct measurement of soil surface roughness on the field scale is not yet appropriately solved. This is leading to strong simplification and considerable uncertainty in the description of spatial soil surface roughness conditions in recent physically based runoff generation modeling efforts

Correspondence to: P. Marzahn
(p.marzahn@iggf.geo.uni-muenchen.de)

Published by Copernicus Publications on behalf of the European Geosciences Union.

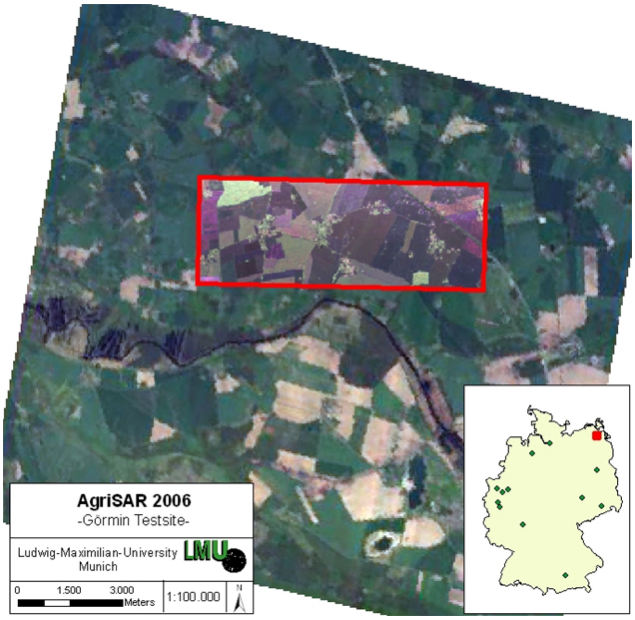

Fig. 1. Overview of DEMMIN-Görmin test site in the North East of Germany.

on the catchment scale. While expensive and labor intensive in-situ measurements are limited to small areas, remote sensing techniques are able to cover larger areas at relatively high frequency, which might offer the opportunity to measure dynamic soil surface characteristics on larger scales (Santanello et al., 2007; Loew and Mauser, 2008). In this study, the derivation of soil surface roughness information on field scale is conducted and evaluated from multi temporal airborne PolSAR data. To investigate the application potential in hydrological modeling, the deployment of multi temporal soil surface roughness maps for the retrieval of soil physical parameters, such as bulk density and void ratio, are presented as first results of a feasibility study.

2 Methods and field data

The study was performed in the frame of the ESA-founded campaign AgriSAR 2006, which was carried out from mid-April to the end of July at the DEMMIN (Durable Environmental Multidisciplinary Monitoring Information Network) test site (Hajnsek et al., 2007). A major component of this study was to generate an image and ground data base on a weekly basis for the examination and validation of bio-/geo-physical parameter retrievals and to simulate ESA's future Sentinel 1 and Sentinel 2 missions. Therefore, weekly E-SAR flights, operated by the German Aerospace Centre (DLR-HR), were accompanied by extensive in-situ measurements.

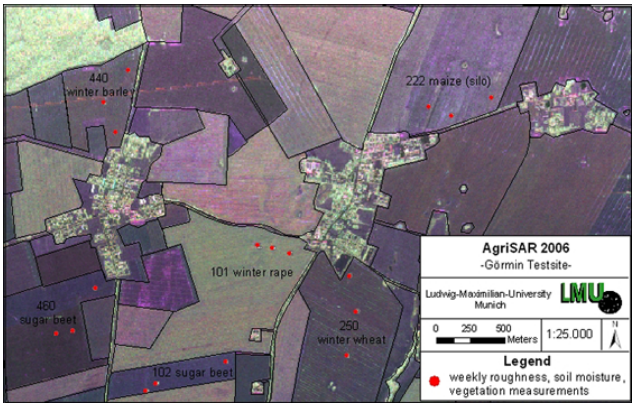

Fig. 2. Location of sample points within the Görmin test site during AgriSAR 2006.

2.1 Test site

DEMMIN is a consolidated test site in Mecklenburg-Western Pomerania in North East Germany, approximately 150 km north of Berlin (Fig. 1). The $3\times8\,km^2$ test site is located in the young moraine area, characterized by smooth topography and intensive agricultural cultivation on high productive soils. The altitudinal range within the test site is about 60 m with its maximum in the north and a minimum in the southern part of the test site near the Peene river. Soil texture ranges from sandy loam to loamy sand. The main crop rotation is winter wheat, winter rape and winter barley. Additionally, maize and sugar beet is sown in spring for livestock feed. The mean field size is 225 ha. Due to very large fields and intensive cultivation, wind, water or tillage induced erosion patterns such as shortened soil columns can be observed within the fields.

18 sample points were chosen to represent soil conditions under the main crops in the test site during the campaign. Figure 2 shows the locations of the sample points. Most of the sampling points are situated in plain areas except for sample points (ESU) 102-1 (SB) and 222-2 (M) which are located in local sinks or in small drainage channels.

2.2 In-field measurements

2.2.1 Roughness characterization

For measuring soil surface roughness a photogrammetric approach was chosen due to its 3 dimensional output and highly accurate estimates. A further advantage for choosing a photogrammetric approach is its efficiency with regard to a decoupled acquisition and analysis compared to similar accurate acquisition setups such as laser devices (Rieke-Zapp and Nearing, 2005). To collect samples over a wide range of roughness states, soil surface roughness measurements were performed on 18 sample points (Fig. 2). Roughness conditions ranged from smooth and crusted surfaces to ploughed

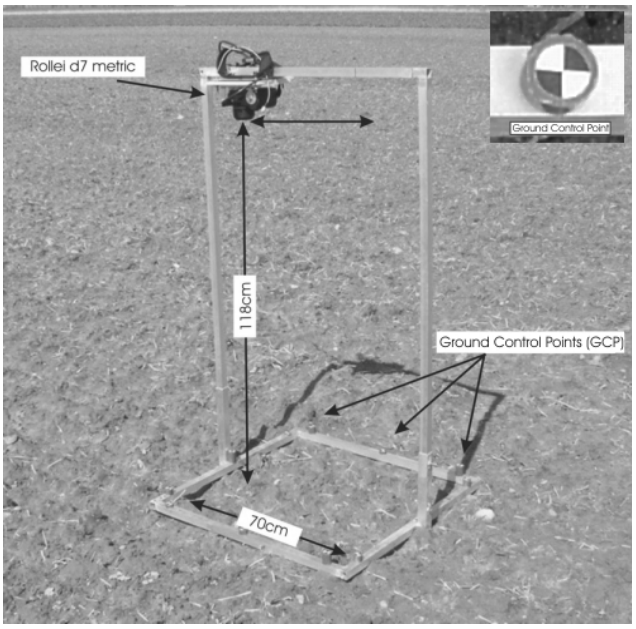

Fig. 3. Camera system for photogrammetric image acquisition (setup and signalized control point).

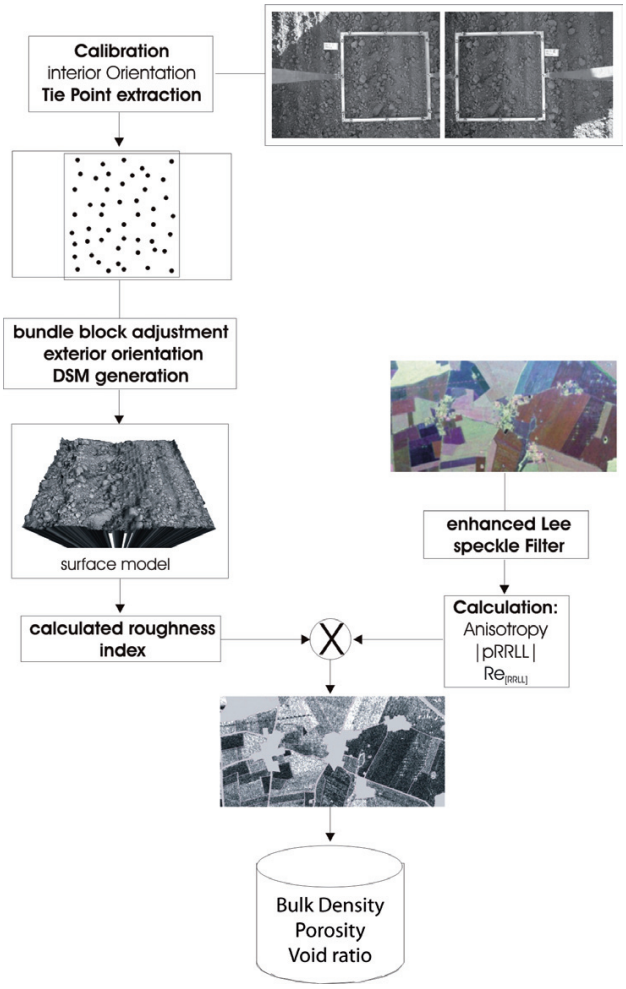

Fig. 4. Scheme of the roughness retrieval approach.

and harrowed fields. For sampling surface roughness on vegetated fields, plants were carefully cut off at the surface and completely removed from the areas covered by photogrammetric image acquisitions, without disturbing the soil surface.

For image acquisition, a Rollei d7 metric camera with known interior orientation was mounted on a tripod approximately 118 cm above the soil surface. The self-developed aluminum tripod (Fig. 3) accommodates 12 ground control points (GCP) whose three dimensional (xyz) coordinates were manually determined, as described by Lascelles et al. (2002), using a caliper rule with an accuracy of 1/10 mm. The horizontal coverage of the sampling area is limited to $70 \times 70\,cm^2$ (approx. $0.5\,m^2$). The camera and tripod setup allows an image acquisition from 1180 mm above ground with a baseline of 480 mm resulting in a height-to-base ratio of 2.5 and an image overlap of approximately 65%, which is appropriate for roughness measurements (Rieke-Zapp and Nearing, 2005; Linder, 2006). Thus, the image block consists of two images at which the acquired images have a spatial resolution of 0.54 mm.

Digital Surface Models (DSM) were generated using Leica Photogrammetry Suite (LPS 9.0). Exterior orientation of the two images was established using the highly accurate GCPs and bundle block adjustment techniques. Therefore, additionally to the 12 known GCPs, tie-points were derived and their three dimensional coordinates were calculated respectively. Best results in bundle block adjustment were achieved by using an additional 12-parameter model (Ebner, 1976). For DSM generation, LPS uses image matching strategies which work in epipolar lines (LPS, 2006). For different roughness states, adjusted matching strategies have been developed, which only vary in the x direction and deliver a good fit to the known GCPs and the highly accurate tie-points. The minimum correlation coefficient for the matching process, calculated from a 11x11 kernel between the two images, was set to 0.65, which is sufficient for epipolar line based matching algorithms (Stojic et al., 1998, Linder, 2006). In a final step, the generated DSMs were interpolated to a regular grid with a nominal resolution of 2 mm. A low-pass filter using a 7×7 kernel was applied to remove outliers.

In order to quantify soil surface roughness as a function of soil geometrical properties, roughness indices can be calculated from the derived DSM using different statistical approaches. Allmaras et. al (1966) and Currence and Lovely (1970) propose different calculation procedures based on the standard deviation of height values with additional terms to remove general slope effects. Due to the tripod geometrics perpendicular to the surface, a superimposition of general

slope effects can be excluded. Thus the calculation of the RMS Height can be simplified to:

$$s = \sqrt{\frac{\sum_{i=1}^{n} (Z_i - \bar{Z})^2}{1-n}} \quad (1)$$

Where s is the RMS Height in (cm) and Z is the height value in (cm).

Some authors (Currence and Lovely, 1970; Römkens and Wang, 1986; Linden and Van Doren, 1986; Sommer, 1997) have criticized these roughness indices for not maintaining the spatial distribution of height measurements for physical interpretation. Still, the RMS Height is the common and generally preferred index to describe soil surface roughness conditions in radar remote sensing and is therefore applied in this study (Oh et al., 1992; Hajnsek et al., 2003; Loew et al., 2006).

In addition, to quantify the non isotropic behavior of the sampled surface, the RMS Height parallel and perpendicular to the tillage direction was calculated separately. The mean RMS Height parallel to the tillage direction is then defined as:

$$\bar{s}_{x(y)} = \frac{\sum_{j=1}^{m} \sqrt{\frac{\sum_{i=1}^{n} (Z_{i(y)} - \bar{Z}_y)^2}{1-n}}}{m} \quad (2)$$

While the average RMS Height perpendicular to the tillage direction is defined as:

$$\bar{s}_{y(x)} = \frac{\sum_{j=1}^{m} \sqrt{\frac{\sum_{i=1}^{n} (Z_{i(x)} - \bar{Z}_x)^2}{1-n}}}{m} \quad (3)$$

As a consequence, the ratio $\bar{s}_{x(y)} / \bar{s}_{y(x)}$ is a measure for the directionality of the surface roughness, where for a value of 1 the surface is an absolute isotropic scatter.

As roughness is a function of wavelength, its appearance changes with different wavelengths. Using lower frequencies, the illuminated targed appears much smoother than at higher frequencies. To compensate this effect, the RMS Height has to be scaled to the actual wavelength using the wavenumber k within the following equation:

$$ks = s \times k = s \times \frac{2\pi}{\lambda} \quad (4)$$

Where ks is the RMS Height normalized to the wavenumber k and λ the wavelength (at the used L-band 23,054 cm).

As demonstrated by different authors (Davidson et al., 2000; Verhoest et al., 2007, 2008) roughness parameters often change with the length of profile over which they are estimated. Davidson et al. (2000) observed an increase in the RMS Height with an increasing profile length (1 and 10 m) in range of 0.5 cm for rolled fields, 0.6 cm for harrowed and 1.2 cm for ploughed fields. While those investigations are mainly focused on roughness data obtained by profile lasers or mesh boards, the effect of larger sample coverage on the RMS Height using 3d information is subject to only few studies. In their extensive work, Taconet and Ciarletti (2007) investigated the accuracy of different roughness estimators with changing sampling coverage. From an initial DSM with 0.77 m width and 2.95 m length they calculated different sub DSMs ranging from 0.4 m to 2.95 m length and a width of 0.77 m and compared those estimated roughness values with the true estimates. Within this study, the acquired sampling area results in an accuracy of 90% for representing the true roughness conditions for ploughed fields and 92.5% accuracy for seedbed structures (Taconet and Ciarletti 2007).

2.2.2 Soil and vegetation parameters

In addition to those above mentioned roughness measurements, a broad variety of focussed in-situ measurements was carried out simultaneous to E-SAR flights. The main sampling routine included soil physical characteristics (soil moisture, roughness, bulk density) as well as vegetation parameters (wet/dry biomass, vegetation cover, plant height, LAI, shoots per m^2).

After photogrammetric image acquisition, soil samples were taken for moisture, bulk density and texture analysis. Soil moisture content was measured gravimetrically (oven drying at 105°C) using 100 cm^2 Kopecky rings, at depth of 0–5 cm and 5–10 cm, with three repetitions each. From the known volume of the Kopecky rings volumetric soil moisture (Vol. %) as well as bulk density (g/cm^3) was calculated subsequently.

2.3 Radar acquisitions and processing

A total of 11 E-SAR flights were carried out on a weekly basis, recording imagery in X-, C-, and L-band with an incidence angle ranging from 25° to 55°. The raw radar data was preprocessed radiometrically and geometrically at DLR-HR. The L-band radar data showed good quality with an absolute error of -2 dB and a phase accuracy of 2° (Scheiber et al., 2007).

Geocoded Single Look Complex (SLC) L-band data with a spatial resolution of 2×2 m^2 was chosen to retrieve roughness information. As shown by Thiel et al. (2001) it is feasible to use geocoded SLC E-SAR L-band data to perform polarimetric image analysis. Prior to further image analysis, the radar imagery was speckle filtered by applying a 7×7 window enhanced LEE-Filter (Lee et al., 1992), which corresponds to approximately 34 looks.

Cloude and Pottier (1996) developed a very useful decomposition theorem which is based on the eigenvalue and eigenvector decomposition of the coherency matrix [**T**]. On base of the diagonalization of the [**T**] matrix, three important

physical parameters arise. The first two parameters are derived from the eigenvalues $\lambda_1-\lambda_3$ and are namely the Entropy H and the Anisotropy A and give an overview about the amount of different scattering mechanisms within a resolution cell (Hellmann et al., 1999). The third parameter, the polarimetric alpha angle α, is derived from the eigenvectors of the coherency matrix [**T**], were each eigenvector $\boldsymbol{e_i}$ can be expressed in terms of five angles as shown in (5) (Cloude and Pottier 1997).

$$\boldsymbol{e_i} = \begin{bmatrix} \cos\alpha_i \exp(i\phi_{1i}) \\ \sin\alpha_i \cos\beta_i \exp(i\phi_{2i}) \\ \sin\alpha_i \sin\beta_i \exp(i\phi_{3i}) \end{bmatrix} \tag{5}$$

The β_i angles can be interpreted as the orientation angle containing information of the rotation of the eigenvector $\boldsymbol{e_i}$ in the plane perpendicular to the scattering plane, while ϕ_{ji} giving information about the phase relations between the elements of $\boldsymbol{e}_i$. To obtain information about the mean scattering angle α Eq. (5) has to be transposed and the mean α angle can by calculated using the probabilities p_i (Cloude and Pottier, 1996):

$$\alpha = p_1\alpha_1 + p_2\alpha_2 + p_3\alpha_3 \rightarrow p_1 + p_2 + p_3 = 1 \tag{6}$$

The polarimetric alpha angle ranges from 0° to 90°. It can be used to represent and differentiate between a wide variety of scatter mechanisms (Cloude and Pottier, 1996, 1997). An alpha angle of α=0° can be interpreted as surface scattering. With an increase in α the surface becomes anisotropic due to the presence of small plants or non isotropic tillage patterns. At an alpha angle of α=45° the illuminated target acts like a dipole where either the *HH* or *VV* backscatter is zero. With a further increase of α the surface is characterized by an anisotropic dihedral scattering where the $HH \neq VV$ and the phase difference is 180°. At its maximum of α= 90°, one can obtain an isotropic double bounce scattering mechanism (Cloude and Pottier, 1997). As a consequence, the polarimetric alpha angle, jointly used with the Entropy, gives a first impression of the dominant scattering mechanisms (Cloude and Pottier, 1997; Hellmann et al., 1999).

Cloude (1999), Cloude and Lewis (2000) as well as Hajnsek et al. (2003) first introduced the Anisotropy as a potential roughness estimator, which is only dependent from the geometrical properties of a given surface and independent from its dielectric properties as well as the local incidence angle. The Anisotropy (A) is defined as:

$$A = \frac{\lambda_2 - \lambda_3}{\lambda_2 + \lambda_3} \tag{7}$$

It ranges from zero to one, where the eigenvalues of the coherency matrix [**T**] are $\lambda_1 \geq \lambda_2 \geq \lambda_3 \geq 0$.

As obvious from (7), the Anisotropy defines the relation between the second and third eigenvalues and is therefore a measure of the secondary scattering mechanisms. As a consequence the Anisotropy is a very noisy parameter due to the measurement of the weak third eigenvalue λ_3 close to the system noise floor (Schuler et al., 2002; Hajnsek et al., 2003).

For low Anisotropy values, two equally strong scattering processes are present, while a high Anisotropy indicates the presence of only one strong secondary scattering process with a negligible third scattering mechanism (Cloude and Pottier, 1997).

However, the deployment of the Anisotropy comprises some constraints which are related to its physical meaning. Under the presence of vegetation, the Anisotropy decreases, due to an increase in importance of the third eigenvalue, and results therefore in an overestimation of roughness (Hajnsek et al., 2003). As a consequence the Anisotropy is only applicable for surface scatter regions, e.g. bare soil areas or areas with sparse vegetation with one strong scattering mechanism (Cloude and Pottier, 1997; Cloude, 1999; Hajnsek et al., 2003). Another limitation is given by an insensitiveness of A for roughness values above ks=1 where A saturates and is therefore almost decorrelated (Hajnsek et al., 2003).

Dependent on the roughness conditions the Anisotropy A, can be inverted using two different linear approaches. For smooth areas Cloude and Lewis (2000) suggest:

$$ks = 1.25 - 2A \tag{8}$$

while for rougher surfaces Cloude (1999) recommends:

$$ks = 1 - A \tag{9}$$

As shown by Mattia et al. (1997), using PolSAR data over the Matera test site (Italy) and the Chickasha test site (USA), the magnitude of the complex circular coherence ($|\rho_{RRLL}|$) is sensitive to roughness and insensitive to dielectric properties, respectively soil moisture of the illuminated target. The magnitude of the complex circular right-right left-left coherence is defined as (Mattia et al., 1997):

$$|\rho_{RRLL}| = \frac{\left\langle \left| S_{RR} S_{LL}^{*} \right| \right\rangle}{\sqrt{\left\langle |S_{RR}|^2 \right\rangle \left\langle |S_{LL}|^2 \right\rangle}} \tag{10}$$

with S_{RR}=right-right handedness, S_{LL}=left-left handedness of the rotation of the electric field vector about the line of sight. By definition $|\rho_{RRLL}|$ ranges similar as the Anisotropy from zero to one. In their investigations, Mattia et al. (1997) proved a nearly linear increase of $|\rho_{RRLL}|$ with a decrease in roughness. For rough fields, they measured values of $|\rho_{RRLL}|$ in a range of 0.2 to 0.05 while smooth fields showed values of $|\rho_{RRLL}|$ in a range of 0.6 to 0.5.

In further investigations Schuler et al. (2002) approved this sensitivity of $|\rho_{RRLL}|$ but established a stronger relationship between the soil surface roughness and the real part of the circular coherence ($Re_{[\rho RRLL]}$) for a wide range of natural soil surfaces and different frequencies. The real part of the circular coherence is defined as (Schuler et al., 2002):

$$Re_{[\rho RRLL]} = \left[\frac{\left\langle |S_{HH} - S_{VV}|^2 \right\rangle - 4\left\langle |S_{HV}|^2 \right\rangle}{\left\langle |S_{HH} - S_{VV}|^2 \right\rangle + 4\left\langle |S_{HV}|^2 \right\rangle} \right] \tag{11}$$

The advantage of using only the real part of the circular coherence as compared to the complex coherence is due to the fact that the imaginary part is very sensitive to unsymmetrical scattering contributions caused by vegetation (Schuler et al. 2002). Its insensitivity to the dielectric constant has further been proven in several investigations (Schuler et al. 2002, Thiel 2003). However for an azimuthal symmetric surface both estimators are the same, e.g. $|\rho_{RRLL}|$ is real and equals therefore $Re_{[\rho RRLL]}$. Using $Re_{[\rho RRLL]}$ rather than $|\rho_{RRLL}|$ has both advantages and disadvantages. When azimuth terrain slopes are present, the magnitude of $Re_{[\rho RRLL]}$ is reduced and therefore $Re_{[\rho RRLL]}$ is sensitive to large scale azimuthal slopes (Schuler et al., 2002). However these effects are correctable by using an external digital elevation model (DEM) (Lee et al., 2000). For this investigation an already terrain corrected SAR product (GTC) is utilized, therefore a further correction of large scale azimuth slopes is not required.

In their investigations Schuler et al. (2002) carried out an extensive comparison of $|\rho_{RRLL}|$ and A. They concluded that both soil surface roughness estimators are in general not the same, however in present of azimuth symmetric scatter the estimators lead to the same results. This condition of azimuthal symmetry is true for some natural scenes and can be illustrated as follows. For the special case of azimuth symmetric scatter the coherency matrix [**T**] is diagonal and the eigenvalues can be expressed as (Hajnsek 2001):

$$\begin{aligned}\lambda_1 &= \left\langle |S_{HH} + S_{VV}|^2 \right\rangle \\ \lambda_2 &= \left\langle |S_{HH} - S_{VV}|^2 \right\rangle \\ \lambda_3 &= 4\left\langle |S_{HV}|^2 \right\rangle\end{aligned} \tag{12}$$

The fact that A and $|\rho_{RRLL}|$ are the same for this case can be easily observed by incorporating (12) in (7) which is than equivalent to (11).

Indeed, for ks <0.5, $Re_{[\rho RRLL]}$ is more sensitive to roughness than A which is related to the noisy third eigenvalue, especially for those smooth areas with low backscatter close to the system noise floor (Schuler et al., 2002). As a consequence, for smooth areas and/or areas covered with vegetation, $Re_{[\rho RRLL]}$ is the preferable roughness estimator.

For the spatial derivation of micro-scale soil surface roughness, the Anisotropy, $|\rho_{RRLL}|$ and $Re_{[\rho RRLL]}$ were calculated by applying a 5×5 boxcar filter on the despeckled L-band single look complex data.

3 Results

3.1 In-field roughness measurements

As described in Sect. 2.2.1, in-field micro-scale soil surface roughness was obtained from micro-DSMs, determined by photogrammetric image analysis. As can be seen from Fig. 5 it is possible to easily distinguish between different soil clods and even between small aggregates. The bundle block adjustment revealed a sub millimeter precision for the object coordinates. Triangulation resulted in a precision z=0.8 mm in the vertical direction and xy=0.37 mm in the horizontal direction related to the manually measured GCPs. The deployed matching strategies lead to a successful matching rate (pixels showing a correlation >0.65) of approximately 72% of all possible matches in all stereo pairs. Mismatches mostly appear in areas where three main factors occur: low image contrast, soil clod obstruction in both images and strong height difference between adjacent pixels. In regions where these factors are valid, the matching algorithm fails or leads to low correlation coefficients (see Fig. 5). However, the aim of the presented study was to develop an easy-to-apply standard procedure which allows for a rapid image acquisition near time the radar data recordings. Nevertheless, the derived DSMs showed good agreement with the highly accurate reference points with a mean absolute error of 1.2 mm and a RMSE of 1.6 mm in vertical direction. Compared to literature, these accuracies are sufficiently high (Rieke-Zapp and Nearing, 2005; Wegmann et al., 2001; Warner, 1995; Taconet and Ciarletti, 2007).

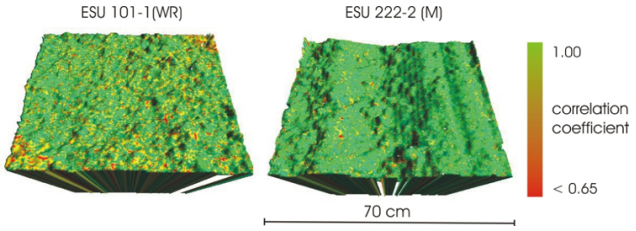

Fig. 5. Correlation coefficients of the matching process for two different sample points (101-1/222-2) and roughness states.

From the obtained micro-DSM, the RMS Heights are calculated for each sample point and date using Eqs. (1)–(3). Table 1 summarizes the main statistics of the calculated in-field RMS Heights for each field separately, while Figs. 6–9 give an overview of the obtained roughness values for each field and campaign date separately. As can be seen from Fig. 6 and Table 1, the highest values for s occur on the maize field 222, while the fields under winter resistant vegetation (101, 250 and 440) are much smoother with $s \approx$1 cm. To assess the directionality of the in-field roughness, $\bar{s}_{x(y)}/\bar{s}_{y(x)}$is calculated and the results are displayed in Fig. 9. As can be seen most sample points are dominated by an anisotropic roughness pattern with a direction perpendicular to the tillage pattern.

As roughness changes with its length/area over which it is estimated (see Sect. 2.2.1), we assessed its under- or overestimation by calculating for each DSM different sub-DSMs for both directions. Therefore we reduced subsequently each DSM by 0.2 mm in the x direction (respectively y direction) and calculated for each reduced DSM the RMS Heights parallel ($\bar{s}_{x(y)}$) and perpendicular ($\bar{s}_{y(x)}$) to the tillage direction.

Table 1. Mean statistical characteristics of RMS Height measurements.

	101 (WR)	102 (SB)	222 (M)	250 (WW)	440 (WB)	460 (SB)
s	0.84	1.07	1.74	0.9	0.9	1.29
s STD	0.14	0.25	0.57	0.13	0.1	0.38
s_x	0.61	0.56	0.77	0.52	0.53	0.65
s_x STD	0.14	0.25	0.36	0.24	0.23	0.28
s_y	0.72	0.81	1.45	0.72	0.71	1.04
s_y STD	0.19	0.42	0.69	0.33	0.31	0.52

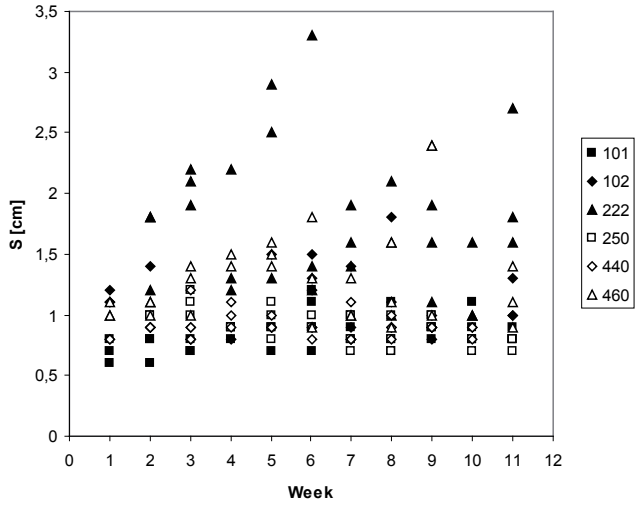

Fig. 6. RMS Height variability for each sample point and campaign date.

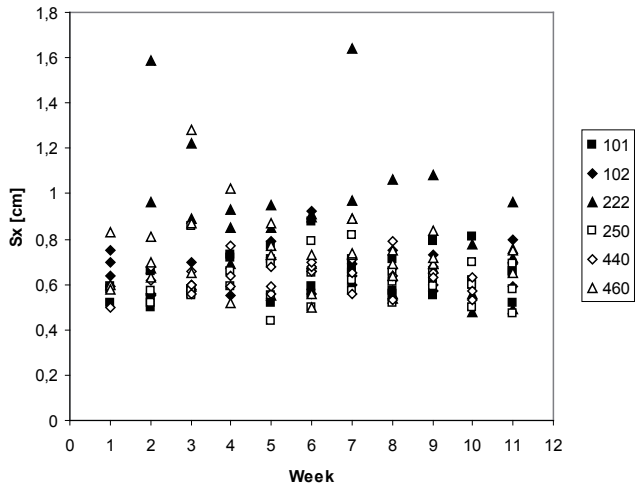

Fig. 7. RMS Height variability parallel to the tillage direction for each sample point and campaign date.

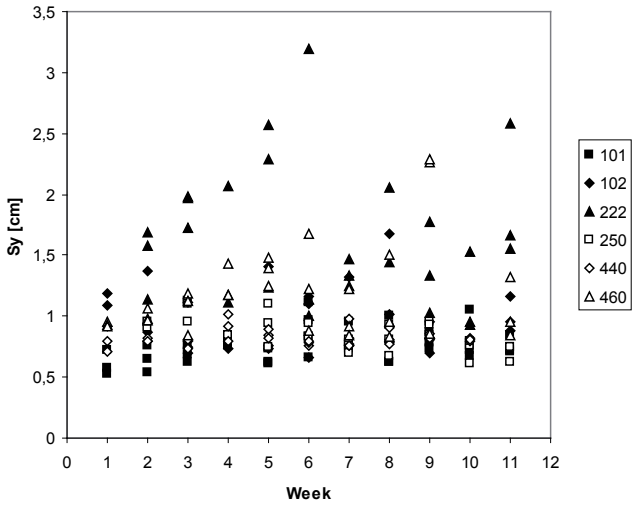

Fig. 8. RMS Height variability perpendicular to the tillage direction for each sample point and campaign date.

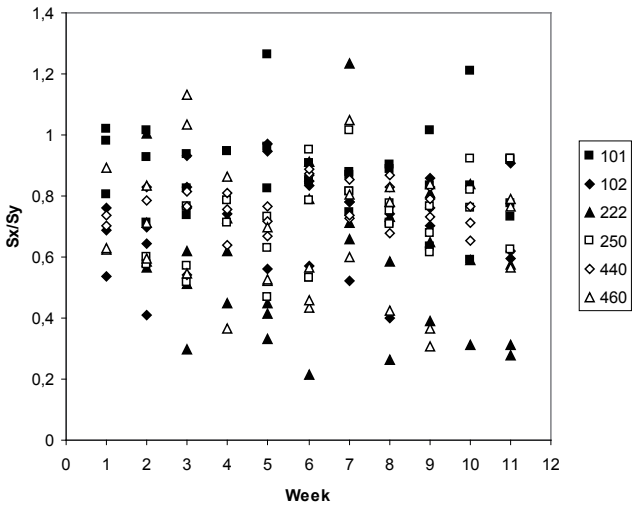

Fig. 9. Variability of the $\bar{s}_{x(y)} / \bar{s}_{y(x)}$ ratio showing directional effects in roughness for each sample point and campaign date.

Results of three representative DSMs (smooth, medium and rough) are given in Fig. 10. It is obvious, that the size of the proper DSM is dependent from the direction of the tillage pattern. As the RMS Height perpendicular to the tillage direction saturates almost after 15–20 cm, the RMS Height parallel to the tillage pattern shows no saturation effects and is nearly random over the acquired area, meaning that the chosen sampling area is to small to represent the roughness in parallel to the tillage direction. However, this needs to be further investigated in future.

3.2 Derivation of soil surface roughness on the field scale

Figure 11 shows the comparison of the calculated potential roughness estimators, based on Eqs. (7), (10) and (11), for 19 April 2006. As theory predicts, the Anisotropy A appears much noisier than $|\rho_{RRLL}|$ and $Re_{[\rho RRLL]}$, due to its calculation from the second and third eigenvalues (see Eq. 7) (Cloude, 1999; Hajnsek, 2001; Schuler et al., 2002). The $Re_{[\rho RRLL]}$ reveals the highest level of detail and does not appear as noisy as the others.

Schuler et al. (2002) and Mattia et al. (1997) showed in their investigations that the polarimetric coherence decreases with an increase in surface roughness. Thus, smooth areas with large enough backscatter intensities appear in bright colours in $|\rho_{RRLL}|$ images (see Fig. 11, middle). Contrary to $|\rho_{RRLL}|$, the images of $Re_{[\rho RRLL]}$ appear different: the values for $Re_{[\rho RRLL]}$ increases with an increase of surface roughness (Thiel, 2003). Note that in contrast to A and $|\rho_{RRLL}|$ values of $Re_{[\rho RRLL]}$ are in the range of -1 to +1. Following the approches of Cloude (1999) as well as Cloude and Lewis (2000), high values for the Anisotropy Aindicate smooth areas while lower Anisotropy regions show rougher areas. As taken from Fig. 11 all three estimators allow to distinguish between different roughness states within and between several fields.

For the derivation of soil surface roughness on field scale, correlation coefficients have been calculated for each field and each campaign date between the RMS Heights and the calculated radar parameters (Figs. 12–13). As can be seen from Fig. 12, the correlation coefficients for all fields over the whole campaign are quit low with a maximum for the Anisotropy on field 102 with r=0.44. Note the positive sign of the correlation for the whole fields (except field 250) and A, which indicates a proportional relationship and is contrary to the proposed inversion schemes by Cloude (1999) as well as Cloude and Lewis (2000). For $|\rho_{RRLL}|$ the mean correlation coefficient is r=0,2 which indicates a weak positive relationship, which is similar to A. Indeed, the theoretical description by Mattia et al. (1997) as well as the investigation of Schuler et al. (2002) showed a negative relationship, meaning that high coherence values indicate a smooth surface. For the real part of the complex circular coherence $Re_{[\rho RRLL]}$ no consistent correlation for the different fields can be observed. Even for the two sugar beet fields (102 and 460) opposite

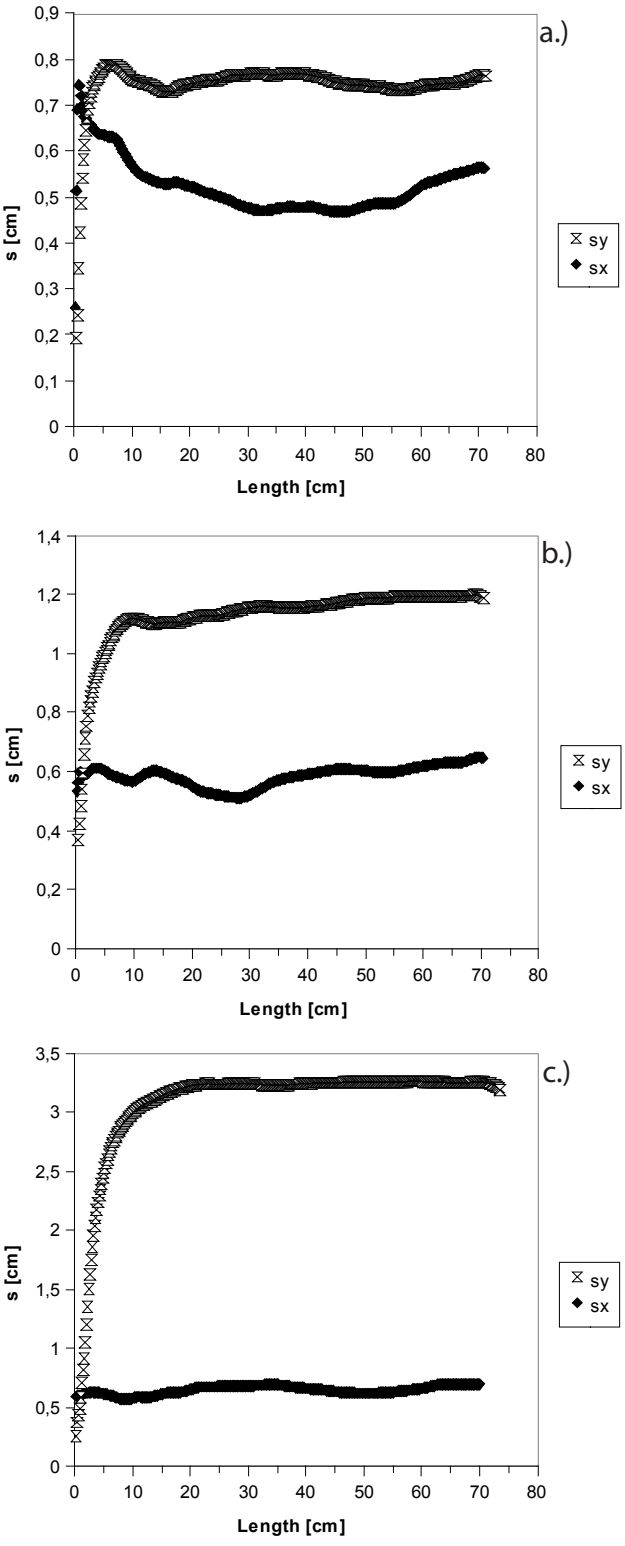

Fig. 10. Variation of RMS Heights in dependency from the size of the sampling area. **(a)** smooth DSM with s=0.6 cm, **(b)** medium DSM with s=1.3 cm and **(c)** rough DSM with s=3.3 cm.

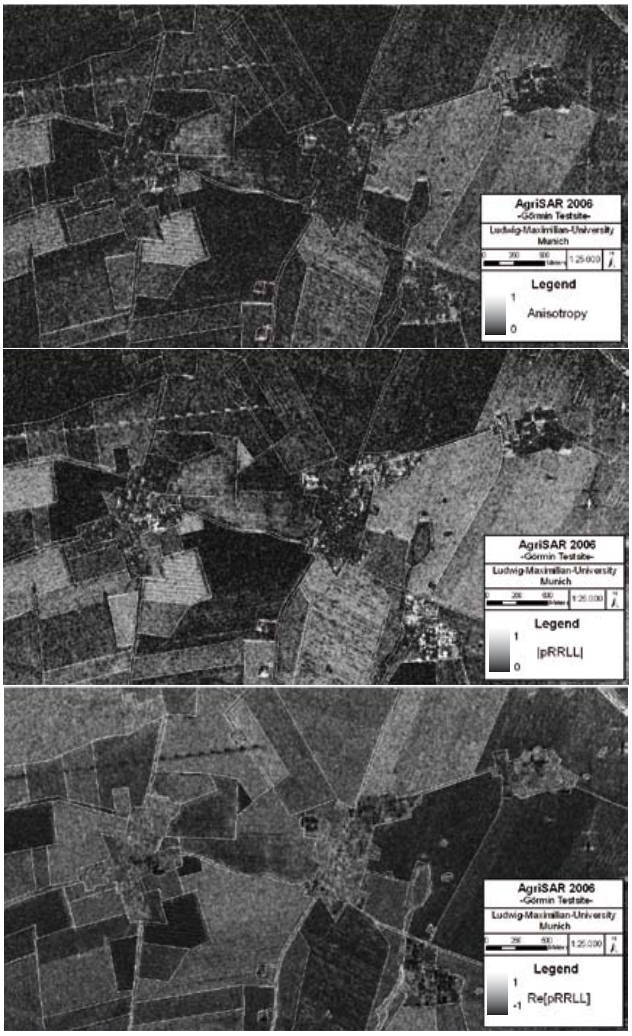

Fig. 11. Calculated roughness estimators (Anisotropy, Circular Coherence and Real Part of the Circular Coherence) for 19 April 2006.

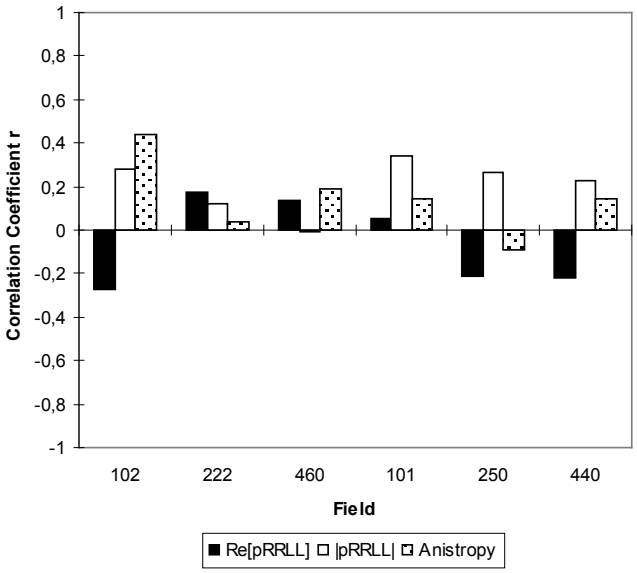

Fig. 12. Correlation coefficients *r* between *ks* and polarimetric roughness estimators for each field and whole campaign.

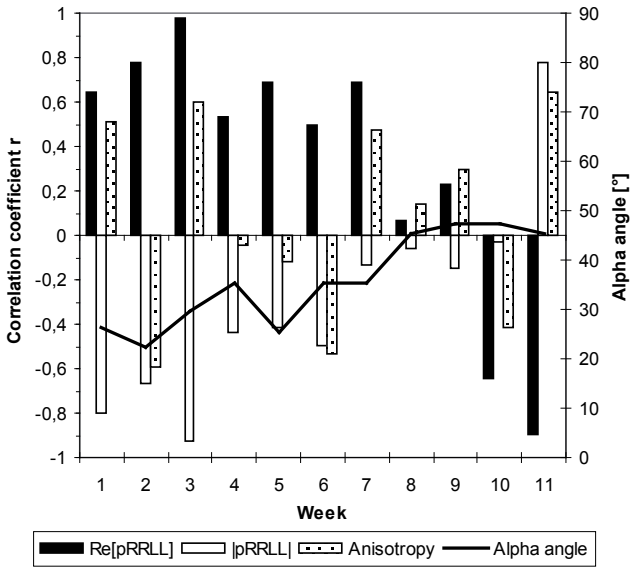

Fig. 13. Correlation coefficients *r* between *ks* and polarimetric roughness estimators and mean polarimetric alpha angle for the summer vegetation field at each campaign.

signs are given for the correlation coefficients. This could be related to the presence of vegetation which cause an overestimation of *ks* and superimposes therefore the good correlation coefficients between *ks* and the radar parameters on bare soil fields (see Fig. 15). As investigations of Thiel (2003) have shown, there is in general a positive proportional relationship between *ks* and $Re_{[\rho RRLL]}$ which is also observable within Fig. 10.

To study the effect of vegetation on the roughness retrieval we calculated for the bare soil fields (102, 222 and 460) for each campaign date the mean correlation coefficient which are shown in Fig. 13. While $Re_{[\rho RRLL]}$ and $|\rho_{RRLL}|$ show a very similar trend over the whole campaign, the Anisotropy *A* changes its sign nearly random, which led us to conclude that it is not suitable for roughness retrieval. Indeed, especially for the first three campaign dates, a strong correlation between $Re_{[\rho RRLL]}$, $|\rho_{RRLL}|$ and *ks* in range of r=0.65 to r=0.97 can be observed. As theory reveals, for an azimuthal symmetric surface both estimators are the same and yield in the same values for r. The small discrepancies can be explained due to the non isotropic behaviour of the fields (Fig. 9) which reduces the similarity of both estimators (Schuler et al., 2002). However, with development of vegetation the correlation between both estimators and *ks* is reduced showing its minimum at the eighth campaign date and then increases with an opposite sign for both estimators revealing the effect of vegetation on the derivation.

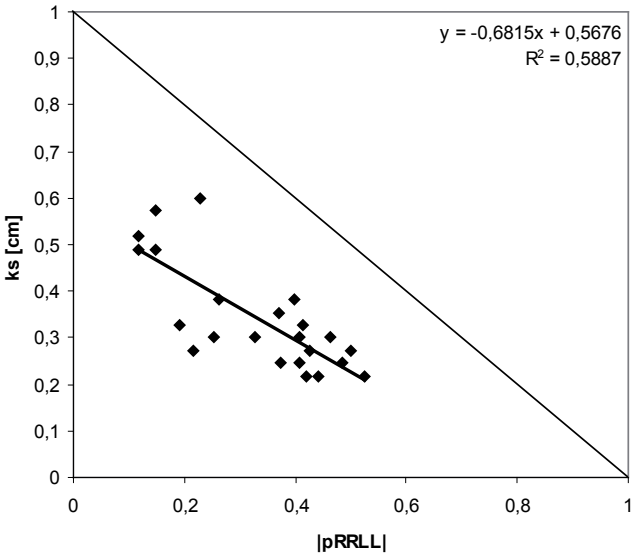

Fig. 14. Scatterplot for *ks* and $|\rho_{RRLL}|$ for areas $\alpha<40°$ at the first three campaign dates.

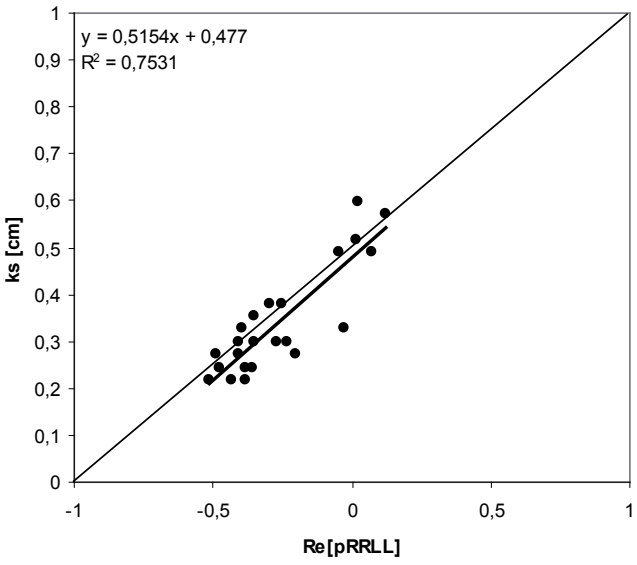

Fig. 15. Scatterplot for *ks* and $Re_{[\rho RRLL]}$ for areas $\alpha<40°$ at the first three campaign dates.

To define a threshold to which a derivation is suitable, we tested several vegetation dependent indices. As argued by Hajnsek (2001) the *HV*/*VV*-ratio <0.07 (−11 dB) is a good measure for the separation of vegetated and bare soil surfaces. However, we could not confirm this threshold (data not shown). As a measure of the different scattering mechanisms, the polarimetric alpha angle is a good indicator of the different phenological stages. Therefore we plotted the α angle against the correlation coefficients as displayed in Fig. 13. As can be seen with an increase in α, a decrease of r for $Re_{[\rho RRLL]}$, $|\rho_{RRLL}|$ and *ks* can be observed until its sign changes. An appropriate threshold seems to be an α angle <40°, which is related to the surface scatter criterion proposed by Cloude and Pottier (1997), however it is not that strict and even allows high roughness values with an high Entropy to be included in the derivation.

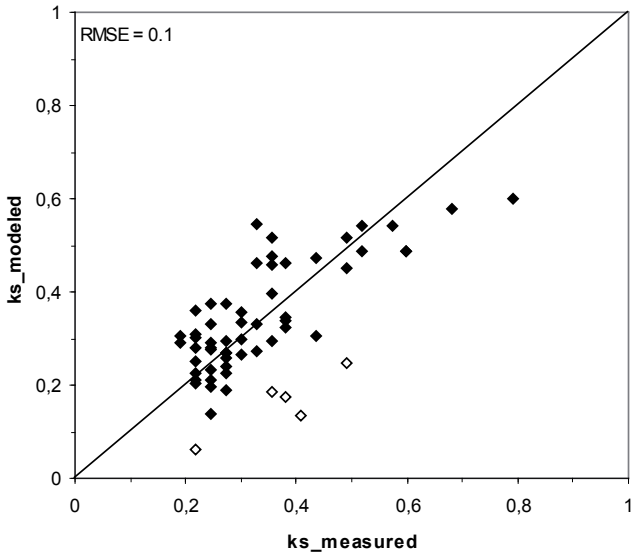

Fig. 16. Modeled versus measured *ks* values for all sample plots with $\alpha<40°$. Hollow rhombuses indicate sample points with strong directional effects.

3.3 Multi temporal roughness derivation

To develop an inversion scheme, we defined for the first three campaign dates an empirical relationship masking out all the values with $\alpha>40°$, which allows us to calculate a regression based on bare soil conditions under a wide variety of roughness values. Scatterplots for both, the $Re_{[\rho RRLL]}$ and $|\rho_{RRLL}|$ show a strong correlation to *ks* and are displayed in Figs. 14 and 15. However the correlation coefficient between *ks* and $Re_{[\rho RRLL]}$ is quite high and outperforms $|\rho_{RRLL}|$. Based on this correlation, we defined a linear inversion scheme which allows us to invert *ks* from $Re_{[\rho RRLL]}$:

$$ks = 0.5154 \times Re_{[\rho RRLL]} + 0.477 \quad (13)$$

Using this relationship, we derived *ks* from $Re_{[\rho RRLL]}$ for each campaign date on the remaining valid areas. A RMSE of 0.1 indicates a very accurate inversion model. Figure 16 shows a scatterplot for the modeled and measured *ks* values. High *ks* values are slightly underestimated while several other roughness values (in Fig. 16 indicated by hollow rhombuses) are also underestimated. However, these measured *ks* values show a significant directional behavior leading to an overestimation of the in-field *ks* values, as can be obtained from Fig. 9.

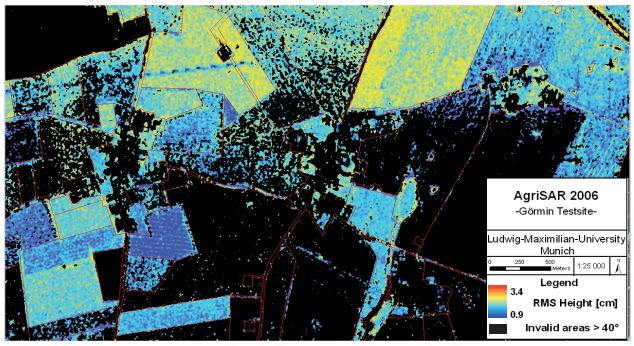

Fig. 17. Spatial distribution of s. Invalid areas with $\alpha > 40°$ are masked out black.

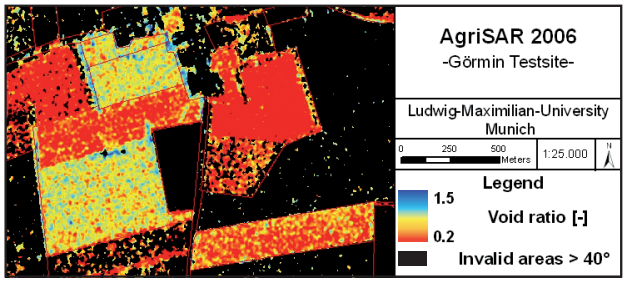

Fig. 18. Spatial derived void ratio for 19 April on both sugar beet fields(102+460). Invalid areas with an alpha angle $\alpha > 40°$ are masked out black.

Finally, Fig. 17 shows the spatially derived values for s, were invalid areas with $\alpha > 40°$ (settlements, forests, vital vegetated areas) are masked out for April 19, 2006. As can be seen, the southern part of field 460 (sugar beet) appears much rougher as the northern part, which is due to ongoing agricultural practice during the first campaign date. While in the southern part the seed bed was already prepared, the northern part is still showing a crusted surface from the bare winter period.

4 Potentials for hydrological model application – retrieval of soil bulk density parameters

This section discusses the potentials and limitations of the proposed roughness retrieval for direct use in hydrological models. As soil surface roughness play a crucial role in physically based soil erosion models, the assimilation of the derived roughness values into such models is considered beneficial to better describe the processes involved. However due to the lack of precipitation a soil erosion assessment is not reasonable. Results of a feasibility study on the use of roughness information in physically based hydro-ecological modeling will be presented.

In addition to soil texture (grain size), bulk density and derived variables such as porosity and void ratio are key parameters in hydrological modeling. Most widely used pedo-transfer-functions (PTF) for the calculation of hydro-ecological properties such as (un-)saturated conductivity are based on these parameters (Cosby et al., 1984; Rawls and Brakensiek, 1985; Woesten et al., 1999; Sobieraj et al., 2001). Further, porosity as well as void ratio are important indicators for the detection of mechanically compacted soils in agricultural environments. Typically, bulk density can be determined using Kopecky rings with known volume, while soil porosity is mostly measured using an air pycnometer (Schlichting et al., 1998; Sun et al., 2006). Alternatively, soil porosity (n) as well as void ratio (ε) can be calculated from bulk density measurements using the following equations (Hartge and Horn, 1999):

$$n = 1 - \frac{\rho_s}{\rho_F} \tag{14}$$

$$\varepsilon = \frac{n}{1-n} \tag{15}$$

Where n denotes soil porosity in (%); ρ_s is the bulk density of the given soil (g/cm^3) and ρ_F is the bulk density of the solid particles, where for quartzous soils $\rho_F \approx 2.65$ g/cm^3.

However, there are some drawbacks in using these classical methods. First, destructive measurements using Kopecky rings or the air pycnometer do not allow for a multi temporal analysis. Secondly, they are limited to a small area (plot scale) and therefore time-, labor- and cost-consuming for field scale assessments.

Sun et al. (2006) introduced the potential of using roughness information, derived from a 3d laser device, to obtain soil porosity. Using a linear fit, they predicted porosity from RMS Heights for different roughness conditions of a silty loam soil. The hypothesis is based on the assumption that changing roughness due to tillage practice or precipitation alters only volume but not mass of the soil column (Hartge and Horn 1999) and thus introduces a change in soil porosity.

To verify the approach suggested by Sun et al. (2006), correlation coefficients between the in-field roughness measurements and the bulk parameters calculated from Eqs. (14) and (15) are determined. To avoid any influence from vegetation, only bare fields were considered. Table 2 summarizes

Table 2. Statistical characteristics for bulk density parameters.

	ρ_s	n [%]	ε [–]
Mean	1.43	45	0.89
Min	1.01	36	0.56
Max	1.69	62	1.6
STD	0.11	4.2	0.15

Table 3. Correlation between s and soil bulk density parameters (R^2=coefficient of determination, r=correlation coefficient, m=slope, b=axis intercept).

Parameter	R^2	r	m	b
ρ_s	0.55	−0.74	−0.32	1.90
n	0.55	0.74	12.14	28.28
ε	0.60	0.78	0.49	0.16

the statistics of measured bulk density values while Table 3 summarizes the results from this analysis.

A good relationship between the indicated parameters can be noted, while the void ratio in the uppermost layer is correlated stronger to s than the bulk density and porosity (see Table 3). This is in good agreement with the results of Sun et al. (2006).

Applying a linear fit, we derived the spatial void ration for 19 April, for the bare soil field 102 and 460, as shown in Fig. 18. A first visual qualitative interpretation of the results indicates a well working algorithm. The still crusted surface on field 102 as well as the crusted northern part of field 460 show a very low void ratio while the already seed bed prepared southern part of field 460 shows significantly higher values. Result in form of an RMSE=0.17 g/cm^3 indicate promising results, however there is still some potential for an enhanced bulk density parameter retrieval that has to be investigated with a larger amount of data in future studies.

5 Summary and conclusions

This study presents an approach for the spatial derivation of soil surface roughness using photogrammetry and radar remote sensing. Therefore several polarimetric roughness estimators have been correlated to a wide range of *ks* values, showing that the real part of the complex circular coherence is outperforming all the other estimators. However, as theory reveals, for azimuth symmetric bare soil surfaces $Re_{[\rho RRLL]}$ and $|\rho_{RRLL}|$ are the same, while for asymmetric surfaces, due to a directional behaviour of the surface, differences in both occur. In presence of vegetation, the retrieval algorithm leads to an overestimation of roughness and is therefore not suitable for an operational use. However, using the polarimetric alpha angle (Cloude and Pottier, 1996) for masking out areas with $\alpha > 40°$ seems to be a suitable threshold for a robust roughness retrieval of various roughness conditions even under (short or dry/ripe) vegetation leading to a RMSE=0.1. However for high *ks* values ($ks \geq 0.8$) an underestimation using the developed inversion scheme could be ascertained. In investigations of Hajnsek (2001) and Schuler et al. (2002), a random distribution of $Re_{[\rho RRLL]}$ and $|\rho_{RRLL}|$ for $ks > 1$ is reported, which is in good accordance with our results.

It is shown that the deployed photogrammetric method allows a fast and adequate retrieval of roughness information. However, the role of the scale dependent calculations of s needs to be further investigated in future studies. Even if earlier papers from Taconet and Ciarletti (2007) proved a good representation of the roughness determination for the deployed horizontal coverage (0.5 m^2), uncertainties remain, which are especially given in parallel to the tillage direction were a larger sampling area is necessary. Future investigations, to assess this effect on roughness retrieval from SAR data, are mandatory.

However, our results indicate that spatially determined soil surface roughness from remote sensing can support the parameterization of spatially explicit hydrological models, in this case by providing distributed values of driving variables. It is shown in a first assessment that soil bulk parameters of the upper few centimetres of the soil column, such as bulk density, porosity and void ratio, can be discriminated from surface roughness. However, even though a dependency of these bulk parameters from roughness can be noted, the approach needs further research with regard to different uncertainties:

– The correlation between roughness parameters and bulk parameters is only strong for fresh harrowed fields. For small values of s$\leq$1 cm the bulk parameters are randomly distributed.

– Using the regionalization approach suggested in this study, error propagation will lead to large RMSE values. Therefore, a better roughness retrieval needs to be achieved.

Besides those constraints, the approach is very promising. For future investigations, an enhanced roughness retrieval has to comprise four major improvements:

– To enhance the in-field roughness retrieval, the image acquisition set up has to be improved by better illumination and to solve the appearance of obstructed areas more than two image pairs could remediate (Luhmann, 2003; Wiggenhagen and Raguse, 2003). To solve the problem of mismatches between adjacent pixels with strong height differences, a broad variety of appropriate matching strategies have to be developed to enhance the matching process.

– The effect of directionality on roughness retrieval needs to be investigated in more depth by comprising a larger amount of roughness in-situ measurements to achieve a better understanding of those effects.

– To reduce uncertainties in roughness measurements, due to too small sampling areas the horizontal coverage of future measurement systems has to be increased especially in the direction parallel to the tillage pattern.

– For a better separation of vegetation effects different decomposition theorems as well as the deployment of PolInSAR techniques will be necessary.

Acknowledgements. The authors would like to thank ESA for funding the AgriSAR 2006 campaign. Rieke-Zapp (University of Bern) is gratefully acknowledged for providing the Rollei d7 metric camera and for assistance and support during the photogrammetric processing.

Edited by: W. Wagner

References

Allmaras, R. R., Burwell, R. E., Larson, W. E., and Holt, R. F.: Total porosity and random roughness of the interrow zone as influenced by tillage, USDA Conservation Research Report, 7, 1966.

Bertuzzi, P., Rauws, G., and Courault, D.: Testing roughness indices to estimate soil surface roughness changes due to simulated rainfall, Soil Till. Res., 17, 87-99, 1990.

Cerdan, O., Souchère, V. Lecomtze, V. Couturier, A., and Le Bissonnais, Y.: Incorporating soil surface crusting processes in an expert-based runoff model: Sealing and Transfer by Runoff and Erosion related to Agricultural Management – STREAM. Catena Vol., 189–205, 2001.

Cloude, S. R.: Eigenvalue parameters for surface roughness studies. Proceedings of SPIE Conference on Polarization: Measurement, analysis and remote Sensing II, Denver, Colorado, USA, 1999.

Cloude, S. R. and Lewis, G. D.: Eigenvalue Analysis of Mueller Matrix for Bead Basted Aluminium Surfaces, SPIE Polarisation Analysis and Measurement III, Proc. SPIE, AM107, July–August 2000, 2000.

Cloude, S. R. and E. Pottier: A review of target decomposition theorems in radar polarimetry. IEEE T. Geosci. Remote Sens., 34, 498–518, 1996.

Cloude, S. R. and Pottier, E.: An entropy based classification scheme for land applications of polarimetric SAR. IEEE T. Geosci. Remote Sens. 35(1), 68–78, 1997.

Cosby, B. J., Hornberger, G. M., Clapp, R. B., and Ginn, T. R.: A statistical exploration of the relationships of soil moisture characteristics to the physical properties of soils, Water Resour. Res., 20, 682–690, 1984.

Currence, H. D. and Lovely, W. G.: The analysis of soil surface roughness, Trans. ASAE, 13, 710–714, 1970.

Darboux, F., Gascuel-Odoux, C. and Davy, P.: Effects of surface water storage by soil roughness on overland-flow generation, Earth Surf. Proc. Landforms, 27, 223–233, 2002.

Davidson, M. W. J., Le Toan, T., Mattia, F., Satalino, C., Manninen, T., and Borgeaud, M.: On the characterization of agricultural soil roughness for radar remote sensing studies, IEEE T. Geosci. Remote Sens., 38, 630–640, 2000.

Ebner, H.: Self calibrating block adjustment. Proceedings XIII Congress of the International Society of Photogrammetry, Helsinki, 1976.

Farres, P. J.: Some observations on the stability of soil aggregates to raindrop impact, Catena, 7, 223–231, 1980.

Fohrer, N., Berkenhagen, J., Hecker, J.-M., and Rudolph, A.: Changing soil and surface conditions during rainfall single rainstorms/ subsequent rainstorms, Catena, 37, 355–375, 1999.

Hajnsek, I.: Inversion of surface parameters from polarimetric SAR. PhD-Thesis Friedrich-Schiller-University Jena, Germany, 238 pp., 2001.

Hajnsek, I., Bianchi, R., Davidson, M., D'Urso, G., Gomez-Sanchez, J., Hausold, A., Horn, R., Howse, J., Loew, A., Lopez-Sanchez, J., Ludwig, R., Martinez-Lozano, J., Mattia, F., Miguel, E., Moreno, J., Pauwels, V., Ruhtz, T., Schmullius, C., Skriver, H., Sobrino, J., Timmermans, W., Wloczyk, C., and Wooding, M.: AgriSAR 2006 Airborne SAR and Optics Campaigns for an improved monitoring of agricultural processes and practices, European Geoscience Union (EGU), General Assembly, 15–20 April 2007, Vienna, Austria, 2007.

Hajnsek, I., Pottier, E., and Cloude, S. R.: Inversion of surface parameters from polarimetric SAR, IEEE T. Geosci. Remote Sens., 41, 727–744, 2003.

Hartge, K. H., and Horn, R.: Einführung in die Bodenphysik, 3. Aufl. Ferdinand Enke, Stuttgart, 304 pp., 1999.

Hellmann, M., Jager, G., Kratzschmar, E., and Habermeyer, M.: Classification of full polarimetric SAR-data using artificial neural networks and fuzzy algorithms, IEEE Proceedings IGARSS'99, Hamburg, 1995–1997, 1999.

Helming, K.: Die Bedeutung des Mikroreliefs für die Regentropfenerosion. Bodenökologie und Bodengenese Nr. 7, Berlin, Germany, 1992.

Lascelles, B., Favis-Mortlock, D., Parsons, T., and Boardman, J.: Automated digital photogrammetry: a valuable tool for small-scale geomorphological research for the non-photogrammetrist?, Trans. GIS, 6, 5–15, 2002.

Le Bissonnais, Y., Benkhada, Chaplot, V., Fox, D., King, D., and Daroussin, J.: Crusting, runoff and sheet erosion on silty loamy soils at various scales and upscaling from m^2 to small catchments, Soil Till. Res., 46, 69–80, 1998.

Lee, J. S., Grunes, M. R., and De Grandi, G.: Polaimetric SAR speckle filtering and its impact on classification, IEEE T. Geosci. Remote Sens., 37, 2363–2373, 1997.

Lee, J. S., Schuler, D. L., and Ainsworth, T. L.: Polarimetric SAR data compensation for terrain azimuth slope variation, IEEE T. Geosci. Remote Sens., 38, 2153–2163, 2000.

Linden, D. R. and Van Doeren, D. M.: Parameters for characterizing tillage induced soil surface roughness, Soil Sci. Soc. Am. J., 50, 1560–1565, 1986.

Linder, W.: Digital Photogrammetry, A Practical Course. Springer Berlin, Heidelberg, New York, USA, 214 pp., 2006.

Loew, A., Ludwig, R., and Mauser, W.: Derivation of surface soil moisture from ENVISAT ASAR WideSwath and Image mode data in agricultural areas, IEEE T. Geosci. Remote Sens., 44, 889–899, 2006.

Loew, A. and Mauser, W.: Inverse modeling of soil characteristics from surface soil moisture observations: potential and limitations, Hydrol. Earth Sys. Sci., 5, 95–145, 2008.

LPS: Leica Photogrammetry Suite User Manual V 9.0, 2006.

Luhmann, T.: Nahbereichsphotogrammetrie – Grundlagen, Methoden und Anwendungen. Heidelberg, Germany, 586 pp., 2003.

Mattia, F., Le Toan, T., Souyris, J. C., De Carolis, G., Floury, N., Posa, F., and Pasquariello, G.: The effect of surface roughness on multi frequency polarimetric SAR data, IEEE T. Geosci. Remote Sens., 35, 954–966, 1997.

Oh, Y., Sarabandi, K., and Ulaby, F. T.: An empirical model and an inversion technique for rader scattering from bare soil surfaces,

IEEE T. Geosci. Remote Sens., 30, 370–381, 1992.

Rawls, W. and Brakensiek, D.: Prediction of soil water retention properties for hydrologic modeling, Watershed Management in the Eighties, Proc. Symposium of Irrig. Drainage Div. ASCE, Denver, CO, USA, 30 April–1 May 1985, 293–299, 1985.

Rieke-Zapp, D. and Nearing, M. A.: Digital close range photogrammetry for measurement of soil erosion, The Photogrammetric Record, 20, 69–87, 2005.

Römkens, M. J. and Wang, J. Y.: Effect of tillage on surface roughness, Trans. ASAE 29, 429–433, 1986.

Santanello, J. A., Peters-Lidard, C. D., Garcia, M. E., Mocko, D. M., Tischler, M. A., Moran, S., and Thoma, D.: Using remotely-sensed estimates of soil moisture to infer soil texture and hydraulic properties across a semi-arid watershed, Remote Sens. Environ., 110, 79–97, 2007.

Scheiber, R., Keller, M., Fischer, J., Horn, R., and Hajnsek, I.: Radar Data Processing, Quality Analysis and Level-1b Product Generation for AGRISAR and EAGLE campaigns. Proceedings AGRISAR and EAGLE Campaigns Final Workshop, 15–16 October 2007 ESA/ESTEC, Noordwijk, The Netherlands, available on CD, 2007.

Schlichting, E., Blume, H. P., and Stahr, K.: Bodenkundliches Praktikum. Blackwell, Berlin, Germany, 295 pp., 1995.

Schuler, D. L., Lee, J. S., and Kasilingam, D.: Surface roughness and slope measurements using polarimetric SAR data, IEEE T. Geosci. Remote Sens., 40, 687–698, 2002.

Sobieraj, J. A., Elsenbeer, H., and Vertessy, R. A.: Pedotransfer functions for estimating saturated hydraulic conductivity: implications for modeling storm flow generation, J. Hydrol., 251, 202–220, 2001.

Sommer, H.: Quantifizierung der Rauigkeit von Bodenoberflächen und Simulation hydromechanischer Prozesse anhand von Oberflächenmodelen. Aachen, Germany, 1997.

Sun, Y., Lin, J., Schulze Lammers, P., and Damerow, L.: Short communication. Estimating surface porosity by roughness measurement in a silt – loam field. J. Plant Nutr. Soil Sci., 169, 630–632, 2006.

Taconet, O. and Ciarletti, V.: Estimating soil roughness indices on a ridge-and-furrow surface using stereo photogrammetry, Soil Till. Res., 93, 64–76, 2007.

Thiel, C.: Measuring surface roughness on base of the circular polarization coherence as an input for simple inversion of the IEM model, Proceedings of PolInSAR Workshop, 14–16 January 2003, Frascati, Italy, 2003.

Thiel, Ch., Gruenler, S., Herold, M., Hochschild, V., Jaeger, G. and Hellmann, M.: Interpretation and Analysis of Polarimetric L-Band E-SAR-Data for the Derivation of Hydrologic Land Surface Parameters, IEEE Proceedings IGARSS'01, Sydney, available on CD, 2001.

Verhoest, N. E. C., De Baets, B., and Vernieuwe, H.: A Takagi-Sugeno fuzzy rule-based model for soil moisture retrieval from SAR under soil roughness uncertainty, IEEE T. Geosci. Remote Sens., 45, 1351–1360, 2007.

Verhoest, N. E. C., Lievens, H. Wagner, W. Álvarez-Mozos, J., Moran, S., and Mattia, F.: On the soil roughness parameterization problem in soil moisture retrieval of bare surfaces from synthetic aperture radar, Sensors, 8, 4213–4248, 2008.

Warner, W. S.: Mapping a three-dimensional soil surface with hand-held 35 mm photography, Soil Till. Res. 34, 187–197, 1995.

Wegmann, H., Rieke-Zapp, D., and Santel, F.: Digitale Nahbereichs-photogrammetrie zur Erstellung von Oberflächenmodellen für Bodenerosionsversuche. Publikationen der Deutschen Gesellschaft für Photogrammetrie und Fernerkundung, 9, 2001.

Wiggenhagen, M. and Raguse, K.: Entwicklung von Kenngrößen zur Qualitätsbeurteilung optischer Prozessketten, PFG, 2, 125–134, 2003.

Woesten, J.: Soil Quality for Crop Production and Ecosystem Health. Development in Soil Science, chap. Pedotransfer functions to evaluate soil quality, Elsevier, The Netherlands, 221–245, 1997.

Zeiger, M.: Assessment of dynamic biotic and abiotic processes at the soil surface affected by different management systems, Kiel, Germany, 185 pp., 2007.

2.2 Paper II: Remote Sensing of Environment - Progress in the understanding of narrow directional microwave scattering of agricultural fields

Paper II shows as an extreme case the impact of soil surface roughness on the backscattering of several SAR sensors and images. As an output of an ESA campaign investigating the existence and occurrence of strong directional scattering (*flashing fields*) a new backscatter model was developed allowing one to address and comprise the different scales of soil surface roughness as well as the orientation of the anisotropic roughness component to the SAR sensor's look direction within the model. The so-called *Modified Shin and Kong Model* (MSK) was used to predict SAR backscatter values for several SAR sensors such as ERS-2, ASAR, Radarsat II, TerraSAR-X and E-SAR.

Wegmüller, U., Santoro, M., Mattia, F., Balenzano, A., Satalino, G., Marzahn, P., Ludwig, R. and Floury, N. Progress in the Understanding of Narrow Directional Microwave Scattering of Agricultural Fields. *Remote Sensing of Environment*, **2011**, 115, 2423-2433

Remote Sensing of Environment 115 (2011) 2423–2433

Contents lists available at ScienceDirect

Remote Sensing of Environment

journal homepage: www.elsevier.com/locate/rse

Progress in the understanding of narrow directional microwave scattering of agricultural fields

U. Wegmüller [a,*], M. Santoro [a], F. Mattia [b], A. Balenzano [b], G. Satalino [b], P. Marzahn [c], G. Fischer [c], R. Ludwig [c], N. Floury [d]

[a] Gamma Remote Sensing AG, CH-3073 Gümligen, Switzerland
[b] Consiglio Nazionale delle Ricerche, ISSIA, I-70126, Bari, Italy
[c] Department of Geography, University of Munich, D-80333 Munich, Germany
[d] ESA,ESTEC, 2201 AZ Noordwijk, The Netherlands

ARTICLE INFO

Article history:
Received 29 November 2010
Received in revised form 14 April 2011
Accepted 16 April 2011
Available online 14 June 2011

Keywords:
Scattering
Directional
Agriculture
Radar
Flashing fields

ABSTRACT

Directional microwave scattering, as investigated in this study, is characterized by a strong and narrow scattering pattern that varies strongly for only minor aspect angle changes. As was noted already in the past directional scattering is relevant for applications and cannot just be ignored. The overall objective of our work was to better understand directional scattering. Suited space- and airborne SAR data over several agricultural sites together with related *in-situ* information were collected for this purpose. Directional scattering was identified by comparison of backscattering acquired with only slightly different aspect angles as available from ERS–ENVISAT pairs with significantly different Doppler Centroids or by comparing azimuth spectrum sub-bands with slightly different Doppler Centroid. Major progress achieved in this work includes the much improved experimental evidence available and significant improvements in the understanding of the scatter phenomenon through the developed scatter model. Good progress was also made in the detection of directional scattering.

1. Introduction

After the launch of ENVISAT in 2002, ENVISAT ASAR–ERS-2 Tandem (EET) pairs acquired within 30 min over the same area revealed strong directional scattering effects on some agricultural fields (Wegmüller, Cordey, Werner, & Meadows, 2006). Examples of backscatter differences ("flashing") larger than 6 dB were observed in EET pairs for look directions differing by less than 1° in the aspect angle over the same area. The discrepancies between the backscatter values appeared not to be related to changing environmental conditions but rather to the fine details of the observing geometries of the two instruments. However, a complete understanding, including the explanation with scatter models, was not achieved, because cases, for which the directional effect could be clearly identified (*e.g.* using an available EET pair acquired with significantly different Doppler Centroids) and *in-situ* information on parameters as crop type and surface geometry was available, were missing.

The presence of poorly characterized anomalies between two subsequent and close SAR acquisitions may have severe implications for the confidence with which satellite SAR data are assimilated in hydrological and/or crop growth models for land applications monitoring, particularly in view of near future missions characterized by short-repeating cycles (*e.g.*, Sentinel-1 (Attema, Davidson, Snoeij, Rommen, & Floury, 2009)) data. Indeed, directionality increasing the backscattering by more than 3 dB is threatening for any kind of quantitative interpretation of SAR backscattering. At C-band the total backscatter range over a bare soil with changing soil moisture is around 6 dB (Wegmüller, 1990), therefore, an increase of the backscattering by 6 dB caused by directionality can change the interpretation from dry to saturated. Furthermore, a crop classification based on the SAR backscattering can be also affected by directional scattering effects.

For these reasons, the investigation of directional scattering was resumed in 2008 (Wegmüller et al., 2010). This time, an important focus was on the modeling of the directional effects. In the following, directional scattering will be referred to narrow scattering pattern of few degrees width in azimuth plane, which differs both from an anisotropic scattering, with a wider pattern, and an isotropic scattering which is independent of the aspect angle. Based on a bibliographic review, two principal conditions originating directional scattering on SAR images were identified:

a) the existence, on the imaged surface, of geometric structures (*e.g.* rows or ditches parallel to the impinging SAR wave front) (Raney, Gray, & Princz, 1988) that can backscatter coherently the incidence field;

* Corresponding author.
E-mail address: wegmuller@gamma-rs.ch (U. Wegmüller).

0034-4257/$ – see front matter © 2011 Elsevier Inc. All rights reserved.
doi:10.1016/j.rse.2011.04.026

b) the presence of regular patterns of these geometric structures (*e.g.* periodic tilled soils (Shin & Kong, 1984) (Yueh, Shin, & Kong, 1988) (Zribi, Taconet, Ciarletti, & Vidal-Madjar, 2002,) or regular grids of plants characterized by a high double-bounce response, *e.g.* machine planted rice in the appropriate phenological stage (Ouchi, Wang, Ishitsuka, Saito, & Mohri, 2006), (Ulander & Le Toan, 1999)), which determine a Bragg scattering reinforcement.

A general conceptual model that can account for very directional scattering patterns represents a resolution cell of the observing system (*e.g.* SAR) as a superposition of a few coherent scatter rather than as a collection of many incoherent scatterers (*e.g.* Attema, 2007). Such a model not only predicts a significant angular anisotropy in the surface scattering but it also implies that the backscattering coefficient depends on the observing system parameters (*e.g.* resolution cell) and its 1-look amplitude pdf is not a Rayleigh distribution (*e.g.* Jakeman & Pusey, 1976). However, in realistic cases (*e.g.* tilled row soils), there are coherent (*e.g.* scattering from parallel periodic rows) and non-coherent (*e.g.* scattering from isotropic surface roughness) contributions whose weights depend on the characteristics of the radar system (*e.g.* frequency, polarization, and incidence angle) and of the soil surface (*e.g.* row distance, vertical and horizontal roughness parameters) and the quantitative prediction of the directional scattering requires to develop new tools or revisit previous models.

In this framework, the objective of this work has been to consolidate the experimental evidence and to support its understanding by a dedicated ground campaign and an improved theoretical model in order to better quantify and assess the relevance of the directional scattering with very narrow scattering pattern.

Section 2 presents the SAR and ground data collected during the dedicated ground campaign in 2009 over agricultural fields in Flevoland Province (The Netherlands). Then, the experimental evidence of the flashing field phenomenon and the scatter modeling development to interpret the directional pattern are presented in Sections 3 and 4, respectively. Section 5 discusses the development of methodologies to reliably detect the directional scattering. Finally, in Section 6 the conclusions are drawn.

2. Materials

Initially, we searched through a quite extensive set of existing campaign data (Wegmüller et al., 2010) with potentially suited SAR data with *in-situ* information. It turned out, however, that either no clear "flashing" could be identified (which was the case for fields with available *in-situ* information) or that no *in-situ* information was available. To ensure an adequate data base, we finally decided to conduct a dedicated campaign over the area at East of Dronten in Flevoland Province, The Netherlands. Historic data over this area and a very recent EET pair acquired on 29-Mar-2009 highlighted the presence of many fields showing directional effects. On 4-May-2009 we conducted our field campaign to observe the conditions of the fields during the ENVISAT ASAR and ERS-2 acquisitions on 3-May-2009.

2.1. Test site and in-situ data

The study area is an agricultural site of approximately 7 km × 4 km located East of Dronten, in Flevoland Province. The very flat topography of the area is an ideal precondition for the occurrence and detection of the directional effects. In addition, the selected area is framed by canals or roads that are either quasi perpendicular or parallel to the ENVISAT ASAR and ERS-2 look direction.

During the survey, information on crop type and status and cultivation direction as well as a general description of surface roughness was collected and documented by photographs over 146 fields, having an average size of 6.7 ha. Fig. 1 shows the boundaries (red polygons) of monitored fields and the main crop types, *i.e.* potato, onion, sugar beet and wheat fields. The longitudinal red and green lines highlight the road and canals bounding the fields.

For approximately half of the fields inspected during the campaign, measurements of soil moisture, row maximum height A and row separation L, crop height and auxiliary information, such as vegetation growth status, cover fraction, field topography, soil texture type (mainly sandy clay or clay) were conducted. Rough visual estimates of the random r.m.s. surface height were also collected. In Table 1, the mean values of soil parameters, *i.e.* soil moisture, random r.m.s. surface height, row height and row separation, for the main crop types and bare soils, are reported.

An accurate GIS-based assessment highlighted that there were two different sub-areas in terms of row direction. More precisely, the row directions following the road/canal directions (red and green longitudinal lines in Fig. 1) were at 9.3° ± 0.3° and at 11.5° ± 0.3° from the North, respectively for the two different sub-areas. This difference is likely due to the slight change (*i.e.* 2°) in the road/canal direction between the two sub-areas, as can be seen in Fig. 1.

It is worth noting that, in early May, vegetation was developed only over wheat fields (end of tillering-beginning of stem elongation), whereas onion, potato and sugar beet fields were mostly bare or sparsely vegetated, as they were probably sown in April or May, according to local agricultural practices (Fig. 2).

2.2. SAR data

From the end of March to mid-July 2009, 4 descending ENVISAT ASAR and ERS-2 Tandem pairs (Wegmüller et al., 2009) were acquired over Flevoland within ~30 min from each other. Table 2 describes the relevant characteristics of the ENVISAT ASAR and ERS-2 pairs.

To determine the accurate radar look direction, the zero Doppler look vector and the squint angle ξ (the angle that the slant range vector makes with the zero Doppler plane) need to be considered. The corresponding corrected angle in the ground surface plane δ depends also on the incidence angle θ and is calculated (approximated for small squint angles) by:

$$\delta = \frac{\xi}{\sin\theta} = \frac{\lambda f_d}{2v\sin\theta},$$

with the sensor velocity, v, the wavelength, λ, and the Doppler frequency, f_d. Over the synthetic aperture an aspect angle range, δ_{bw}, related to the azimuth bandwidth, bw, is covered:

$$\delta_{bw} = \frac{\lambda bw}{2v\sin\theta}.$$

As a consequence, the corrected aspect angle in the ground surface plane can be evaluated (Table 2).

For the satellite C-band SARs operated at an incidence angle of 23°, a Doppler difference of 1000 Hz will cause an incidence direction difference of approximately 0.5°. It is worth noting that the EET pair acquired on 3-May-2009 contained a significant Doppler Centroid (DC) difference (2131 Hz), so that it was a good candidate to reliably identify directional scattering. For ERS-2 the antenna diagram azimuth 3 dB beam-width is 0.288°, which corresponds to a Doppler bandwidth of 1263 Hz. This means that within a single acquisition an aspect angle range of 0.74° is covered.

From April to June, 10 quad-pol RADARSAT-2 images at different incidence angles were also acquired over the Dronten site (Table 3), in the framework of European Space Agency (ESA) AGRISAR '09 campaign, in preparation of methodologies and retrieval algorithms for the near future ESA SAR system Sentinel-1 (Attema et al., 2009). The RADARSAT-2 data could complement the ENVISAT and ASAR data as additional observations, in particular to study the dependence of

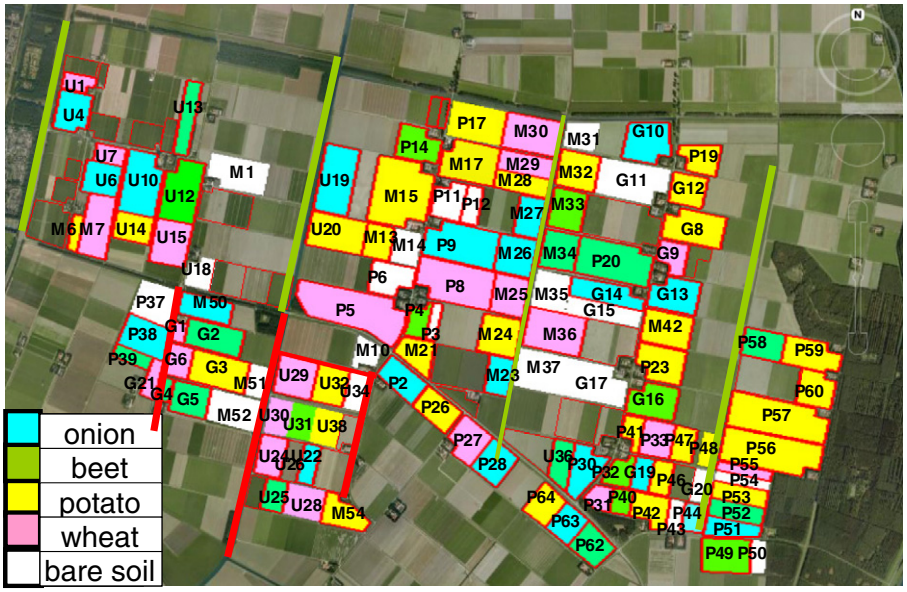

Fig. 1. Boundaries (red polygons) of visited fields and the main cultivated crops in the Dronten site (Flevoland Province, The Netherlands). The longitudinal red and green lines highlight canals or roads bounding the fields. Field names are also reported.

directional scattering on polarization. Although the 3 RADARSAT-2 FQ13 ascending data reported in Table 3 did not cover the Dronten site, they were interesting as acquired on the same dates as the FQ12 descending data with just about 12 hour difference.

For all SAR data, azimuth sub-band images were also generated. The available bandwidth was divided into 5 sub-bands (with 50% overlap between neighboring sub-bands). The sub-band Single Look Complex images were multi-looked and geocoded. A radiometric scaling relative to the full bandwidth scene was applied (Moreira, 1992).

The ERS-2, ENVISAT and RADARSAT-2 backscattering coefficients of the monitored area were extracted from full and sub-band geocoded multi-look intensity images with 20 m pixel size, averaging at field scale.

3. Consolidation of experimental evidence

Fig. 3 shows the ENVISAT ASAR and ERS-2 Tandem HSI (Hue–Saturation–Intensity) composite of the backscatter ratio (hue), backscatter change (saturation) and backscattering in the first image of the pair (intensity) over the Dronten site on 3-May-2009. Backscatter ratio (hue) ranges from −6 to +6 dB; mean intensity (intensity) from −22 dB to +3.5 dB; backscatter change (saturation) is defined as the absolute value of the ratio expressed in dB and ranges from 0 to +6 dB. The red arrow indicates the radar look direction. For fields showing red (green) color the ENVISAT ASAR backscatter is between 3 dB and 10 dB higher (lower) than the ERS-2 backscatter.

As the corrected aspect angles of ENVISAT and ERS-2 images were 10.5° and 9.3° respectively (Table 2) and the row direction of red and green "flashing fields", were at 9.3° ± 0.3° and at 11.5° ± 0.3° from the North, it results that the flashing field rows were quasi perpendicular to the radar look directions, whereas the not flashing field rows were quasi parallel to the radar look directions.

The relationship between the high directional scattering and the cultivation direction can also be seen, in Fig. 4 which shows the ENVISAT ASAR (left) and ERS-2 (right) backscattering coefficients of sugar beet flashing (red and green) and not flashing (black) fields as a function of the row direction. Moreover, the backscatter values of flashing fields with row direction quasi perpendicular to the radar look direction are spread with respect to the backscatter values of not flashing fields. This is due to the fact that little changes around the perpendicular direction to the radar look direction can cause a high variability in the field response (narrow directional scattering pattern), so that flashing effect can disappear, for example as in case of the sugar beet field P49.

Nevertheless, flashing fields with row direction not approximately perpendicular to the observation direction were also observed in an area adjoining the Dronten site. These cases seem to be rather exceptional and we assume that the explanation for this directionality may be different.

It is worth noting that the list of the flashing fields includes fields with very significant row structures, such as potato and carrot fields, as well as fields with quite weak row structures, such as onion, sugar beet and wheat (Table 1).

Different look directions over the same area can be also compared by splitting the azimuth spectrum of one single image into sub-bands. For the RADARSAT-2 FQ8, sub-band HSI images (first sub-band image combined with last sub-band image) on 1st May at HH (top left), VV (top right), HV (bottom left) and VH (bottom right) polarization are shown in Fig. 5. At HH- and VV-polarization directional scattering effects of similar level were observed, whereas at cross-polarization no effects were observed at a comparable level.

Table 1
Mean values of soil parameters of onion, sugar beet, potato, wheat fields and bare soils: soil moisture, random r.m.s. height, row height and row separation.

	Soil moisture [%]	Random rms height [cm]	Row height [cm]	Row separation [cm]
Onion	18	<1	2.5	15
Sugar beet	21	<1	1.5	50
Potato	12	<1	13	70
Wheat	16	1–1.5	1.5	13
Bare soil	15	1–1.5	3	30

3.1. Occurrence of directionality effects and influence of surface parameters

The significant difference observed for many fields within the 1°. directional angle range of the synthetic aperture of the spaceborne C-band SARs (ERS-2, ENVISAT, and RADARSAT-2) indicates that narrow

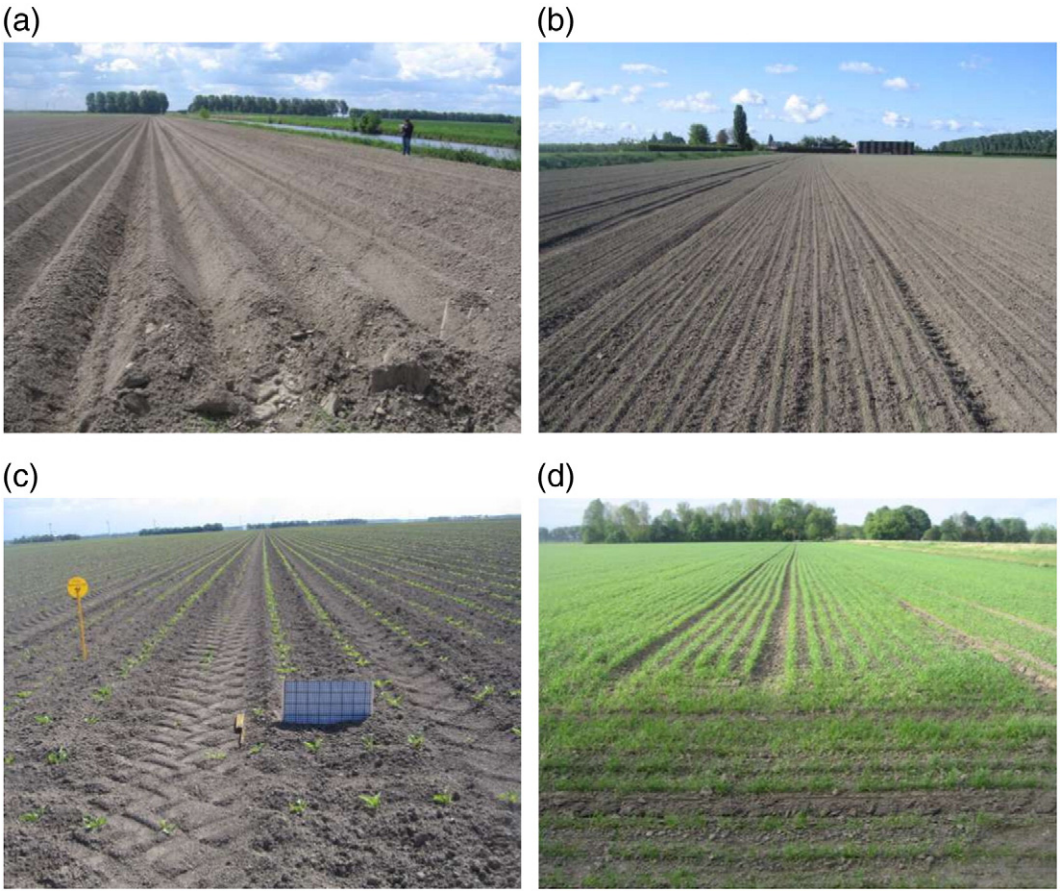

Fig. 2. Examples of potato (a), onion (b), sugar beet (c), wheat (d) fields over the Dronten site.

directionality patterns (*e.g.* <3° width) are often observed. For a 3° directionality pattern width, a 0.5° aspect angle range covered over the synthetic aperture, and assuming an isotropic distribution of cultivation directions results in an occurrence estimate of (4°/180°) = 2.2%.

However, the field topography was found to be a very important factor for the presence of directional scattering. In flat terrain row structures are more often very straight. Even in the case of small slopes, the geometry of the rows relative to the sensors often changes within a field. In more hilly terrain, fields are generally also smaller than in flat terrain which makes the detection of directional scattering more difficult. So the high occurrence stated relates to flat terrain only.

Furthermore, vegetation canopy on top of the soil seems to quench the directionality effect from the soil, adding a random screen. As an example, Fig. 6 shows the temporal behavior of backscatter coefficient of an onion flashing field. The directional effect decrease may be due to the vegetation growth, as the ENVISAT ASAR and ERS-2 DC difference (Table 2) does not significantly change from March to July 2009.

Finally, surface roughness is expected to disturb or reduce directional scattering from sufficiently straight rows. However, quite different random roughness was observed on the fields showing directional effects. In some cases the fields were recently prepared and showed small scale random roughness typical for such fields with small 1–2 cm aggregates (soil clods) on the surface. Other fields, *e.g.* some onion and sugar beet fields were already prepared further back in the past and so the surface was slain by precipitation (no more aggregates visible).

4. Scatter model development

4.1. Modification of model by Shin and Kong (1984)

On the basis of the experimental considerations over the Dronten site and of the previous experimental studies (*e.g.* Ferro-Famil,

Table 2
ENVISAT ASAR and ERS-2 Tandem pairs available in descending (desc) tracks over the Dronten site.

Sensor	Date	Track	Mode	Polarization	Swath	Incidence angle [°]	Doppler Centroid [Hz]	Corrected aspect angle [°]
ERS2	29-Mar-2009	380	desc	VV		25.4	1109	10.0
ASAR	29-Mar-2009	380	desc	VV	IS2	25.4	211	10.5
ERS2	3-May-2009	380	desc	VV		25.4	2350	9.3
ASAR	3-May-2009	380	desc	VV	IS2	25.4	219	10.5
ERS2	7-Jun-2009	380	desc	VV		25.4	1791	9.6
ASAR	7-Jun-2009	380	desc	VV	IS2	25.4	213	10.5
ERS2	12-Jul-2009	380	desc	VV		25.4	1630	9.7
ASAR	12-Jul-2009	380	desc	VV	IS2	25.4	212	10.5

Table 3
RADARSAT-2 descending (desc) and ascending (asc) images available in fine beam (FQ) quad polarization mode over the Dronten site.

Sensor	Date	Mode	Polarization	Mode	Incidence angle [°]
RADARSAT-2	18-Mar-2009	desc	Quad-pol	FQ4	25.6
RADARSAT-2	07-Apr-2009	desc	Quad-pol	FQ8	27.5
RADARSAT-2	1-May-2009	desc	Quad-pol	FQ8	27.5
RADARSAT-2	25-May-2009	desc	Quad-pol	FQ8	27.5
RADARSAT-2	8-May-2009	desc	Quad-pol	FQ12	31.9
RADARSAT-2	1-Jun-2009	desc	Quad-pol	FQ12	31.9
RADARSAT-2	25-Jun-2009	desc	Quad-pol	FQ12	31.9
RADARSAT-2	8-May-2009	asc	Quad-pol	FQ13	34.9
RADARSAT-2	1-Jun-2009	asc	Quad-pol	FQ13	34.9
RADARSAT-2	25-Jun-2009	asc	Quad-pol	FQ13	34.9

Reigber, Pottier, & Boerner, 2003; Wegmüller et al., 2006), the observed directional scattering on SAR images mainly concerned agricultural surfaces either bare or at an early vegetation stage. For this reason, the modeling activity focused on the study of scattering from agricultural soil surfaces showing a periodic or quasi periodic tillage row pattern disregarding the presence of vegetation.

The scattering from anisotropic quasi-periodic soils has been studied in a number of theoretical works in the 1980s (Shin & Kong, 1984; Ulaby, Kouyate, Adrian, & Sieber, 1982; Yueh et al., 1988). In those studies, the strong impact of anisotropic roughness component in modulating the isotropic surface scattering was clearly identified and quantified. Indeed, large variations of backscatter (up to 10–20 dB) for off-azimuth incidence angle (*i.e.* the angle between sensor azimuth and row tillage direction) ranging between 0° and 90°, corresponding to incidence perpendicular and parallel to tillage row directions, were predicted.

Shin and Kong(1984) provided a rigorous mathematical framework to describe the scattering from quasi periodic surfaces, modeled as the superposition of three components: a deterministic periodic function, a zero mean isotropic stationary Gaussian random process, and a narrow band Gaussian process. Therefore, the soil roughness is described by six parameters, the standard deviation (s) and the correlation coefficient (l) of the isotropic random roughness component, and the standard deviation (s_y) and the correlation coefficient (l_y) of the anisotropic random roughness component, the amplitude (A) and the spatial periodicity (L) of the rows. In (Shin & Kong, 1984), it is demonstrated that the total backscatter of quasi periodic surfaces consists of three terms:

- the first one due to the coherent field related to the scattering of the deterministic periodic function (σ^c_{pp});
- the second one representing the incoherent scattering of the combined isotropic and anisotropic random roughness components modulated by the deterministic periodic function $\sigma^{nc_1}_{pp}$;
- the third one due to the incoherent field scattered only by the anisotropic random component modulated by the deterministic periodic function $\sigma^{nc_2}_{pp}$:

$$\sigma_{0pp} = \sigma^c_{pp} + \sigma^{nc_1}_{pp} + \sigma^{nc_2}_{pp} \quad (1)$$

where *p* stands for vertical or horizontal polarization.

However, all the simulations reported in (Shin & Kong, 1984; Yueh et al., 1988) only dealt with the incoherent scattering of the isotropic random roughness components modulated by the deterministic periodic function, which could not predict highly directional backscattering patterns. The other terms were discarded because their expressions were found depending on the Dirac-δ function and

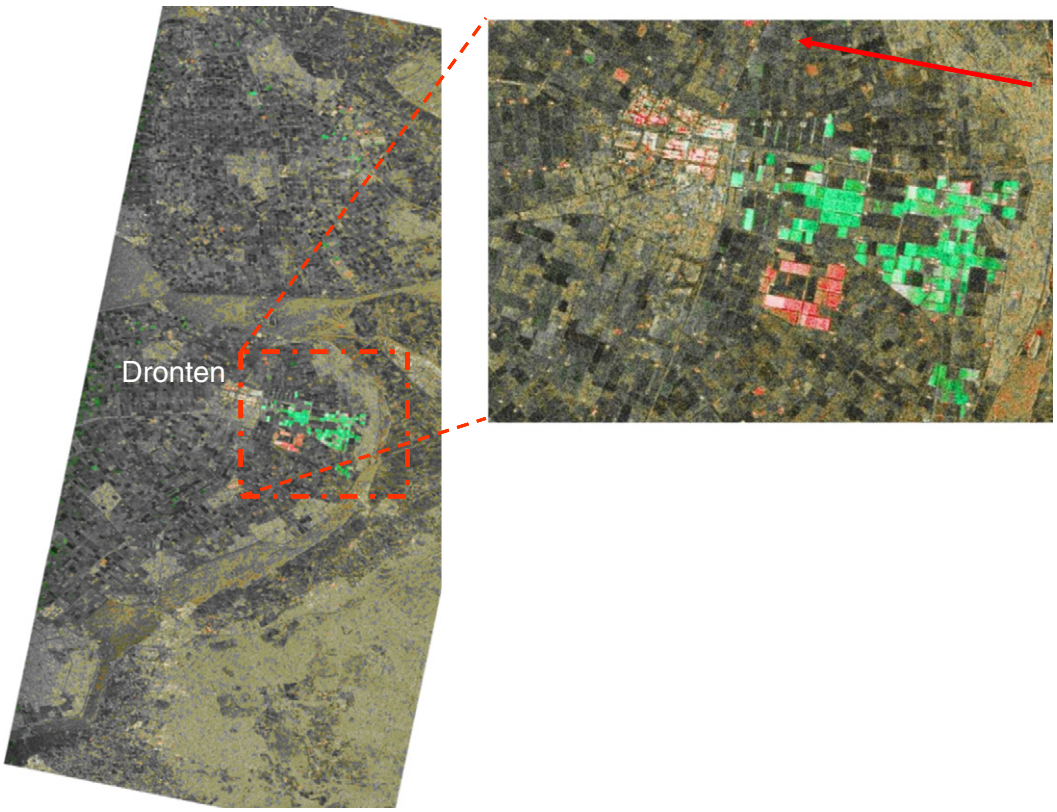

Fig. 3. ENVISAT ASAR and ERS-2 Tandem HSI (Hue–Saturation–Intensity) composite of the backscatter ratio (hue), backscatter change (saturation) and backscattering in the first image of the pair (intensity) over Dronten site on 3-May-2009. Backscatter ratio (hue) ranges from −6 to +6 dB; mean intensity (intensity) from −22 dB to +3.5 dB; absolute backscatter change (saturation) from 0 to +6 dB. Red indicates higher intensity for ENVISAT ASAR, and green higher intensity for ERS-2.

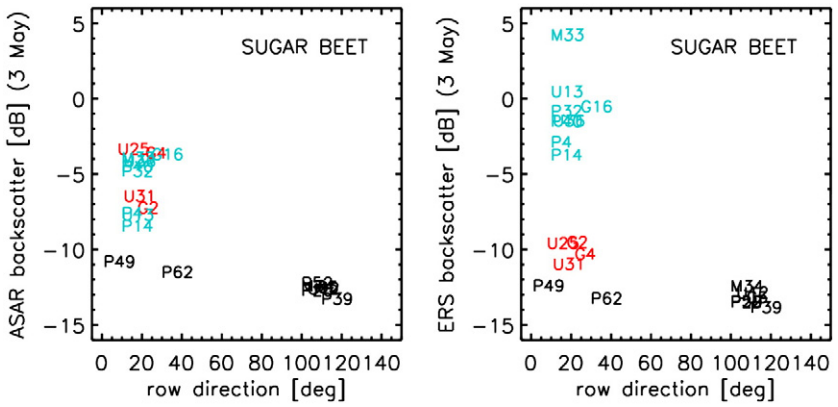

Fig. 4. ENVISAT ASAR (left) and ERS-2 (right) backscatter of sugar beet flashing (red and green) and not flashing (black) fields *versus* the row direction with respect to North.

therefore were not given in a finite form. In other words, the study by Shin and Kong (1984) was able to predict large variations (*i.e.* several dBs) of backscattering for changes of the off-azimuth angle of several degrees but could not predict strong changes of the backscatter (*i.e.* 3–6 dB) for variations of the off-azimuth angle of few degrees (*i.e.* 1–3°), as it is observed in the case of flashing fields imaged by spaceborne SAR sensors.

The improved scatter model (Mattia, 2011) consisted of deriving finite expressions for all the three backscatter terms of quasi periodic surfaces. This was accomplished by introducing two principal changes in the theoretical approach.

Firstly, the surface scattered field was computed using the Kirchhoff diffraction integral under the Fresnel approximation rather than the Fraunhofer approximation as performed in the original Shin and Kong model. This change is important to obtain a more accurate expression of the coherent term contributing to the total backscatter whenever the observed soil surface is located in the near field of the radar system (as is the case of spaceborne SAR systems).

Secondly, the antenna pattern of the radar system, characterized by the system spatial resolutions (*i.e.* ρx and ρy), was included in the computation of the scattered field, which permits to obtain a finite form for all the terms contributing to the total backscatter.

In the modified model, the total backscattering is still expressed as the superposition of the three terms of Eq. (1), having the same physical meaning as in the original Shin and Kong (1984) model but different analytical expressions, which depend not only on the surface parameters but also on the radar spatial resolutions (*i.e.* ρx and ρy). The new derived expressions reproduce as a particular case the Shin and Kong model expressions in (Shin & Kong, 1984) and assume finite values in the entire azimuthal and zenithal planes. The main difference is that the new model can predict very narrow backscatter peaks (*i.e.* a few tenths of a degree angular aperture in the azimuth

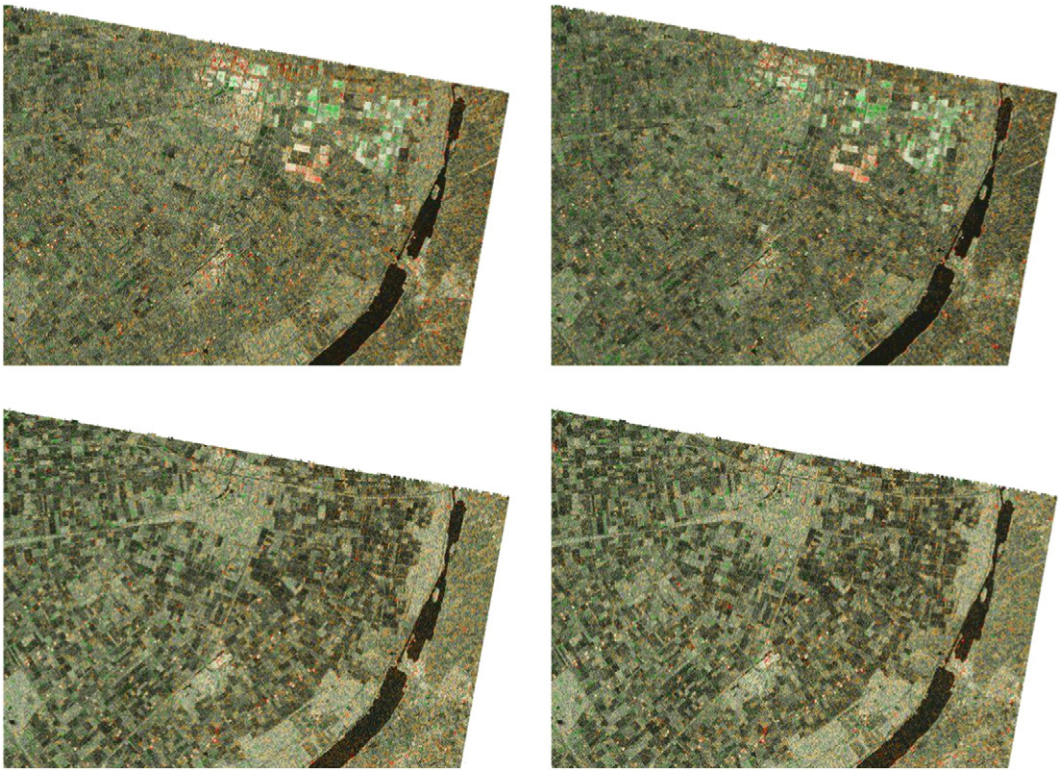

Fig. 5. Radarsat-2 FQ8 sub-band HSI images (first sub-band image combined with last sub-band image) acquired on 1st May at HH (top left), VV (top right), HV (bottom left) and VH (bottom right) polarization.

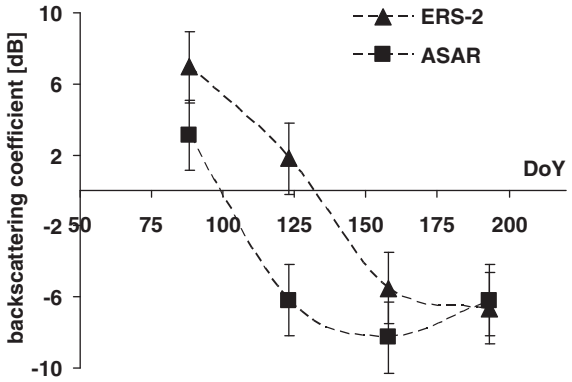

Fig. 6. Backscattering coefficient of an onion flashing field *versus* DoY (Day of Year). The error bars account for the measurement error.

plane) when the impinging electromagnetic wave is perpendicular to the row tillage direction. The amplitude and the width of this peak depend on the radar (system) spatial resolution (the amplitude is directly proportional to ρx whereas the width is inversely proportional to ρx).

4.2. Widening of directionality pattern

One limitation of the adopted roughness description is that all the periodic or quasi-periodic roughness components are perfectly parallel. In other words, the surface roughness model accounts for a randomness in the amplitude and phase of the periodic components but it does not permit to consider quasi-parallel directions. In the real world the tillage rows of agricultural fields can change direction within the same field. To account for such imperfectly parallel tillage rows, the developed scattering model was not modified but an agricultural field was considered as composed of different sub-patches with slightly different row directions, assuming a normal distribution with zero mean and a given standard definition. The backscatter of such a field is obtained by averaging the backscattering from all its sub-patches. The resulting backscatter pattern is characterized by broader peaks whose width increases with the standard deviation of the row direction distribution. As an example, Fig. 7 shows the effect of the peak broadening due to the averaging of quasi-periodic tillage rows considering a standard deviation Δε of parallel direction equal to 0.25° or 0.5°. The broadening effect is evident.

4.3. Simulation of measured directionality

In a further step, it was investigated to what extent the modified model could predict the directional scattering effects observed in the ENVISAT ASAR and ERS-2 data acquired on 3-May-2009 over the Dronten site. This was done over bare or sparsely vegetated agricultural surfaces (potato, onion, sugar beet and bare fields). To increase the number of SAR observations and refine the resolution of the directional pattern, the 5 azimuth sub-look images were also considered. The ground measurements of surface parameters (*i.e.* A, L, and soil moisture content) and the visual estimates of the random RMS surface height (s) collected during the ground campaign over the Dronten site (Table 1) were used as input to the simulations. The remaining surface roughness parameters (*l*, *sy* and *ly*), which were not measured in the field, were used as free parameters to tune the match with the measured data. A difference between the ENVISAT ASAR and ERS-2 aspect angles of 1.2° in May was considered (Table 2). A standard deviation of the row direction (*i.e.* Δε) of 0.7° was assumed in order to reproduce the measured azimuth pattern width. As an example, Fig. 8 shows the simulated backscattering coefficient (continuous lines) of sugar beet fields for both ERS-2 (continuous line) and ENVISAT ASAR (dotted line) acquisitions as a function of the off-azimuth angle ranging between −5° and 5° for ERS-2 acquisition and −6.2° and 3.8° for ENVISAT ASAR acquisition around 0°, meaning that the impinging wave is perpendicular to the row direction. The off-azimuth angles were evaluated considering the ERS-2 and ENVISAT ASAR corrected aspect angles and the measured mean row direction.

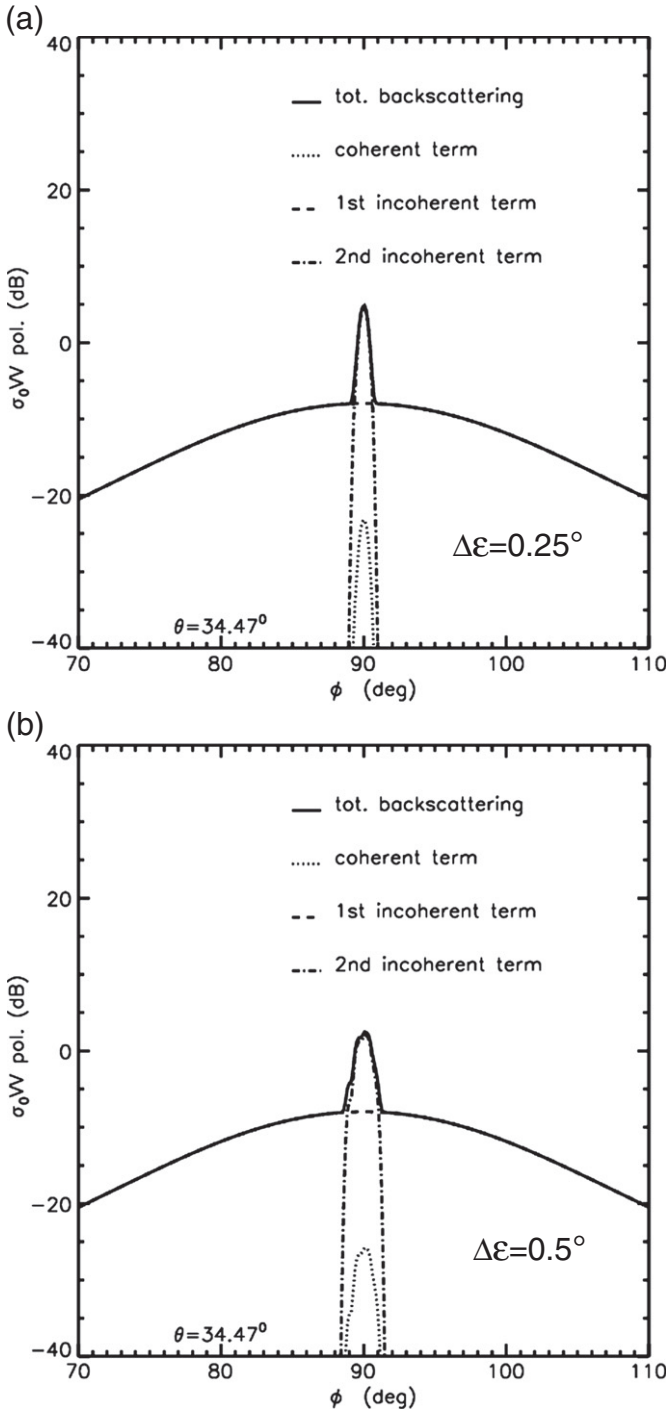

Fig. 7. Azimuth pattern of total backscattering coefficient (blue line) at VV polarization and its components. The standard deviation Δε characterizing the row direction of the quasi-periodic surfaces is: 0.25° (a); 0.5° (b). The surface roughness parameters of the quasi-periodic surface are: $A=1$ cm, $L=25$ cm, $s=0.5$ cm, $l=10.0$ cm, $sy=1.0$ cm, $ly=10.0$ cm while the spatial resolutions are ρ*X*, ρ*Y* = 500 cm.

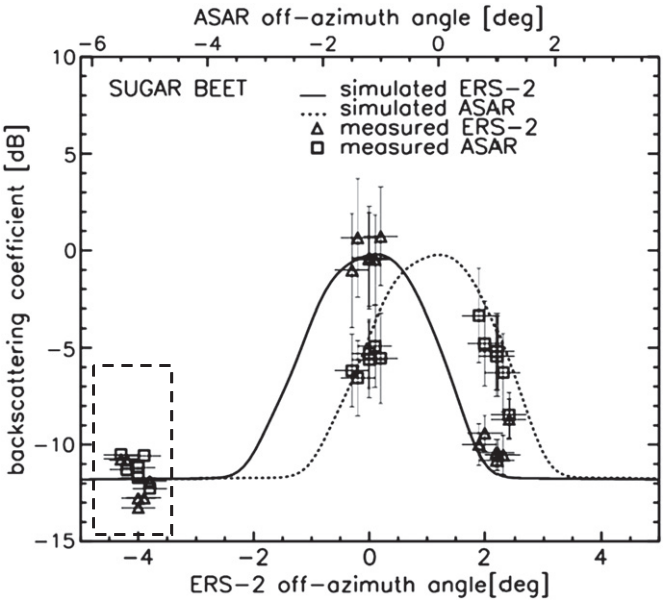

Fig. 8. Comparison between the simulated (continuous and dotted lines) and mean observed backscattering coefficients of sugar beet fields (with row direction almost perpendicular to the radar look direction) for the ERS-2 (triangles) and the ENVISAR ASAR (squares) full and sub-look images. The standard deviations of measured backscatter values in dB and the standard deviations of the row directions of the two different areas in the Dronten site are also shown. The backscattering values of not flashing fields are shown in the dashed rectangle, at a guessed off-azimuth angle outside the range [−2°, +2°], within which the directionality effect appears. The model parameters are: $A=1.5$ cm, $L=50$ cm, $s=0.22$ cm, $l=5.0$ cm, $sy=0.64$ cm, $ly=20.0$ cm, dielectric constant $=10+j2$, while the spatial resolutions are ρx and $\rho y=250$ cm and $\Delta\varepsilon=0.7°$.

The measured mean values of the backscattering coefficient of the fields with row direction almost perpendicular to the look direction of ENVISAT ASAR and ERS-2 full images and the relative sub-image backscattering coefficient (triangles and squares refer to ERS-2 and ENVISAT ASAR, respectively) are compared. The standard deviations of measured backscatter values in dB and the standard deviations of the row directions of the two different areas in the Dronten site are also shown. The backscatter of fields with row direction quasi perpendicular to the look direction of ENVISAT ASAR and ERS-2 but not flashing is reported in the dashed rectangles, at a guessed off-azimuth angle. Since the row direction of the not flashing fields was not precisely measured, it may be inferred that their off-azimuth angles are outside the range [−2°, +2°], within which the directionality effect appears. This is also supported by the fact that their actual backscatter level is approximately −12 dB, and thus in good agreement with the modified model predictions for off-azimuth angles between 2° and 5° or −2° and −5°.

An overall comparison between simulated and mean measured backscattering coefficients of all flashing and not flashing fields with row direction almost perpendicular to the incidence plane for ERS-2 and ENVISAT ASAR full and sub-look images shows that model results reproduce the experimental data acquired in May 2009 with an accuracy ranging between 1.2 dB and 1.9 dB.

5. Detection of directional scattering

The "directionality level" is defined as the increase of the scattering in dB compared to a field of the same type observed with the same or a very similar instrument, with the only relevant difference being the angle between the look direction and the cultivation direction.

The basic approach used to detect directional scattering is to compare the backscattering measured under different aspect angles.

5.1. Detection in multiple scenes

The detection of "directional effects" in multiple observations acquired over the same area under different observational geometries consists typically of the following steps:

- SAR processing with radiometric calibration
- Co-registration of data sets
- Spatial and multi-temporal filtering (Quegan, Le Toan, Yu, Ribbes, & Floury, 2000)
- Calculation of ratio image
- Thresholding on ratio image

For visualization purposes we often generate a HSI (Hue–Saturation–Intensity) composite of the backscatter ratio (hue), backscatter change (saturation) and backscattering in the first image (intensity). Examples are shown in Figs. 3 and 5.

This procedure was successfully applied to ENVISAT ASAR and ERS-2 pairs (Fig. 3) and to ascending/descending orbit pairs (Fig. 9). In ideal cases (both scenes are acquired at almost the same time, with the same polarization and incidence angle, but under a sufficiently different aspect angle) directional scattering can reliably be detected. In many cases the available data do not meet all these requirements,

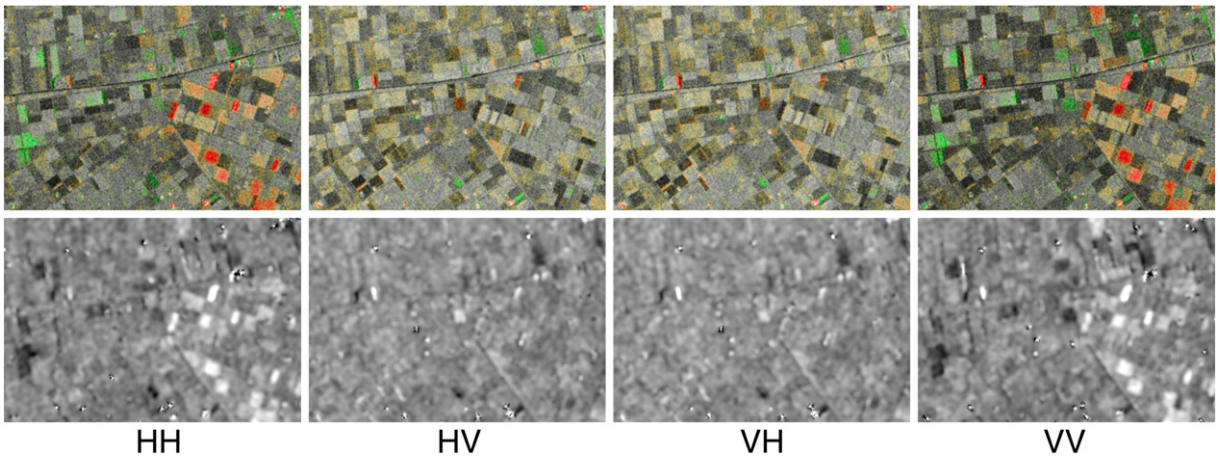

Fig. 9. Flevoland RADARSAT-2 desc. FQ12 and asc. FQ13 data on 1-Jun-2009. Descending/ascending orbit HIS (upper row) and ratio images (lower row) at HH, HV, VH, and VV polarization.

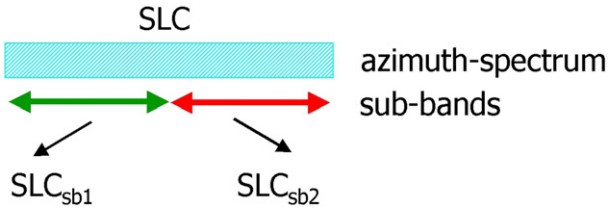

Fig. 10. Azimuth sub-band spectral look images scheme.

so that a change in backscattering between the two scenes may not result from directional scattering but from:

- temporal change
- polarization difference
- incidence angle difference

Note that high ratios in ascending/descending orbit pairs may also relate to anisotropic scattering which has a much wider directionality pattern than the directional scattering.

5.2. Detection in a single scene

Reliable methods to detect directional scattering effects in a single SAR scene would be very useful. The use of azimuth sub-band images and the use of the cross- to like-polarization ratio prove to be the most promising methods presently available for the detection of directional scattering in C-band space-borne SAR data.

Splitting the azimuth spectrum into two sub-bands, as shown in Fig. 10, results in two co-registered SLC with slightly different Doppler Centroids. The DC difference which can be achieved is limited by the azimuth or Doppler bandwidth. In the case of ENVISAT this is around 1600 Hz, resulting in DC differences up to around 1200 Hz, which corresponds to an aspect angle difference of about 0.6°.

Starting from the sub-band images the methodology to detect directional scattering corresponds to that of the methodology used for ERS–ENVISAT Tandem pairs. Examples showed that strong, very narrow directional scattering patterns can be detected using the azimuth sub-band method (Fig. 11).

It has been shown that high levels of directional scattering are observed at HH and VV polarization, but not at cross-polarization. Therefore, very low HV/HH and VH/VV polarization ratios are expected for fields with strong directional scattering.

To assess the potential of the cross- to like-polarization ratios to detect directional scattering we considered the descending orbit swath FQ12 and the ascending orbit swath FQ13. As these two acquire data on the same day with just about 12 h difference so that ascending/descending combinations permitted identifying directional scattering. Fig. 12 shows the HSI calculated for the ascending/descending pair together with the HV/HH ratios for the descending swath FQ12 and for the ascending orbit swath FQ13. Very low HV/HH ratios are characteristic for the fields with strong directional scattering, indicating some potential of the HV/HH and VH/VV ratios to detect strong directional scattering. There are limitations though to detect lower level (<3 dB) directional scattering because of the influence of roughness and vegetation on the cross- to like-polarization ratios.

Finally, the analysis of several polarimetric decomposition approaches (Krogager, Cloude-Pottier, and Freeman-Durden) confirmed that the primary nature of directional scattering is pure surface scattering. For the detection of directional effects, the polarimetric tools investigated did not seem to provide significantly more information compared to what is provided by the cross- to like-polarization ratio.

6. Conclusions

The 2009 Flevoland field campaign dramatically improved the experimental evidence for directional scattering. Well suited SAR imagery, including several ENVISAT ASAR–ERS-2 pairs and fully polarimetric RADARSAT-2 data sets, and related *in-situ* information became available over many fields showing strong directional scattering effects. A significant number of flashing fields and the relevant geometric parameters on the row structure, the random roughness, soil moisture, and the vegetation cover were assessed. Strong directional scattering is observed for fields with a cultivation direction approximately perpendicular to the look direction. It is very important to realize that such fields include potato and carrot fields with very strong row structures as well as onion, sugar beet and wheat fields with rows having amplitudes comparable or even smaller than the random roughness.

The directionality of the scattering was validated reliably thanks to well suited ENVISAT ASAR–ERS-2 pairs acquired within 30 min with significantly different Doppler Centroids.

The fully polarimetric RADARSAT-2 data set demonstrated the polarization dependence of the directional scattering, showing

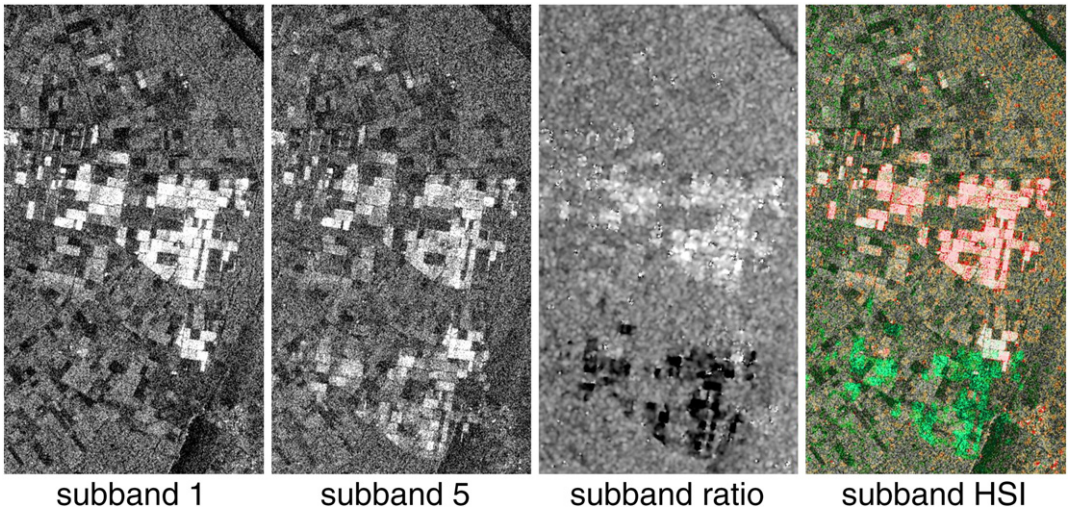

Fig. 11. ENVISAT ASAR azimuth sub-band images of 22-May-2009 over Dronten area, sub-band image ratio using logarithmic gray scale between −10 dB and +10 dB, and sub-band HSI composite (using 6 dB scaling).

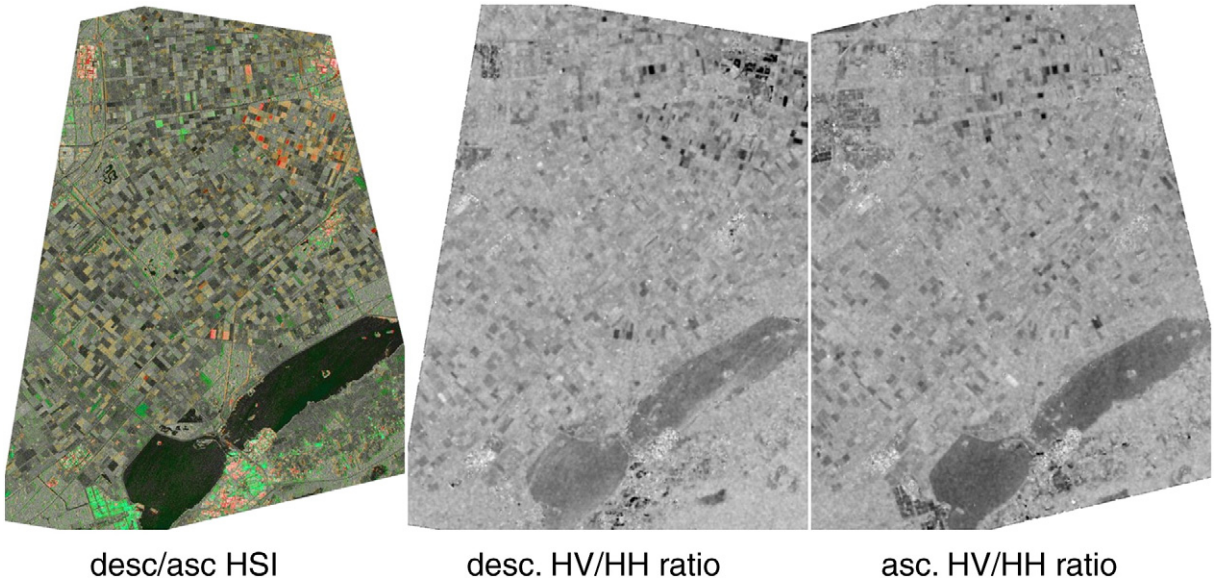

Fig. 12. Radarsat-2 FQ12 and FQ13 data acquired on 1st June over Dronten. In the HSI, red color indicates higher backscattering in the descending orbit data. The HV/HH ratio images have a logartihmic scale between −20 dB and 0 dB. Fields with directional scattering show a very low HV/HH ratio.

similarly high levels at HH and VV polarization and much reduced or no directionality at cross-polarization.

Significant progress was achieved concerning the understanding of the directional scattering. The modified Shin and Kong model (Mattia, 2011) was developed and assessed *versus* the experimental data. Unlike the original Shin and Kong(1984) model, the modified model is able to predict the narrow directional scattering patterns observed, both in amplitude and angular width, over fields with row tillage directions quasi perpendicular to the radar look direction.

Model and experimental results indicate that anisotropic tillage patterns can produce, on one hand, strong (*e.g.* 3–6 dB) though fairly rare (*e.g.* 2.2% of total fields, based on the assumption of uniformly distributed tillage orientation) backscatter changes between spaceborne SAR acquisitions with the same nominal geometry (*e.g.* descending/descending). On the other hand, it can likely produce important (*e.g.* 1–10 dB) changes in the backscatter observed between spaceborne SAR acquisitions with different geometry (*e.g.* ascending/descending).

The basic approach used to detect directional scattering is to compare the backscattering measured under different aspect angles. In the case of a single SAR acquisition this is possible because targets are observed under varying aspect angles along the synthetic aperture. Processing and comparing azimuth sub-band images can be used and showed with some potential.

When using multiple observations to detect directional scattering the angular difference between the two observations can be significantly larger. In the case of using ascending/descending pairs the angular difference is often around 20°, which is excellent to have one image being affected by directional scattering and the other one not. On the other hand directional scattering (with a narrow pattern) and anisotropic scattering (with a wide pattern) cannot be separated reliably.

An important disadvantage of multiple observations is that they are typically acquired at different times, so that temporal change may be confused with directional scattering effects.

For the planned Sentinel-1 the effective azimuth bandwidth available is only about 320 Hz (20% of the value of ENVISAT). Nevertheless, in the so-called TOPS mode this bandwidth available over a certain surface area is split into a few bursts which differ in their Doppler frequency by up to >1000 Hz, so that there may indeed be some potential for detecting directional scattering using azimuth sub-band images.

Very interesting in the context of the detection of directional scattering in Sentinel-1 data is also the observation that the HV/HH ratio (and the VH/VV ratio) is particularly low. Cross- and like polarization data should be available for most Sentinel-1 acquisitions.

The detection based on the low HV/HH ratios and the azimuth sub-band based method use very different schemes and can be considered quite independent of each other. A combination of the two is expected to permit a quite reliable detection at least for strong directional scattering. To detect lower levels on the other hand will not as easily be possible.

Acknowledgement

This work was supported by ESA under contract 21659/08/NL/lvH on *Understanding Directionality in Surface Scattering by Imaging Radar*. ERS-2, ASAR and AGRISAR'06 data copyright ESA (CAT 5862). ESA and MDA are acknowledged for providing RADARSAT-2 data in the frame of the AGRISAR'09 campaign.

References

Attema, E. (2007). The GRAY SAR calibration algorithm applied to “flashing field” phenomena. *Canadian Journal of Remote Sensing*, *33*(1), 12–19.

Attema, E., Davidson, M., Snoeij, P., Rommen, B., & Floury, N. (2009, July 12–17). Sentinel-1, the European Radar Constellation I. *IEEE IGARSS Symposium, Cape Town, South Africa.*

Ferro-Famil, L., Reigber, A., Pottier, E., & Boerner, W. M. (2003, October). Scene characterization using sub-aperture polarimetric SAR data. *IEEE Transactions on Geoscience and Remote Sensing*, *41*(10).

Jakeman, E., & Pusey, P. (1976, November). A model for non-Rayleigh sea echo. *IEEE Transactions on Antennas and Propagation*, *24*(6).

Mattia, F. (2011). Coherent and incoherent scattering from anisotropic tilled soil surfaces. *Waves in Random and Complex Media*, *21*(2), 278–300.

Moreira, A. (1992, July). Real-time synthetic aperture radar (SAR) processing with a new subaperture approach. *IEEE Transactions on Geoscience and Remote Sensing*, *30*, 714–722.

Ouchi, K., Wang, H., Ishitsuka, N., Saito, G., & Mohri, K. (2006). On the Bragg scattering observed in L-band synthetic aperture radar images of flooded rice fields. *IEICE Transactions on Communications*, *E89-B*(8).

Quegan, S., Le Toan, T., Yu, J. J., Ribbes, F., & Floury, N. (2000). Multitemporal ERS SAR analysis applied to forest mapping. *IEEE Transactions on Geoscience and Remote Sensing*, *38*, 741–753.

Raney, R. K., Gray, A. L., & Princz, J. G. (1988). An effect of coherent scattering in spaceborne and airborne SAR images. *International Journal of Remote Sensing*, *9*(5).

Shin, R. T., & Kong, J. A. (1984). Scattering of electromagnetic waves from a randomly perturbed quasiperiodic surface. *Journal of Application Physics*, *56*(1).

Ulaby, F. T., Kouyate, F., Adrian, A. K., & Sieber, A. J. (1982, October). A backscatter model for a randomly perturbed periodic surfaces. *IEEE Transactions on Geoscience and Remote Sensing*, *GE-20*(4).

Ulander, L., & Le Toan, T. (1999). Bragg-scattering resonance in VHF-SAR forestry data. *Proceedings IEEE IGARSS '99*, *vol. 4*.

Wegmüller, U. (1990, August). The effect of freezing and thawing on the microwave signatures of bare soils. *Remote Sensing of Environment*, *33*(2), 123–135.

Wegmüller, U., Cordey, R. A., Werner, C., & Meadows, P. J. (2006). Flashing fields in nearly simultaneous ENVISAT and ERS-2 C-Band SAR images. *IEEE Transactions on Geoscience and Remote Sensing*, *44*(4).

Wegmüller, U., Santoro, M., Werner, C., Strozzi, T., Wiesmann, A., & Lengert, W. (2009). DEM generation using ERS–ENVISAT interferometry. *Journal of Applied Geophysics*, *69*, 51–58, doi:10.1016/j.jappgeo.2009.04.002.

Wegmüller, U., Santoro, M., Werner, C., Marzahn, P., Fischer, G., Ludwig, R., Mattia, F., Satalino, G., & Balenzano, A. (2010, May). Understanding directionality in surface scattering by imaging radar. *Final Report*. : ESA/ESTEC Contract n. 21659/08/NL/LVH.

Yueh, H. A., Shin, R. T., & Kong, J. A. (1988). Scattering of electromagnetic waves from a periodic surface with random roughness. *Journal of Application Physics*, *64*(4).

Zribi, M., Taconet, O., Ciarletti, V., & Vidal-Madjar, D. (2002, September 10). Effect of row structures on radar microwave measurements over soil surface. *International Journal of Remote Sensing*, *23*(24).

2.3 Paper III: ISPRS - Assessment of soil surface roughness statistics for microwave remote sensing applications using a simple photogrammetric acquisition system

As a consequence of the different roughness scales and occurring problems in Paper I, related to the small acquisition area of the measurement system, Paper III describes the development of a new, simple and efficient roughness acquisition system. In a very detailed analysis, the utilization of the system has been studied and evaluated in the context of representativeness of the calculated roughness values. For the proposed roughness value autocorrelation length l, an efficient method was proposed, which allows l to be calculate from 3D datasets quickly using geostatistics and variogram analysis. In this paper, a method was established to quantify the impact of the sample size on the derived roughness values. Therefore, the roughness values were calculated over a wide range of different sample sizes using a moving window-based approach, which also accounts for anisotropic effects. Further more in this paper, the performance of the system is evaluated compared to synthetic profile measurements, extracted from the generated digital surface models. It was shown, that the developed system is more robust in the assessment of roughness values compared to conventional profile measurements.

Marzahn, P., Rieke-Zapp, D. and Ludwig, R. Assessment of Soil Surface Roughness Statistics for Microwave Remote Sensing Applications using a Simple Photogrametric Acquisition System *ISPRS*, **2012**, 72, 80-89

ISPRS Journal of Photogrammetry and Remote Sensing 72 (2012) 80–89

Contents lists available at SciVerse ScienceDirect

ISPRS Journal of Photogrammetry and Remote Sensing

journal homepage: www.elsevier.com/locate/isprsjprs

Assessment of soil surface roughness statistics for microwave remote sensing applications using a simple photogrammetric acquisition system

Philip Marzahn [a,*], Dirk Rieke-Zapp [b], Ralf Ludwig [a]

[a] Department of Geography, Ludwig-Maximilian University Munich, Luisenstrasse 37, 80333 Munich, Germany
[b] Institute of Geological Sciences, University of Bern, Baltzerstrasse 1+3, 3012 Bern, Switzerland

ARTICLE INFO

Article history:
Received 21 July 2011
Received in revised form 22 April 2012
Accepted 1 June 2012

Keywords:
Photogrammetry
Soil surface roughness
Remote sensing
SAR
Soil science

ABSTRACT

In this paper we present a simple and efficient method to measure soil surface roughness in an agricultural environment. With the deployed system one can generate digital surface models (DSMs) with a minimum size of 1×2.5 m^2 extendable to any desired size. Using this approach, we generated a set of 22 DSM with sizes ranging from 2.5 m^2 to 4 m^2 and an *x*-, *y*-resolution of 2 mm. The DSM were acquired over different roughness conditions representing ploughed, harrowed as well as crusted fields. For roughness characterization we calculated different roughness indices (RMS-height *s*, autocorrelation length *l*). In an extensive statistical investigation we show the behavior of the roughness indices for different acquisition sizes of the proposed method. Results indicate, compared to results from profiles generated out of the dataset, that using a three dimensional measuring device, the calculated roughness indices are more robust in their estimation. Results also indicate a strong directional dependency of the proposed roughness indices.

1. Introduction

Micro-scale soil surface roughness is a crucial parameter in a wide range of environmental applications. In the sense of soil erosion modeling applications, the role of soil surface roughness is quite well understood and investigated (Fohrer et al., 1999; Farres, 1987; Cremers et al., 1996; Helming et al., 2006). However, the availability of micro scale soil surface roughness information is still not sufficiently solved, introducing several soil erosion estimation errors especially at large-scale modeling applications (Cremers et al., 1996; De Roo et al., 1996). Remote sensing, especially in the microwave domain, offers the potential for monitoring surface features on the regional scale, thus theoretically allowing the retrieval of soil surface roughness for soil erosion studies (Marzahn and Ludwig, 2009; Schuler et al., 2002).

In the sense of soil moisture retrieval from space or airborne microwave sensors, the ambiguity of the received signal is still an unsolved problem due to the inherent dependency of the signal on both geometric and dielectric properties. While the dielectric properties of a natural medium (e.g. soil) are directly given by the soil water content, soil texture, bulk density and soil temperature (Dobson and Ulaby, 1981, 1986; Dobson et al., 1985), the geometrical properties of a surface correspond to the roughness of the soil surface (Dobson and Ulaby, 1981). For single-polarized single-frequency SAR systems this ambiguity cannot be solved leading to large soil moisture retrieval errors (Hajnsek et al., 2003; Verhoest et al., 2008). By using multi-polarized multi-frequency SAR systems or multi-temporal SAR acquisitions it is possible to invert both soil moisture and soil surface roughness separately (Allain et al., 2003; Hajnsek et al., 2003, 2009). However, available soil moisture retrieval algorithms lead to sufficient results with acceptable root mean square errors only in experimental studies and not in an operational use (Loew et al., 2008; Verhoest et al., 2008). One of the main reasons for this insufficiency is the parametrization of soil surface roughness and its description in the available backscatter models (Lievens et al., 2009; Verhoest et al., 2008).

Regarding a natural soil surface in the environment, soil surface roughness is a superimposition of different roughness scales. According to Roemkens and Wang (1986) soil surface roughness can be divided into several roughness classes addressing the scale dependency of the appearing roughness spectra (see Table 1). In addition Allmaras et al. (1966) classified roughness into two terms due to their geometrical appearance: orientated and random roughness. While orientated roughness is dependent on the tillage tool or general slope effects, the latter is the result of the fortuitous occurrence of peaks and depressions resulting from soil clods and organization of aggregates which cannot be addressed to orientated roughness (Allmaras et al., 1966).

* Corresponding author. Tel.: +49 (0)89 2180 6698; fax: +49 (0)89 2180 6675.
E-mail address: p.marzahn@iggf.geo.uni-muenchen.de (P. Marzahn).

0924-2716/$ - see front matter © 2012 International Society for Photogrammetry and Remote Sensing, Inc. (ISPRS) All rights reserved.
http://dx.doi.org/10.1016/j.isprsjprs.2012.06.005

Table 1
Roughness classification after Roemkens and Wang (1986).

Roughness class	Scale (mm)	Topographic elements
Micro roughness	⩽2	Texture dependent roughness, very small soil aggregates
Random roughness	2–200	Soil aggregates and clods
Orientated roughness	200–400	Rows, tillage patterns
Higher order roughness	⩾400	Slope, field borders

In classical approaches, soil surface roughness is described as a single scale random stationary process which can be characterized by two terms: a) a vertical component, characterized by the standard deviation of the height values (RMS Height *s*) compared to a reference plane (e.g. the mean height), and b) a horizontal component, numerically described by an autocorrelation function and length (*ACF, l*) (Fung et al., 1992). With respect to the complexity and superimposition of different roughness scales, several studies considered soil surface roughness as fractals or self affine surfaces (Zribi et al., 2000; Sommer, 1997). Fractals are based on the formulations of Mandelbrot and Benoait (1995) describing a self affinity at different scales of irregular and fragmented structures. However, there is considerable uncertainty in the parametrization of soil surface roughness which led to enormous soil moisture retrieval errors (Verhoest et al., 2008). Bryant et al. (2007) reported that the main retrieval errors are the result of differences in soil roughness parametrization due to different roughness measurement techniques and transect analysis. While the common measurement technique for soil surface roughness uses mesh boards or needle profilers (Hajnsek et al., 2003; Bryant et al., 2007), recent studies used laser profilers (Davidson et al., 2000; Alvarez-Mozos et al., 2009) or three-dimensional high-resolution photogrammetric approaches (Marzahn and Ludwig, 2009; Blaes and Defourny, 2008).

Several studies have shown the scale dependency of different roughness indices. Davidson et al. (2000) have shown an increasing behavior of *s* and *l* with increasing profile length. In a theoretical experiment, Lievens et al. (2009) confirmed this behavior using Monte Carlo simulation techniques and synthetic profiles. However, this is only based on 1d profile data. For three-dimensional data, little information is available on the behavior of the proposed roughness indices. Taconet et al. (2007) investigated the reliability of different roughness indices with increasing acquisition size, using a photogrametric approach. However, they only determined a certain percental error for reduced acquisition sizes based on the larger initial acquisition size defining the true roughness index.

In this study, we will investigate and evaluate the behavior of different roughness indices in regard to their spatial sampling size and sampling form. We therefore introduce a simple and efficient photogrammetric acquisition setup Section 2.2, and analyze the derived roughness values using (geo-) statistical analysis in detail Section 3.2.

2. Methods

2.1. Description of soil surfaces

In order to characterize a wide range of roughness conditions, 22 samples have been acquired on different agricultural fields, representing surface conditions from smooth (crusted) fields to rough ploughed fields at two different test sites – Steinbeissen and Puch. Both test sites are part of the SMOS CalVal experimental campaign (Schlenz et al., 2010a,) located in Bavaria, Germany. While the Steinbeissen test site represents a typical Bavarian agricultural landscape, located in Lower Bavaria next to the village Landau an der Isar, the Puch test site consists of the fields of a research farm, operated by the Bavarian agency for agriculture (LfL), located near the village Puch, approximately 30 km west of Munich.

The initial campaign took place over the Steinbeissen test site in late July 2009. The region is mainly agricultural in character and the main crops are winter wheat, winter barley, corn and sugar beet. During the campaign most of the crops had reached their mature stadium and several cereal fields were already harvested. Therefore several tillage operations, mainly ploughing and grubbing using a row cultivator, were ongoing during the campaign. Four different fields were selected, representing different roughness conditions within the test site. The main soil texture of the sample points is loess loam, which contains a high fraction of silt. Sample points SP 11-45 were acquired over the Steinbeissen test site.

The second and third campaign took place at the Puch test site. As the Puch test site is an experimental farm, various crops and tillage practices are available. However the main crops are winter rape, winter wheat and potatoes. For this study a winter rape field was chosen to measure soil surface roughness on a multi-temporal basis. Therefore roughness was measured in October 2009 and March 2010 over the same field and the same locations. In October 2009 winter rape was recently sown, however it was already well developed, thus preserving the seedbed structure against splash erosion. The already developed vegetation layer was carefully removed from the scene without disturbing the surface conditions during the measurements. In March 2010 the soil surface was crusted due to rainfall events and the long winter season in southern Bavaria. The main soil type of the sample points is sandy loam. Sample points SP 51-64 were acquired over the Puch test site. Table 2 summarizes the main characteristics of the sample points.

2.2. Acquisition setup

In this section we will describe the acquisition setup, which consists of customized Canon EOS 5D digital camera and reference frame marked with targets. The derivation of the DSM is done with *Leica Photogrammetry Suite 9.3* (LPS) Software.

2.2.1. Camera description

Using photogrametric approaches in surface reconstruction requires high-precision cameras with respect to interior orientation. Metric cameras satisfy such requirements at high costs. In recent years, working with cameras that are not particularly designed for the requirements of photogrametry has become common in close range applications (Rieke-Zapp, 2010). While one can achieve high precision results with such cameras under several circumstances, it is well known that the geometric stability of these cameras is the limiting factor for the accuracy that can be achieved (Chandler et al., 2005; Rieke-Zapp and Nearing, 2005; Rieke-Zapp, 2010). While mechanical problems are highlighted to be the main sources for geometrical instability, recent studies have shown that mechanical fixation of the lens and/or the sensor help increase the accuracy in object space (Rieke-Zapp and Nearing, 2005; Rieke-Zapp et al., 2009).

In this study we use a customized Canon EOS 5D with a Canon EF 2/35 mm lens. Table 3 summarizes the characteristics of the EOS 5D and its calibration results. As shown by Rieke-Zapp et al. (2009), the off-the-shelf Canon 5D in combination with the Canon EF 35 mm lens produces a maximum absolute Length Measurement Error (LME) of 330 μm, without fixation of the focusing tube at a maximum object distance of 2.5 m. Fixing the lens by placing epoxy resin between the focusing tube and the outer lens tube reduces the maximum absolute LME to 47 μm. The fixation of

Table 2
Characteristics of the sample points for roughness measurements.

Sample point	Preparation status	Characteristics
SP 11–13	Ploughed	Large soil clods with several plant residua
SP 11p–13p	Ploughed	Large soil clods with several plant residua, perpendicular to rows
SP 21–23	Crusted	Smooth crusted field, recently harvested, rape seed residua
SP 31–35	Harrowed	Recently harrowed field, random appearance of soil aggregates
SP 51–54	Seedbed structure	Recently prepared seedbed under winter rape, 24 mm precipitation received
SP 61–64	Crusted	Smooth soil surface under winter rape after 291 mm precipitation received

Table 3
Canon EOS 5D characteristics and calibration results. Calibration with Aicon 3D studio (Aicon 3d Systems, 2009) – parameters converted for input in LPS. K1 = 3rd-order term of radial distortion correction, K2 = 5th-order term of radial distortion correction, K3 = 7th-order term of radial distortion correction, P1 and P2 = coefficient of decentering distortion.

Parameter	Values	Standard error
Camera	Canon EOS 5D	–
Lens	Canon EF 2/35 mm, fixed focus at 2.5 m	–
Resolution	4368 × 2912 pixels	–
Pixel width, *xy* (mm)	0.0082	–
Focal length, *c* (mm)	35.8919	0.0000
Principal point offset, *xp* (mm)	−0.2026	0.0000
Principal point offset, *yp* (mm)	0.2092	0.0000
K1 (mm)	7.30312e−005	8.2836e−008
K2 (mm)	−5.30725e−008	5.535e010
K3 (mm)	−2.33223e−011	1.1034e−012
P1 (mm)	3.2677e−005	1.296e−007
P2 (mm)	−1.3050e−005	1.167e−007

the Canon EF 35 mm lens was done by "Photogrammetrie Perrinjaquet AG" Guemmlingen, Switzerland.

2.2.2. Reference frame

Since LPS needs ground control points (GCPs) with known coordinates for the calculation of the exterior orientation, a reference frame was designed providing 28 horizontally and vertically distributed GCPs. To keep the reference frame handy, the horizontal size of the lightweight aluminum frame is set to $2.5 \times 1\ m^2$. Fig. 1 shows the reference frame as well as a detailed view of a marked GCP. Co-ordinates of the reference frame were measured with a caliper ruler with an accuracy of 0.10 mm in *x, y, z* direction. To cover an area inside the frame with sufficient resolution, six images were necessary with a forward overlap of 60% and a sidelap of 50%. Table 4 summarizes the image acqusition schedule for the coverage of each frame.

In this case we relied on the normal (nadir) case of photogrammetry which appeared most natural for our needs. Wackrow and Chandler (2008, 2011) on the other hand have shown that especially when working with cameras where the interior orientation is not well defined, a convergent setup of the camera positions can be favorable, reducing systematic errors in DSMs.

To ensure that the roughness measurements are not limited to the acquisition size of the frame, an approach is developed which allows for an acquisition of several consecutive subplots which can be merged to a single roughness plot during post processing using image matching techniques. Therefore the frame is levelled along an exact horizontal plane with a given length. After the images for one frame are acquired, the frame is moved to the next position with an overlap of 30%. Fig. 2 shows this approach in a schematic manner. During post processing, for each subplot a DSM is generated in its local coordinate system. To merge the subplots to a single plot, homogenous points were calculated in the overlapping regions using a cross correlation aproach and the offsets of the (homogenous) points in the *x*-, *y*-direction were

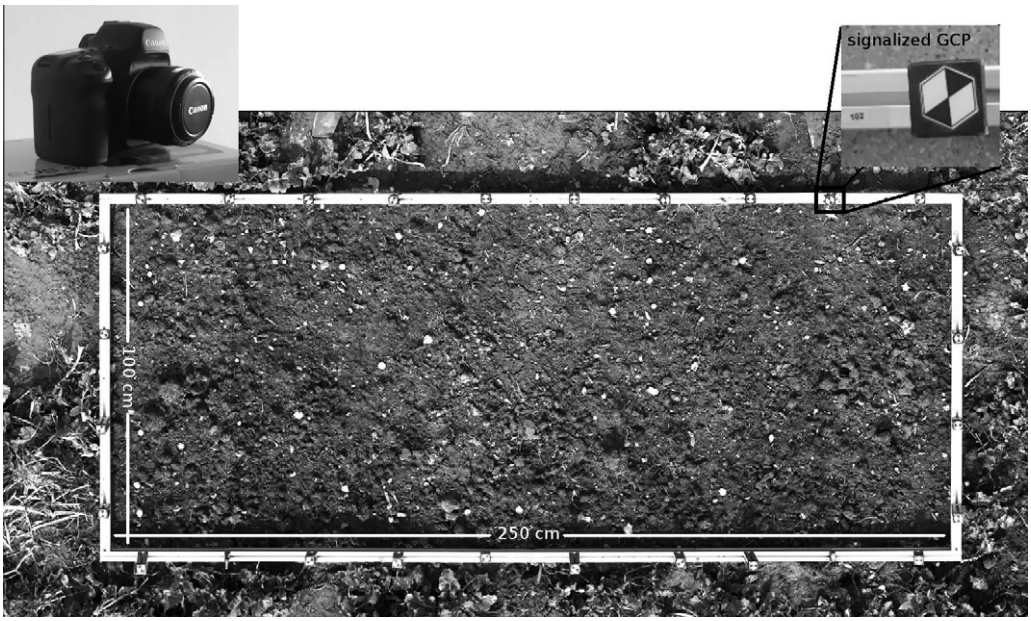

Fig. 1. Reference frame for relative orientation of the images acquired for DSM generation and detailed view of a GCP.

Table 4
Acquisition plan for the coverage of the reference frame.

Parameter	Values
Camera altitude, *h* (mm)	2500
Base length, *b* (mm)	1000
Height to base ratio, *h/b*	2.5
Image scale	1:69.65
Ground sample distance (mm)	0.57
Forlap, *x* (%)	50
Sidelap, *y* (%)	60
Number of images per strip	3
Number of strips	2

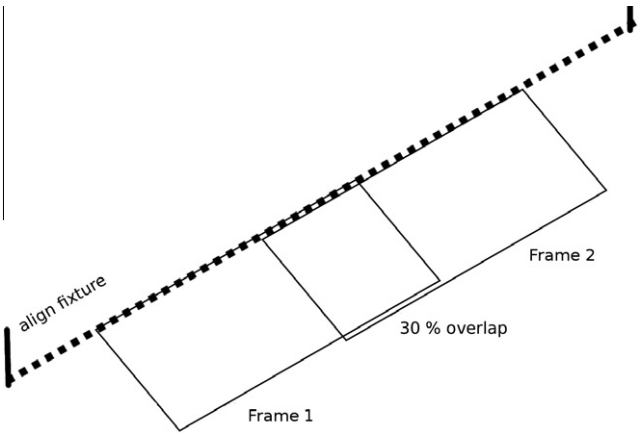

Fig. 2. Acqusition scheme for the sampling of roughness measurements with a given length and its components using a single reference frame.

calculated. Afterwards each subplot is (linearly) shifted to its final position in the global DSM.

2.2.3. Generation of Digital Surface Models (DSMs)

For the generation of the DSMs *Leica Photogrametry Suite 9.3* (LPS) (Leica Geosystems, 2010) is used. LPS uses epipolar constraints during image matching based on the established exterior orientation of the imagery, the exterior orientation of the block first has to be established. We therefore used the GCPs installed on the frame and improved the original camera calibration by using the Ebner model (Ebner, 1976) which is implemented in LPS. After the exterior orientation has been established, the DSMs were generated using different matching strategies depending on the roughness classes occurring. Table 5 summarizes the applied strategies based on a ground pixel size of 0.57 mm. For rougher surfaces a larger search window is chosen. Indeed, the size of the correlation window is smaller for rougher surfaces due to the significant topographic changes within the window. This is based on the fact that the smoother surface images are lower in contrast and therefore a larger correlation window is necessary to obtain large correlation coefficients. Using an epipolar based approach, Linder (2009) suggests a correlation coefficient threshold for matching for such applications of 0.65. In a laboratory experiment, Heng et al. (2010) as well as Rieke-Zapp and Nearing (2005) used a correlation coefficient of 0.80. In our investigations, a threshold of 0.75 seems to be appropriate for a successful matching, as Fig. 3 (left) reveals, yielding good results based on visual inspection. As obvious, most correlation coefficients during DSM generation are above this threshold. After successful generation of DSMs, a 7×7 pixel low pass filter was applied to remove peaks, smoothen the DSMs and resample to a regular resolution of 2×2 mm^2.

Table 5
Matching strategies used during DSM generation as required by LPS based on a pixel size in ground space of 0.57 mm in the *x* and *y* direction.

Roughness class	Search window (pixel)	Correlation window (pixel)	Correlation coefficient threshold
Ploughed	41×3	7×7	0.75
Harrowed I	33×3	7×7	0.75
Harrowed II	25×3	7×7	0.75
Seedbed	17×3	9×9	0.75
Smooth crusted	11×3	11×11	0.75

2.3. Roughness indices

In order to describe soil surface conditions numerically for remote sensing applications, roughness indices are necessary. In the literature several roughness indices are described. Sommer (1997) and Taconet et al. (2007) give a good introduction to the available roughness indices. In this study, the focus is on the application of the RMS height *s* and the autocorrelation length *l* since both are roughness indices used by default in radar remote sensing applications for the characterization of soil surface roughness (Davidson et al., 2003; Verhoest et al., 2008; Zribi et al., 2000). While the RMS height describes the vertical roughness component as the standard deviation of the heights (Z) to a reference height ($\overline{Z}$),

$$s\ [\mathrm{cm}] = \sqrt{\frac{\sum_{i=1}^{n}(Z_i - \overline{Z})^2}{n-1}} \tag{1}$$

the autocorrelation length *l* describes the horizontal component of the roughness spectra. While, *l* is usually determined along 1d-profiles, the derivation of *l* using three-dimensional roughness measurements is more complex. For an efficient estimation of *l*, a variogram analysis was used and inverted the autocorrelation function (ACF) from a calculated theoretical omnidirectional variogram ($\tilde{\gamma}$), where *l* is defined as the distance (h) at which the ACF drops under e^{-1} (Blaes and Defourny, 2008). This implies an exponential fit of the theoretical variogram and therefore of the ACF. Several models were tested, however best fit was always achieved with an exponential model (data not shown). Blaes and Defourny (2008) and Davidson et al. (2000) reported similar observations.

The theoretical variogram ($\tilde{\gamma}$) with an exponential shape is fitted to the experimental variogram ($\hat{\gamma}$), which is defined as (Webster and Oliver, 2007)

$$\hat{\gamma}(h) = \frac{1}{2n}\sum_{i=1}^{n}[Z(x_i) - Z(x_i + h)]^2 \tag{2}$$

From the theoretical variogram ($\tilde{\gamma}$) the ACF ($\tilde{\rho}$) can be derived as follows:

$$\tilde{\rho}(h) = 1 - \frac{\tilde{\gamma}(h)}{\tilde{\gamma}(\infty)} \tag{3}$$

where $\tilde{\gamma}(h)$ is the semi variance at distance h between two points and $\tilde{\gamma}(\infty)$ is the semi variance at distance where the sill of the variogram is reached. For the assumed exponential model, where the sill is asymptotically approached, $\tilde{\gamma}(\infty)$ corresponds to the distance where 95% of the sill is reached (Blaes and Defourny, 2008).

Due to the good resolution of DSMs, *l* was calculated using only a random sub sample of 15000 points, while *s* was calculated for the whole DSM.

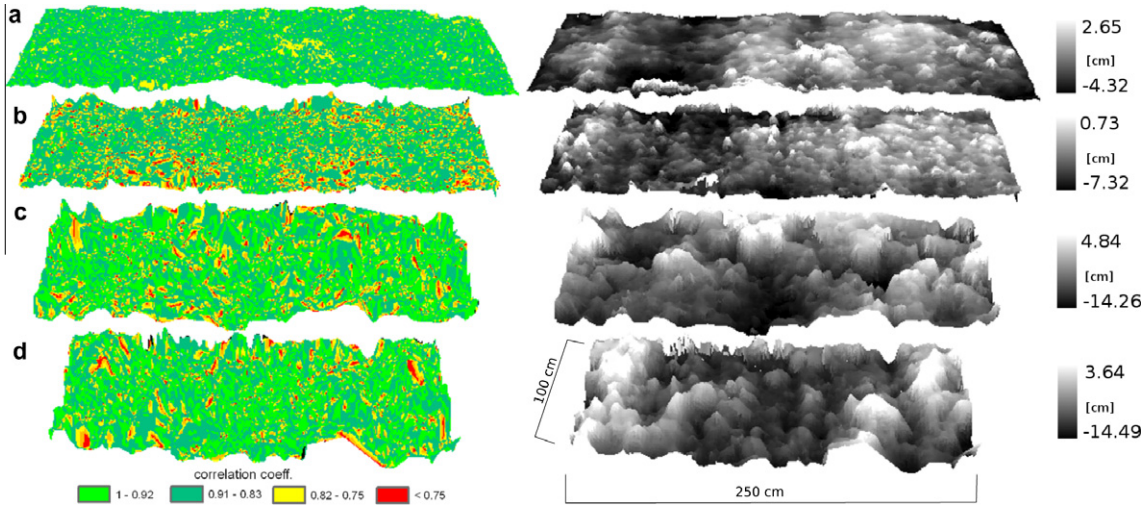

Fig. 3. Results of DSM generation (2× exaggerated heights), from top to bottom, of (a) crusted (SP61), (b) seedbed (SP51), (c) harrowed (SP31) and (d) ploughed surface (SP12). Left: Quality Map draped over DSM, which shows the correlation coefficients of the matching process during DSM generation. Red pixels ($r \leqslant 0.75$) indicate that no match was possible, the height value is then interpolated from its surrounding pixels. Right: Derived DSM values [cm] resulting from applying a 7 × 7 pixel low pass filter.

Table 6
Overall accuracy of generated DSMs compared to GCPs (RMSE = root mean square error (mm); ME = mean error (mm); MAE = mean absolute error (mm)).

Parameter	Value (mm)
Mean RMSE	1.77
Min. RMSE	0.5
Max. RMSE	3.01
ME	−0.98
MAE	1.45

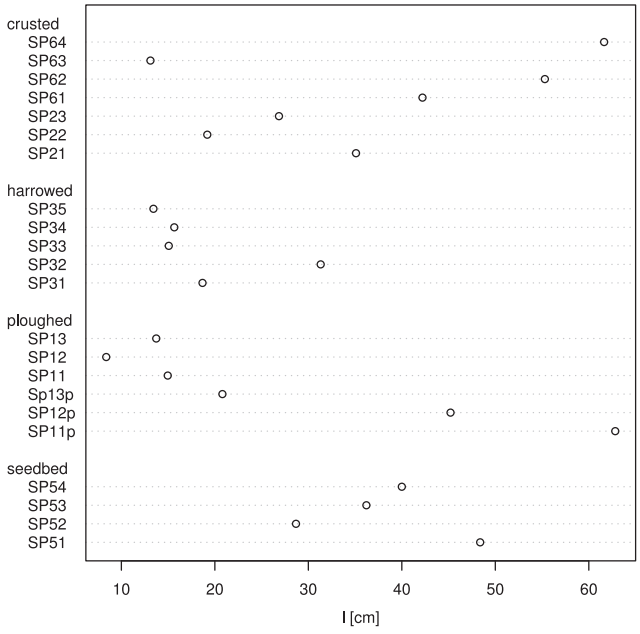

Fig. 4. Calculated autocorrelation length values *l* [cm] for each sample plot. Sample size for each plot is 2.5 m^2, except for SP54 and SP64 where sample size is 4 m^2.

3. Results and discussion

3.1. DSM quality

The generated DSMs showed good accuracy with an overall RMSE of 1.77 mm compared to GCPs as shown by Table 6. As reported by Lievens et al. (2009), an acquisition setup accuracy below 2 mm produces a negligible error in soil moisture estimation.

As Fig. 3 reveals, systematic errors such as dome effects (Wackrow and Chandler, 2011) were not apparent during the matching process. However, for the rough ploughed and/or harrowed surface, several mismatches could be identified, which originated due to shadow effects of the soil aggregates in the images. Image acquisitions from several positions could eliminate this problem in future investigations. Indeed, for the smoother surfaces several low correlation values can be observed, resulting in possible mismatches or in gaps. Those low correlation coefficients resulting from lower contrast in the images not enhanced during post processing could not be absorbed by the larger correlation window size (see Table 5). As proposed by Vozikis et al. (2003), local optimization using Hough transformation could help improving

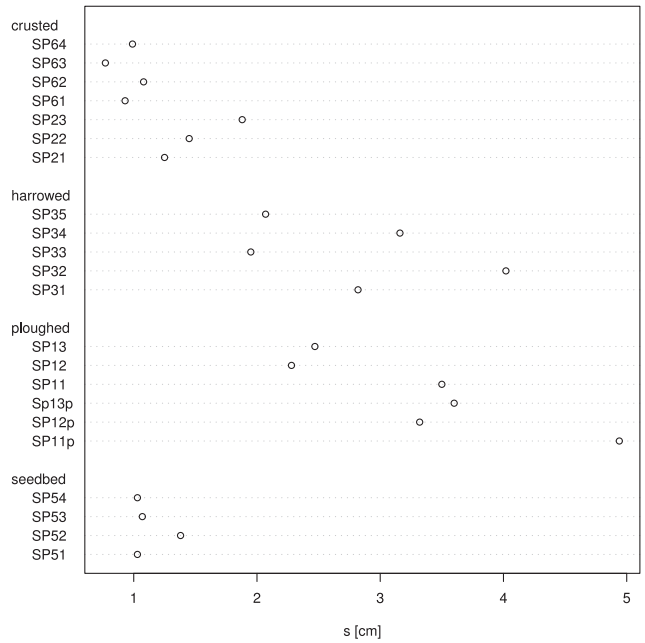

Fig. 5. Calculated RMS height values *s* [cm] for each sample plot. Sample size for each plot is 2.5 m^2, except for SP54 and SP64 where sample size is 4 m^2.

contrast disparities within the imagery due to the lighting conditions. Indeed, a visual inspection of the images allows a good discrimination of the soil aggregates and even small aggregates can be distinguished easily as shown by Fig. 3.

3.2. Statistics of roughness indices

The roughness indices calculated from the DSMs are displayed in Figs. 4 and 5. There is a dependency of s on the different roughness conditions allowing to classify RMS height values s into different roughness classes. While the ploughed fields return a value for s in range of 2.3–5.0 cm, the harrowed fields show lower values ($2.0 \leqslant s \leqslant 4.0$ cm). Anisotropic effects can be observed for the ploughed sample points. While the samples perpendicular to the row direction (SP11p–SP13p) are in range of $3.6 \leqslant s \leqslant 4.9$ cm, the calculated values for s parallel to the row direction are significantly lower ($2.3 \leqslant s \leqslant 3.5$ cm) and have to be excluded for this classification. However, theses findings are only based on a small sample size ($n = 6$); further investigations have to verify this. Indeed, there is an overlap between the seedbed prepared fields and the slightly smoother crusted fields. While the seedbed prepared fields show s values in range of $1.0 \leqslant s \leqslant 1.5$ cm, the crusted surfaces have similar s values.

For autocorrelation length l this trend could not be observed, as the determined values for l are more randomly distributed. Verhoest et al. (2008) as well as Davidson et al. (2000) related this to a too short estimation length for l. Oh and Kay (1998) suggested for a precise measurement of l a minimum length of the acquisition size of $200l$. Using the highest obtained value for l (SP11p l = 62.8 cm), this would result in an acquisition length $A_x \approx 120$ m. Indeed, while SP51 (l = 48.4 cm) and SP52 (l = 28.7 cm) are sub DSMs of SP54, with an acquisition size of 4 m^2, SP54 gives a more realistic estimate with l = 40.0 cm. The lower value for l of SP52 is related to a wheel track occurring in the sampled area assuming an increase in roughness. With a row distance of 25 cm (±5 cm) the results for l are 1.5 times larger than the row separation.

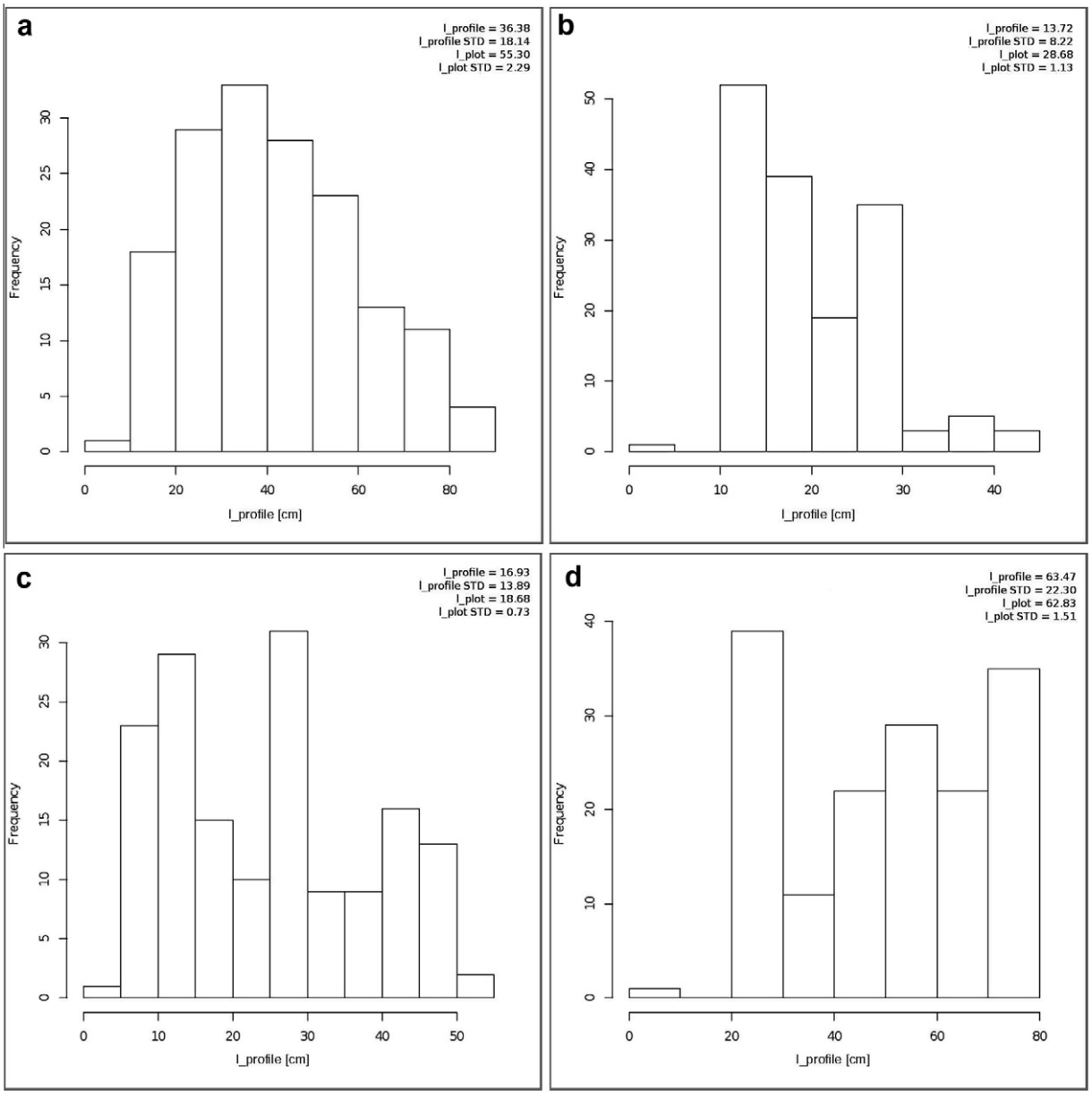

Fig. 6. Histogram of autocorrelation length for profile data ($l_{profile}$) in cm of a, (a) crusted (SP61), (b) seedbed (SP51), (c) harrowed (SP31), (d) ploughed (SP11) surface. (Upper right corner: $l_{profile}$ = modalvalue of the 500 profiles; l_{plot} = modalvalue of 500 calculations of l.)

For SP53 this is not valid, due to its acquisition direction being parallel to the row direction.

Regarding a multi-temporal analysis, which is an important point for soil erosion studies, both roughness indices are sensitive to changes in roughness conditions due to precipitation. As shown above, a sensitivity of the roughness indices to huge changes in roughness is given (e.g. ploughed, harrowed, crusted fields). In addition, it is also possible to detect small changes in roughness due to crusting effects by precipitation. As shown in Table 2, SP51-54 and SP61-64 are the same plots with a difference in received precipitation which causes a smoother appearance of the latter samples. In general, this smoothing could be quantified using the roughness indices and is visible by a decline of s and an increase in l (see Figs. 4 and 5). Indeed, the alteration is more prominent for the rougher sample point SP52 (SP62) where a wheel track is present. This could be related to the very smooth seedbed structure present at the acquisition date after sowing, such that a relative change in roughness is higher for the rougher sample point.

It is to notice that the small value of l = 13.11 cm (SP63) can be directly related to the poor accuracy of the DSM SP63 with an RMSE of 3.01 (see Table 6). Correspondingly, for s there is no significant impact.

3.2.1. Influence of acquisition type on roughness indices

As roughness indices are often determined along profiles, we calculated $s_{profile}$ and $l_{profile}$ along each image row (pixel line). As a result, we generated a set of 500 profiles for each DSM. To compare the obtained data, we calculated l_{plot} with a repetition of 500 for the whole dataset, since we used only a subset of data points for the calculation of l. Fig. 6 summarizes the statistics of four DSMs (ploughed, harrowed, seedbed, crusted) and shows the comparison between the profile data $l_{profile}$ and the results calculated for the whole plots (l_{plot}). Obviously, the values obtained for l_{plot}

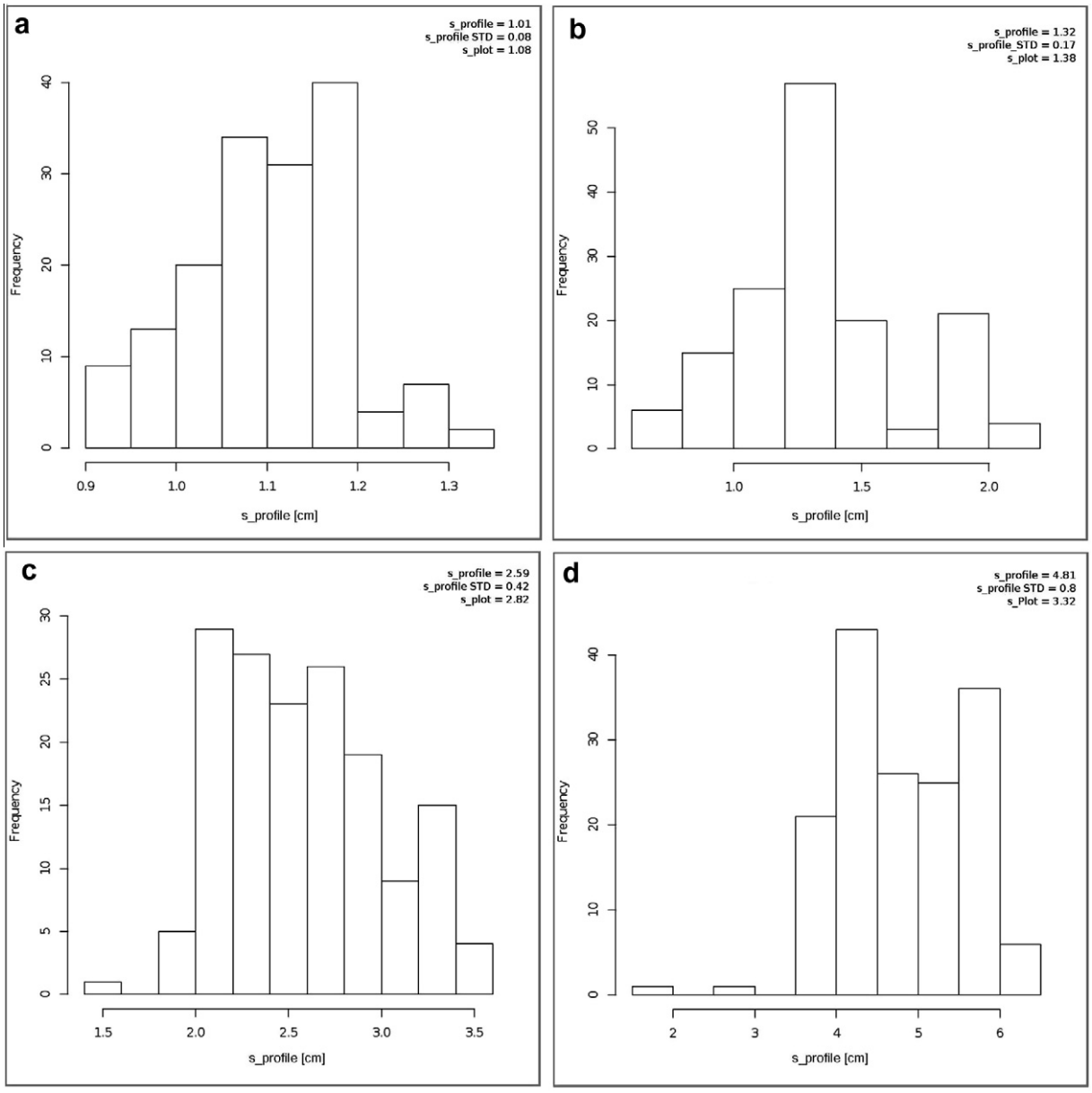

Fig. 7. Histogram of RMS Heights ($s_{profile}$) for profile data in cm of a, (a) crusted (SP61), (b) seedbed (SP51), (c) harrowed (SP31), (d) ploughed (SP11) surface. (Upper right corner: $s_{profile}$ = mean of 500 profiles, $s_{plot} = s$ for the whole plot.)

are more robust in their estimation than using only the values obtained from the single profiles ($l_{profile}$), as the standard deviation of the calculated $l_{profile}$ values reveals, which are on average ten times higher than the standard deviation for l_{plot}.

The same could be observed for s_{plot} (see Fig. 7). While the profile data gives a wide range of different $s_{profile}$-values ranging from $1.89 \leqslant s\,[\text{cm}] \geqslant 6.20$ for a ploughed surface (SP11), the estimates of s_{plot} for the whole acquisition area is more robust ($s_{plot} = 3.32$). However, a clear trend could be observed, as Fig. 8 shows. For smooth surfaces, the profiles give nearly the same results for $s_{profile}$ as for the whole plot standard deviation of r_{plot} STD = 0.17; RMSE = 0.15. Indeed, with an increase in roughness the results of $s_{profile}$ could misrepresent the values for s_{plot} and would result in an underestimation of s_{plot}. The standard deviation of $s_{profile}$ (STD = 0.53) as well as the larger RMSE of 0.64 support this assumption. Oh and Kay (1998) as well as Lievens et al. (2009) describe this as the number of average profiles needed for a robust estimation of the used roughness indices. However, as shown this is only reliable for smooth surfaces where an anisotropic impact is negligible contrary to rougher surfaces.

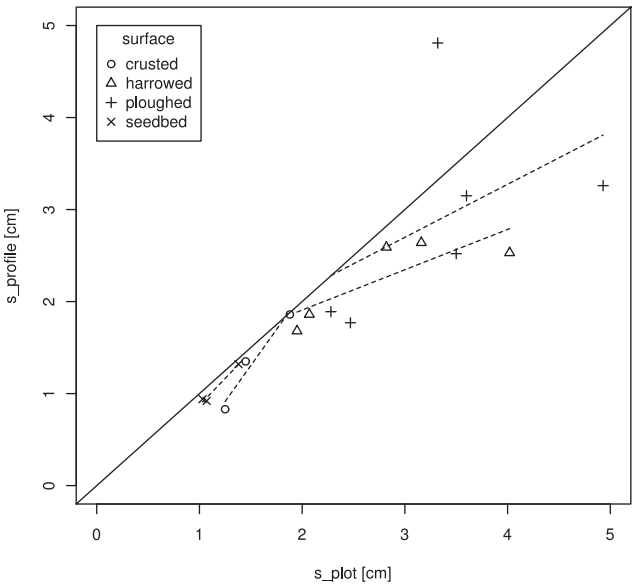

Fig. 8. Scatter plot of s_{plot} versus $s_{profile}$ values for all DSMs. Solid line corresponds to the zero error line. Dashed lines linear regression between s_{plot} and $s_{profile}$ for each surface type.

3.2.2. Influence of acquisition size on roughness indices

As both roughness indices are scale dependent (Davidson et al., 2000; Verhoest et al., 2008), the goal is to find the best acquisition size of DSMs for the characterization of roughness conditions. Taconet et al. (2007) introduced a relative accuracy approach for the evaluation of optimal DSM size. However, this approach has several drawbacks, as roughness can be considered as anisotropic (especially for rougher surfaces, as shown) and without the knowledge of the indices' true values it is not well suited for the determination of representative acquisition size. Therefore we propose the *Representative Elementary Area* (REA) approach according to the *Representative Elementary Volume* approach introduced by Bear (1972), which allows accounting for anisotropic effects of the soil surfaces using a moving window approach. Therefore we recalculated both roughness indices for various given window sizes. In our definition, the sample size of a given surface could be considered as representative when the calculated roughness indices are in range of the final estimation plus the accuracy of the acquisition setup (RMSE = 1.77 mm). Fig. 9 shows, as an example, the result of the REA approach for a given surface (SP12). The two horizontal dashed lines display the range at which the sample size could be considered representative. For small acquisition sizes, a wide range of different roughness values are determined, which were concentrated to a more precise value when increasing the acquisition size. Indeed, by having a closer look at the data, one could observe an increase from small acquisition sizes to larger ones for the mean $\bar{s}_A$ values (solid line). For nearly all surfaces, this increase of $\bar{s}_A$ could be described with a positive exponential fit.

For most surfaces, the optimum sample size is in good accordance with the sample size of the frame (see Fig. 10). However, for SP13, SP22 and SP53 the optimum sample size is larger than 2.5 m^2. Thus, for these sample points, the size of the sampled area

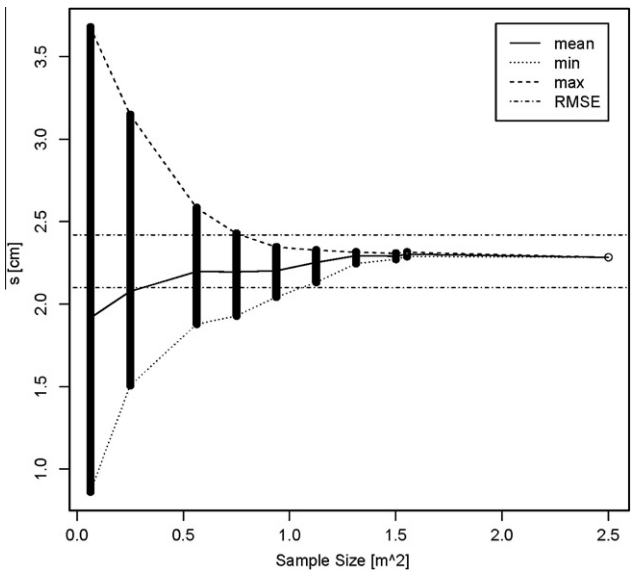

Fig. 9. Results of the REA approach for SP12. (Horizontal dashed lines (RMSE) display the acceptable range of variance in *s*.)

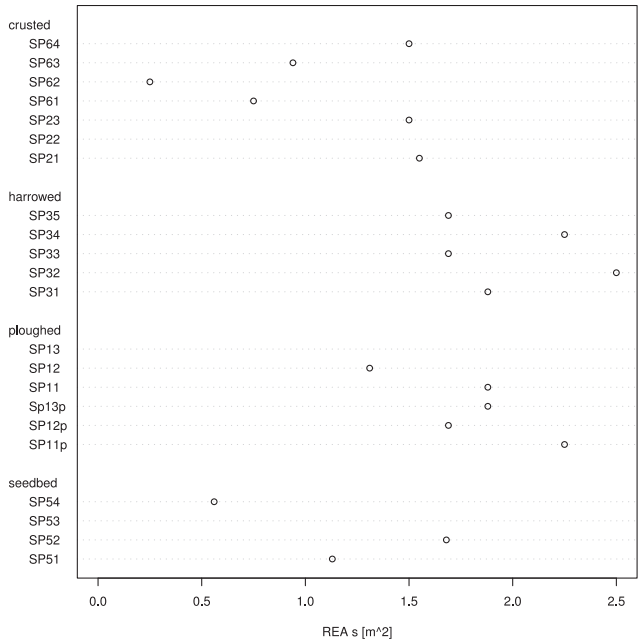

Fig. 10. Results of the REA s approach for the whole data set. For SP13, SP22 and SP53 the optimum sample size is larger than 2.5 m^2.

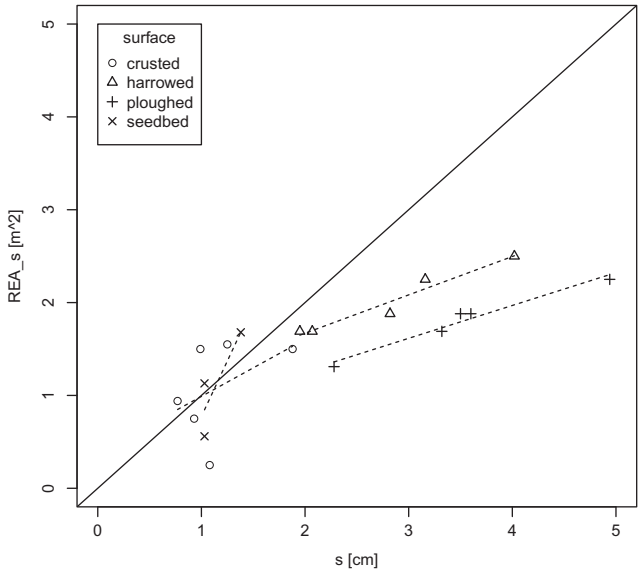

Fig. 11. Results of the REA approach vs. *s* values grouped by their surface appearance. (Black solid line zero error line, black dashed line linear trend of REA vs. *s*.)

is too small and leads to a misinterpretation of the true estimate. Indeed, there is no direct dependency of the acquisition size and *s*. However it is to observe that for smooth surface (small *s*) smaller acquisition sizes are necessary and for rougher surfaces larger ones. It is obvious that values of $s \leqslant 2$ cm could be reliably retrieved from acquisition areas in size of 2 m^2. Indeed, larger values for *s* up to 5 cm could be reliably retrieved by using an acquisition area up 3 m^2 (see Fig. 11).

4. Conclusions

In this paper we proposed a simple and practical approach for the measurement of soil surface roughness for microwave remote sensing applications. The deployed system consists of a consumer grade Canon EOS 5D digital camera with a customized Canon EF 35 mm lens and a reference frame providing ground control points for the photogrammetric derivation of digital surface models. The derived DSMs provide the basis for the quantitative characterization of soil surface roughness by means of RMS height values *s* and autocorrelation lengths *l* and showed a good accuracy compared to the known GCPs. With an overall RMSE of 1.77 mm, the impact for an error-prone soil moisture retrieval could be neglected (Lievens et al., 2009). Therefore the system is well suited for roughness parametrization in soil moisture modeling for microwave remote sensing applications.

In our investigations, of the acquired data the calculated index values allowed us to classify four different soil surface roughness classes: crusted surface, seedbed, harrowed and ploughed. While the harrowed and ploughed surfaces, by excluding the in-parallel acquisitions, could be clearly classified, the crusted surface and the seedbed showed overlapping values of *s*, which could be related to a very smooth seedbed. However, the classification is in good accordance with other studies (Alvarez-Mozos et al., 2009; Davidson et al., 2003).

The acquisition setup deployed allows an estimation of the directional effects in soil surface roughness quantification. By analyzing sample points acquired perpendicular and parallel to the row direction of the agricultural fields, a clear directional behavior is observable. While the in-perpendicular roughness indices indicated always a higher roughness, the in-parallel indices showed a smoother roughness pattern. This is especially valid for rougher surfaces, while for the smoother surface where no roughness pattern (e.g. seedbed, drill-rows) is present, the effect could be neglected. As we have shown with profile data generated from the DSMs, the anisotropic effects are more dominant for a roughness profile compared to the three dimensional approach. This is obvious when comparing the estimated roughness indices from both profile and plot data. While the first one gives a wide range of different roughness values, the estimated roughness values for the plot data are more robust. The variety of the estimated roughness values for the profile data is proportional to an increase in roughness. Thus, as shown, by using a profile measurement device, the estimated roughness values are less reliable leading to misinterpretations. Due to the anisotropic behavior of roughness, profile measurements are only valid for smooth surfaces. Contrary to most authors (Verhoest et al., 2008; Taconet et al., 2007; Lievens et al., 2009; Alvarez-Mozos et al., 2009) we conclude that roughness has to be considered as non isotropic, thus a 3d measurement device is preferable for the characterization of soil surface roughness

As most roughness indices are dependent on the acquisition size over which they are estimated, we tried to find the optimum sample size by using the REA approach. Results show that an acquisition size of 3 m^2 provides a good basis for the derivation of soil surface roughness indices. However for a smooth surface a smaller acquisition size up to 2 m^2 is sufficient. As the REA approach showed, an increase of *s* with an increase of the acquisition area could be observed. This is also in good accordance to values from the literature. The observed increase for the plot data is not very strong and could be described with an exponential shape.

Future investigations on soil surface roughness statistics should include the periodic roughness component in more detail. As the impact of the periodic component for backscatter modeling is not well understood, the deployed system gives the possibility to characterize this component over large acquisition sizes. In addition as we considered roughness as anisotropic, future investigations should also include narrow directional effects in roughness parametrization in only a few degrees width. As results from the *Flashing Fields!* study, Wegmuller et al. (2011) have shown that a very narrow change in the look vector of a microwave sensor causes a backscatter difference of several dB, it is to investigate if this could also be identified in roughness parametrization. As we have shown, for a width of 90° a significant impact on roughness retrieval could be observed.

References

Aicon 3d Systems, 2009. Aicon 3d Studio – User Manual (CD-ROM).

Allain, S., Ferro-Famil, L., Pottier, E., 2003. Surface parameter retrieval from polarimetric and multi-frequency SAR data. In: Proceedings of IEEE International Geoscience and Remote Sensing Symposium IGARSS '03, vol. 2, 21–25 July 2003, pp. 1417–1419.

Allmaras, R.R., Burwell, R.E., Larson, W.E., Holt, R.F., 1966. Total Porosity and Random Roughness of the Interrow Zone as Influenced by Tillage. USDA Conservation Research Report 7. USDA.

Alvarez-Mozos, J., Verhoest, N., Larranaga, A., Casalf, J., Gonzlez-Audfcana, M., 2009. Influence of surface roughness spatial variability and temporal dynamics on the retrieval of soil moisture from SAR observations. Sensors 9 (1), 463–489.

Bear, J., 1972. Dynamics of Fluids in Porous Media. American Elsevier.

Blaes, X., Defourny, P., 2008. Characterizing bidimensional roughness of agricultural soil surfaces for SAR modeling. IEEE Transactions on Geoscience and Remote Sensing 46 (12), 4050–4061.

Bryant, R., Moran, M.S., Thoma, D.P., Holifield Collins, C.D., Skirvin, S., Rahman, M., Slocum, K., Starks, P., Bosch, D., Gonzalez Dugo, M.P., 2007. Measuring surface roughness height to parameterize radar backscatter models for retrieval of surface soil moisture. IEEE Geoscience and Remote Sensing Letters 4 (1), 137–141.

Chandler, J.H., Fryer, J.G., Jack, A., 2005. Metric capabilities of low-cost digital cameras for close range surface measurement. The Photogrammetric Record 20 (109), 12–26.

Cremers, N.H.D.T., Dijk, P.M.V., Roo, A.P.J.D., Verzandvoort, M.A., 1996. Spatial and temporal variability of soil surface roughness and the application in

hydrological and soil erosion modeling. Hydrological Processes 10 (8), 1035–1047.
Davidson, M.W.J., Toan, T.L., Mattia, F., Satalino, C., Manninen, T., Borgeaud, M., 2000. On the characterization of agricultural soil roughness for radar remote sensing studies. IEEE Transactions on Geoscience and Remote Sensing 38 (2), 630–640.
Davidson, M.W.J., Mattia, F., Satalino, G., Verhoest, N.E.C., Le Toan, T., Borgeaud, M., Louis, J.M.B., Attema, E., 2003. Joint statistical properties of rms height and correlation length derived from multisite 1-m roughness measurements. IEEE Transactions on Geoscience and Remote Sensing 41 (7), 1651–1658.
De Roo, A.P.J., Offermanns, R.J.E., Cremers, N.H.D.T., 1996. Lisem: a single-event, physically based hydrological and soil erosion model for drainage basins. II: Sensitivity analysis, validation and application. Hydrological Processes 10 (8), 1119–1126.
Dobson, M.C., Ulaby, F., 1981. Microwave backscatter dependence on surface roughness, soil moisture, and soil texture: Part III – Soil tension. IEEE Transactions on Geoscience and Remote Sensing 19 (1), 51–61.
Dobson, M.C., Ulaby, F.T., 1986. Active microwave soil moisture research. IEEE Transactions on Geoscience and Remote Sensing 24 (1), 23–36.
Dobson, M.C., Ulaby, F.T., Hallikainen, M.T., El-Rayes, M.A., 1985. Microwave dielectric behavior of wet soil – Part II: Dielectric mixing models. IEEE Transactions on Geoscience and Remote Sensing 23 (1), 35–46.
Ebner, H., 1976. Self calibrating block adjustment. International Archives of Photogrammetry 21 (Part 3), 1–17.
Farres, P.J., 1987. The dynamics of rainsplash erosion and the role of soil aggregat stability. CATENA 14 (1–3), 119–130.
Fohrer, N., Berkenhagen, J., Hecker, J.M., Rudolph, A., 1999. Changing soil and surface conditions during rainfall: single rainstorm/subsequent rainstorms. CATENA 37 (3–4), 355–375.
Fung, A., Li, Z., Chen, K., 1992. Backscattering from a randomly rough dielectric surface. IEEE Transactions on Geoscience and Remote Sensing 30 (2), 356–369.
Hajnsek, I., Pottier, E., Cloude, S.R., 2003. Inversion of surface parameters from polarimetric SAR. IEEE Transactions on Geoscience and Remote Sensing 41 (4), 727–744.
Hajnsek, I., Jagdhuber, T., Schoen, H., Papathanassiou, K.P., 2009. Potential of estimating soil moisture under vegetation cover by means of PolSAR. IEEE Transactions on Geoscience and Remote Sensing 47 (2), 442–454.
Helming, K., Rubio, J.L., Boardman, J., 2006. Soil erosion across Europe: research approaches and perspectives. CATENA 68 (2–3), 71–72.
Heng, P.B.C., Chandler, J.H., Armstrong, A., 2010. Applying close range digital photogrammetry in soil erosion studies. The Photogrammetric Record 25 (131), 240–265.
Leica Geosystems, 2010. Leica Photogrammetry Suite v.9.3 Users Manual (CD-ROM).
Lievens, H., Vernieuwe, H., Alvarez-Mozos, J., De Baets, B., Verhoest, N., 2009. Error in radar-derived soil moisture due to roughness parameterization: an analysis based on synthetical surface profiles. Sensors 9 (2), 1067–1093.
Linder, W., 2009. Digital Photogrammetry A Practical Course. Springer, Berlin/Heidelberg.
Loew, A., Hajnsek, I., Schoen, H., Jagdhuber, T., Hoekman, D., 2008. Exploiting Longer Wavelength SAR Data for the Improvement of Surface Modelling. Tech. Rep. ESA Contract No. 19569/06/NL/HE. ESA.
Mandelbrot, Benoait, B., 1995. Les Objetcs Fractals. Champs, Flammarion, Paris.
Marzahn, P., Ludwig, R., 2009. On the derivation of soil surface roughness from multi parametric PolSAR data and its potential for hydrological modeling. Hydrology and Earth System Sciences 13, 381–394.
Oh, Y., Kay, Y.C., 1998. Condition for precise measurement of soil surface roughness. IEEE Transactions on Geoscience and Remote Sensing 36 (2), 691–695.
Rieke-Zapp, D.H., 2010. A digital medium-format camera for metric applications - alpa 12 metric. The Photogrammetric Record 25 (131), 283–298.
Rieke-Zapp, D., Nearing, M., 2005. Digital close range photogrammetry for measurement of soil erosion. The Photogrammetric Record 20 (109), 69–87.
Rieke-Zapp, D., Tecklenburg, W., Peipe, J., Hastedt, H., Haig, C., 2009. Evaluation of the geometric stability and the accuracy potential of digital cameras – comparing mechanical stabilisation versus parameterisation. ISPRS Journal of Photogrammetry and Remote Sensing 64 (3), 248–258.
Roemkens, M.J., Wang, J.Y., 1986. Effect of tillage on surface roughness. Transactions on ASAE 29, 429–433.
Schlenz, F., Dall'Amico, J., T., Loew, A., Mauser, W., 2010a. SMOS validation in the upper danube catchment (UDC): a status report eight month after launch. In: Proceedings of ESA Living Planet Symposium 2010 Bergen, Norway.
Schlenz, F., Gebhardt, T., Loew, A., Marzahn, P., Mauser, W., 2010b. L-band radiometer experiment in the SMOS test site upper danube. In: Proceedings of ESA Living Planet Symposium 2010 Bergen, Norway.
Schuler, D.L., Lee, J.-S., Kasilingam, D., Nesti, G., 2002. Surface roughness and slope measurements using polarimetric SAR data. IEEE Transactions on Geoscience and Remote Sensing 40 (3), 687–698.
Sommer, H., 1997. Quantifizierung der Rauigkeit von Bodenoberflaechen und Simulation hydromechanischer Prozesse anhand von Oberflaechenmodellen. FAM-Bericht 18, Forschungsverbund Agraroekosysteme Muenchen.
Taconet, O., Ciarletti, V., 2007. Estimating soil roughness indices on a ridge-and-furrow surface using stereo photogrammetry. Soil and Tillage Research 93 (1), 64–76.
Verhoest, N., Lievens, H., Wagner, W., Alvarez-Mozos, J., Moran, M., Mattia, F., 2008. On the soil roughness parameterization problem in soil moisture retrieval of bare surfaces from synthetic aperture radar. Sensors 8 (7), 4213–4248.
Vozikis, G., Jansa, J., Fraser, C., 2003. Alternative sensor orientation models for high-resolution satellite imagery. Photogrammetrie, Fernerkundung, Geoinformation (PFG) 2003 (12), 179–186.
Wackrow, R., Chandler, J.H., 2008. A convergent image configuration for DEM extraction that minimises the systematic effects caused by an inaccurate lens model. The Photogrammetric Record 23 (121), 6–18.
Wackrow, R., Chandler, J.H., 2011. Minimising systematic error surfaces in digital elevation models using oblique convergent imagery. The Photogrammetric Record 26 (133), 16–31.
Webster, R., Oliver, M.A., 2007. Geostatistics for Environmental Scientists, second ed. John Wiley & Sons, Ltd..
Wegmuller, U., Santoro, M., Mattia, F., Balenzano, A., Satalino, G., Marzahn, P., Ludwig, R., Floury, N., 2011. Progress in the understanding of narrow directional microwave scattering of agricultural fields. Remote Sensing of Environment 115 (10), 2423–2433.
Zribi, M., Ciarletti, V., Taconet, O., PaillT, J., Boissard, P., 2000. Characterisation of the soil structure and microwave backscattering based on numerical three-dimensional surface representation: analysis with a fractional Brownian model. Remote Sensing of Environment 72 (2), 159–169.

2.4 Paper IV: Remote Sensing - Decomposing dual-scale soil surface roughness for microwave remote sensing applications

Paper IV addresses the multi-scale appearance of soil surface roughness in agricultural environments. Over large sample plots, roughness was measured using the proposed soil surface roughness measurement techniques from Paper III. To quantify the multi-scale appearance, an approach to decompose the several roughness scales into sub-scales based on geostatistical analysis is proposed. Results indicate that, over agricultural fields, the present roughness scales can be decomposed and quantified reliably using the proposed approach. In this paper, it is shown that the quantified roughness scales differ significantly for the same crop types and sowing techniques. Thus, in Paper IV major progress was made in the understanding of the multi-scale properties of soil surface roughness in agricultural environments and the impact of the different scales on the backscattering of available SAR datasets showing the directional scattering problem described in Paper II.

Marzahn, P., Seidel, M. and Ludwig, R. Decomposing Dual-Scale Soil Surface Roughness for Microwave Remote Sensing Applications. *Remote Sensing*, **2012**, 4, 2016-2032

Remote Sens. **2012**, *4*, 2016-2032; doi:10.3390/rs4072016

OPEN ACCESS

Remote Sensing

ISSN 2072-4292

www.mdpi.com/journal/remotesensing

Article

Decomposing Dual Scale Soil Surface Roughness for Microwave Remote Sensing Applications

Philip Marzahn *, Moritz Seidel and Ralf Ludwig

Department of Geography, Ludwig-Maximilians University, Luisenstrasse 37, D-80333 Munich, Germany; E-Mails: moritzseidel@gmx.de (M.S.); r.ludwig@lmu.de (R.L.)

* Author to whom correspondence should be addressed;
E-Mail: p.marzahn@iggf.geo.uni-muenchen.de; Tel.: +49-89-2180-6698; Fax: +49-89-2180-6675.

Received: 15 May 2012; in revised form: 28 June 2012 / Accepted: 30 June 2012 / Published: 6 July 2012

Abstract: Soil surface roughness, as investigated in this study, is decomposed in a dual scale process. Therefore, we investigated photogrammetrically acquired roughness information over different agricultural fields in the size of 6–22 m^2 and decomposed them into a dual scale process by using geostatistical techniques. For the characterization of soil surface roughness, we calculated two different roughness indices (the RMS height s and the autocorrelation length l) differing significantly for each scale. While we could relate the small scale roughness pattern clearly to the seedbed rows, the larger second scale pattern could be related to the appearance of wheel tracks of the tillage machine used. As a result, major progress was made in the understanding of the different scales in soil surface roughness characterization and its quantification possibilities.

Keywords: soil surface roughness; photogrammetry; SAR; synthetic aperture radar; detrending; RMS height; autocorrelation

1. Introduction

Soil surface roughness has a strong impact on the backscattered signal of an imaged surface by a microwave signal. For the parametrization of available backscatter models (e.g., IEM, Oh's model), the illuminated soil surface is strongly generalized and assumed to be a single scale stationary isotropic process [1]. However, recent studies have shown a strong non-isotropic behaviour of soil surfaces

under agricultural use [2,3]. Thus, the inadequate representation of soil surface roughness leads to insufficient results in the derivation of geophysical variables, e.g. soil moisture. In addition, recent studies have shown a huge impact of soil surface roughness and its orientation on the backscattered signal under slightly different look directions of the sensor [4]. This causes a backscatter difference of several dB due to the anisotropic appearance of the soil surface in agricultural landscapes. In several theoretical studies, Ulaby *et al.* [5] as well as Shin *et al.* [6] investigated the scattering from anisotropic quasi-periodic surfaces and described scattering with three coherent and incoherent terms originating from an anisotropic roughness component, a combined isotropic and anisotropic component and a deterministic periodical function. Using this model one can predict the anisotropic dependency of the scattering for row orientations with a width of 90°. On the *ground truth* site, Marzahn *et al.* [7] showed a significant difference in roughness values originating from the orientation of roughness measurements to the seedbed rows. Mattia [8] developed a backscatter model based on the findings of [6] which is able to reproduce the very narrow directional scatter pattern observed in [4] of only a few tenths of a degree. From the findings of [6] and especially of [4,8], the periodical roughness component has a strong impact on the backscattered signal. Besides the anisotropic appearance, different scales of soil surface roughness have an impact on the backscattered signal. Roemkens *et al.* [9] defined different scale dependent roughness classes in the context of a landscape (see Table 1). However, there exist some disparities in the classification scheme, for example a typical grain crop (wheat, barley) shows a row distance of 5–15 cm, thus the borders of the class *orientated roughness* are ambiguous.

Table 1. Roughness classification after [9].

Roughness Class	**Scale** [mm]	**Topographic Elements**
micro roughness	$\leq$2	texture dependent roughness
random roughness	2–200	soil aggregates and clods
orientated roughness	200–400	rows, tillage patterns
higher order roughness	$\geq$400	slope, field borders

In the context of microwave remote sensing, only the random and orientated roughness components as well as the higher order roughness class have a direct impact on the backscattered signal. However the latter can be reliably corrected by applying a terrain correction comprising a digital elevation model. In the available backscatter models, the random and orientated roughness components are usually treated as a single scale process, simplifying the proposed definition of [9]. Thus, available roughness measurements and their characterization of roughness patterns are mostly carried out by using a laser profiler, or mesh board, providing a generalized single scale roughness description [10–12]. Indeed, state of the art descriptions of soil surface roughness patterns included the measurements of soil surface roughness by photogrammetric acquisition systems (e.g., [2,13–16]. Especially Aguilar *et al.* [14] highlighted the advantage of using a photogrammetric acquisition system instead of a laser device due to the in-field acquisition speed. In their study, Blaes *et al.* [2] first described a dual scale approach for the characterization of soil surface roughness in an agricultural environment. At sizes of $3.4 \times 2.4\ m^2$, they characterized for a single sample plot two different roughness scales which they related to the seedbed rows and, as a superimposition, the random appearance of soil clods. However, they only defined these

two scales for the autocorrelation length l differing only in a range of 10–20 cm, while for another roughness index, common in microwave remote sensing, the RMS-height s is not considered. Zribi *et al.* [16] characterized the multi-scale appearance of an agricultural soil surface by a fractal model and for the large scale roughness component with the RMS height and the autocorrelation length respectively autocorrelation function. They evaluated the impact of these three roughness scale dependent terms on the backscattering and concluded a better understanding of the backscattering by incorporating such terms and scales in future backscatter models. In a theoretical experiment Shin *et al.* [6] and Mattia [8] developed a scatter model comprising a two scale roughness description.

The findings of [16] as well as [2] were evaluated on samples of $1 \times 1\ m^2$, respectively $3.4 \times 2.4\ m^2$. However, the size of the sample plot determines the ability to characterize soil surface roughness in an agricultural environment. As shown by several authors [17,18], the length (size) of a sampling area has a strong impact on the retrieved roughness indices. Thus, with an increase in the sampling size, one can observe a significant change in the estimated roughness indices. To characterize the periodicity of an agricultural soil surface, it is necessary to acquire sample plots larger than the proposed size by [2] in order to describe a statistically robust roughness index for the different scales of soil surface roughness.

In this paper, we will present a method to characterize soil surface roughness using high resolution, photogrammetrically acquired digital surface models (DSM). As the periodical (horizontal) roughness component has a significant impact on the backscattered signal [4], we will analyze the periodical roughness component and propose a method to decompose its multi-scale appearance in its single contributions. We first describe the generation of the DSMs, which provides the basis for the calculation of two different roughness indices. In an extensive analysis, the proposed method for the decomposition of the different roughness scales is described and the effect of detrending the acquired DSMs on the retrieval of the roughness indices is highlighted. Section 3 summarizes the results of the proposed methods in the context of microwave remote sensing applications.

2. Methods

2.1. Roughness Acquisition

The setup for acquisition of soil surface roughness information consists of a customized Canon EOS 5D used with a Canon EF 2/35 mm lens and a reference frame (see Figure 1). Usually, metric cameras are used for photogrammetric image acquisitions. However, recent studies [19] have shown the usability of non-metric cameras for photogrammetric applications at reduced costs. Indeed, the geometric stability of these cameras is mostly the limiting factor in terms of achievable accuracy [20,21] and thus altering the interior orientation. To increase the stability of the camera, one can mechanically stabilize the lens by using glue or fix the sensor to the camera's body using screws [22]. The off-the-shelf Canon EOS 5D in combination with the Canon EF 35 mm lens produces a maximum absolute Length Measurement Error (LME) of 330 μm, without fixation of the focusing tube at a maximum object distance of 2.5 m. Fixing the lens by placing epoxy resin between the focusing tube and the outer lens tube reduces the maximum absolute LME to 47 μm [19]. After fixation of the lens, the camera was calibrated and its interior orientation estimated by Aicon 3D Studio in conjunction with an external three dimensional calibration test field [19]. Table 2 shows the results of the calibration process.

Figure 1. Reference frame for relative orientation of the images acquired for DSM generation and detailed view of a GCP.

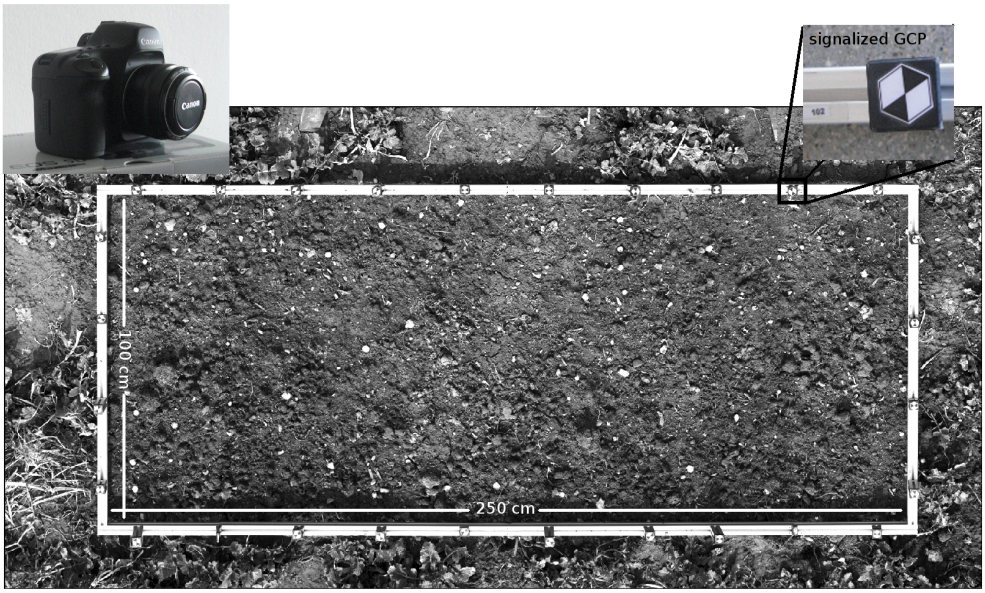

Table 2. Canon EOS 5D characteristics and calibration results. Calibration with Aicon 3D Studio [23]—parameters converted for input in LPS, K1 = 3rd-order term of radial distortion correction, K2 = 5th-order term of radial distortion correction, K3 = 7th-order term of radial distortion correction, P1 and P2 = Coefficient of decentering distortion.

Parameter	**Values**	**Standard Error**
Camera	Canon EOS 5D	-
Lens	Canon EF 2/35 mm, fixed focus at 2.5 m	-
Resolution	4,368 × 2,912 pixels	-
Pixel width *xy* $[mm]$	0.0082	-
Focal length *c* $[mm]$	35.8919	0.0000
Principal point offset *xp* $[mm]$	–0.2026	0.0000
Principal point offset *yp* $[mm]$	0.2092	0.0000
K1 $[mm]$	7.30312e-005	8.2836e-008
K2 $[mm]$	–5.30725e-008	5.535e010
K3 $[mm]$	–2.33223e-011	1.1034e-012
P1 $[mm]$	3.2677e-005	1.296e-007
P2 $[mm]$	–1.3050e-005	1.167e-007

To numerically characterize soil surface roughness, DSMs generated out of the acquired imagery are the basis for further analyses. The generation of the DSMs was done using *Leica Photogrammetry Suite (LPS)*. As LPS needs to establish exterior orientation for DSM generation, known ground control points (GCPs) with xyz coordinates are mandatory. Therefore a reference frame measuring 1 × 2.5 m^2 was set-up, providing 28 horizontally and vertically distributed GCPs. The co-ordinates of the GCPs were determined using a calliper ruler with an accuracy of 0.1 mm in the z direction. Six images acquired from a height of 2.5 m are necessary to cover the whole frame. Table 3 summarizes the characteristics of

the image acquisition. As the frame is limited in size to $1 \times 2.5\ m^2$, it is necessary, for larger roughness acquisitions, to acquire consecutive image acquisitions of the frame by moving the frame along a leveled plane which is ensured by an align fixture (see Figure 2).

Table 3. Flight plan for the coverage of the reference frame.

Parameter	**Values**
Sensor altitude h $[mm]$	2,500
Base length b $[mm]$	1,000
h/b	2.5
Image scale	1:69.65
Ground sample distance $[mm]$	0.57
Forlap x $[\%]$	50
Sidelap y $[\%]$	60
Number of images per strip	3
Number of strips	2

Figure 2. Roughness acquisition scheme and image arrangement for stereo coverage of the frame.

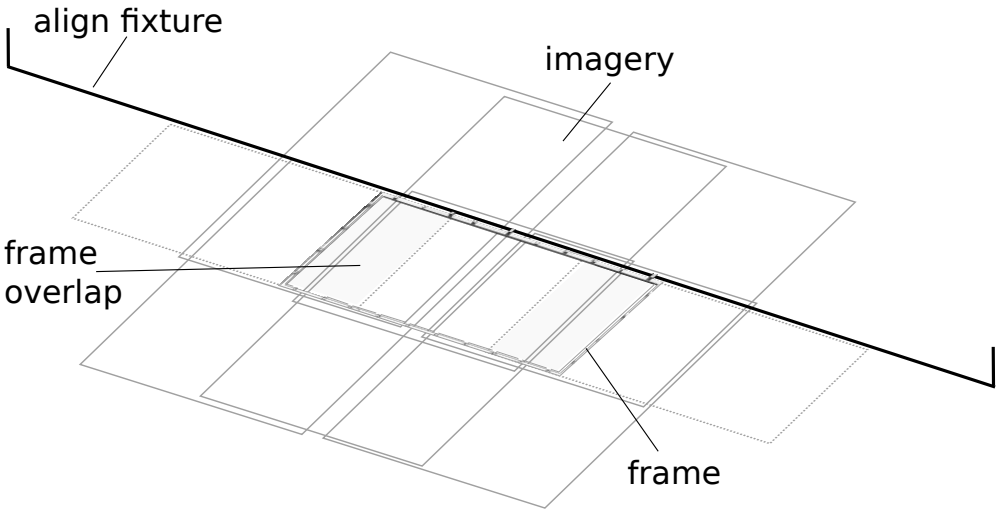

From the acquired imagery, DSMs were generated using LPS. As LPS uses epipolar constraints during image matching based on the established exterior orientation of the imagery, the exterior orientation of the block first has to be established. We therefore used the GCPs installed on the frame and improved the original camera calibration by using the Ebner model [24] which is implemented in LPS. After the exterior orientation has been established, the DSMs were generated using different matching strategies depending on the differences in elevation. Table 4 summarizes the applied strategies based on a ground pixel size of 0.57 mm. For rougher surfaces a larger search window is chosen. Indeed, the surfaces showed similar smooth roughness classes without any significant change in roughness, therefore the applied strategies vary only little. Using an epipolar based approach, Linder [25] suggests a correlation coefficient threshold for the matching process for such applications of 0.65. In a laboratory experiment,

Heng *et al.* [26] as well as Rieke-Zapp *et al.* [22] used a correlation coefficient of 0.80. In our study, under field conditions, the correlation coefficients for matching two pixels showed good results at 0.75. After successful generation of DSMs, a 7 × 7 pixel low pass filter was applied to remove peaks to smoothen the DSMs and resampled to a regular resolution of 2 × 2 mm^2.

Table 4. Matching strategies used during DSM generation as required by LPS based on a pixel size in ground space of 0.57 mm in the x, y direction.

Roughness Class	**Search Window** $[pixel]$	**Correlation Window** $[pixel]$	**Correlation Coefficient Threshold**
seedbed	25 × 3	11 × 11	0.75
crusted seedbed	21 × 3	11 × 11	0.75
smooth crusted	17 × 3	11 × 11	0.75

Roughness Samples

Several field campaigns for the measurement of soil surface roughness were scheduled in May 2011 over the Wallerfing test site, which is part of the SMO Cal/Val activities [27] located in the Upper Danube watershed approximately 100 km northeast of Munich. The region, which has a low relief energy, is mainly agricultural in character, soils mainly consist of loess loam and the main crops are winter wheat, winter barley, corn and sugar beet. During the campaign most of the crops had been already sown several weeks ago and were already at the beginning of their growth. The seedbed structure was at all sample points still well developed, however the random occurrence of soil clods was limited due to precipitation (see Figure 3). Thus, the sample points (***E**lementary **S**ample **U**nit*, ESU) all represent an already prepared seedbed pattern, which is the main conditions of fields at this time in the region. As soil surface roughness can be considered anisotropic [3], roughness should be measured in the perpendicular and parallel directions to the seedbed rows. As [4,8] showed a significant impact on the backscattered signal from the periodical roughness component, we focused in this study only on measurements perpendicular to the row directions which is mainly influenced by the periodical component. Table 5 summarizes the main characteristics of each sample point.

2.2. Geostatistical Analysis

For the characterization of surface roughness, geostatistical methods were chosen to describe the spatial properties of the soil surface. As variography describes the spatial structure of random spatial objects, it is well suited for the characterization of spatial processes such as soil surface roughness. The omnidirectional sample variogram $\hat{\gamma}(h)$ of a data set can be expressed by:

$$\hat{\gamma}(h) = \frac{1}{2n} \sum_{i=1}^{n} [Z(x_i) - Z(x_i + h)]^2 \quad (1)$$

Table 5. Characteristics of sample points acquired within this study, ESU = ***E**lementary **S**ample **U**nit*.

ESU	**Landuse**	**Surface Type**	**Size** $[m^2]$
R11	maize	seedbed	6
R12	onion	smooth crusted	6
R13	sugarbeet	crusted seedbed	8
R14	sugarbeet	crusted seedbed	8
R21	sugarbeet	crusted seedbed	6
R22	sugarbeet	crusted seedbed	6
R23	sugarbeet	crusted seedbed	6
R30	winter rape	seedbed	22

Figure 3. Overview of roughness sample point on a sugar beet field, acquired on 23 May 2011 at the Wallerfing test site.

where h is the distance between the two variables $Z(x_i)$ [28]. As the sample design in our study introduces strong anisotropy, one can calculate the sample variogram for a defined direction as

$$\hat{\gamma}\left(h_{\vec{j}}\right) = \frac{1}{2n}\sum_{i=1}^{n}\left[Z(x_i) - Z\left(x_i + h_{\vec{j}}\right)\right]^2 \tag{2}$$

where $\vec{j}$ is the anisotropic direction, in our case 90°. As an example, Figure 4 shows three sample DSMs while Figure 5 shows the corresponding sample variograms of the three samples, calculated on a basis of 15,000 randomly sampled points out of the DSMs. The inherent appearance of the sample variograms displays two major issues: first the surface in Figure 4(b) shows a clear trend, which has to be corrected;

second, the DSMs perpendicular to the row direction show a two scale process (Figure 4(a)) which has to be quantified for microwave remote sensing separately.

Figure 4. Three sample DSMs of different roughness plots showing (**a**) a significant two scale roughness pattern (R12), (**b**) a spatial trend (R14) and (**c**) no spatial trend with an insignificant two scale roughness pattern (R21). Units are in cm.

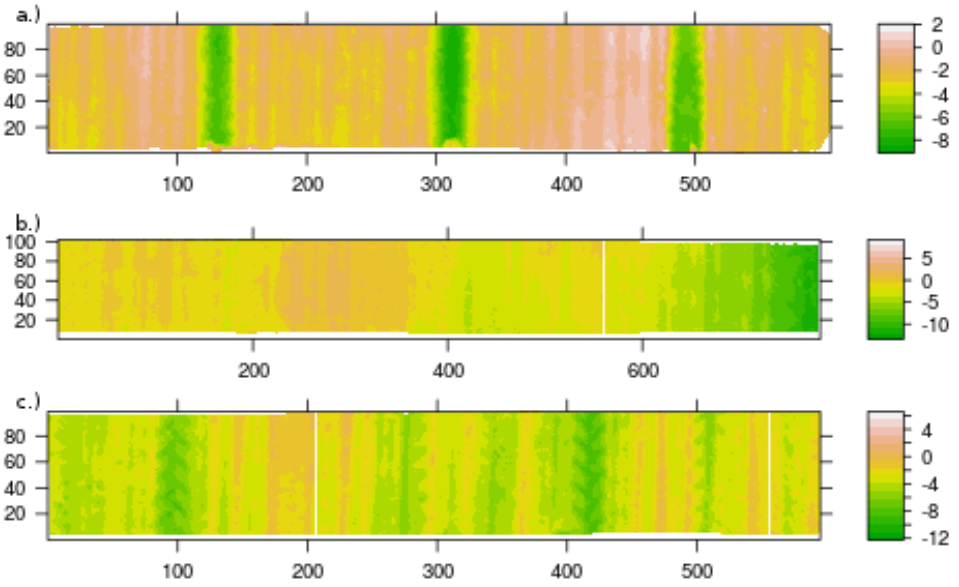

Figure 5. Sample variograms of the roughness plots from Figure 4 showing (**a**) a significant two scale roughness pattern (R12), (**b**) a spatial trend (R14) and (**c**) no spatial trend with an insignificant two scale roughness pattern (R21).

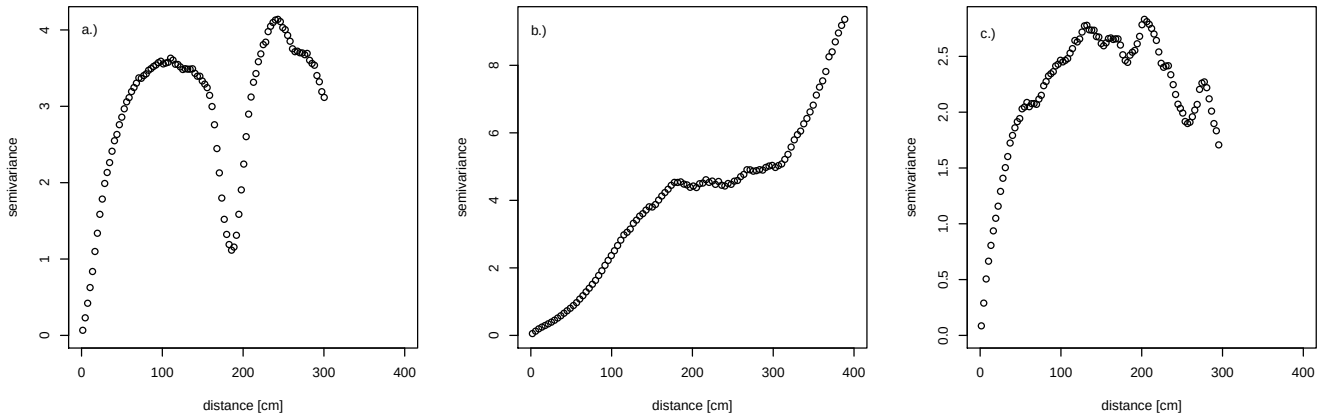

Detrending

As obvious from Figure 4(b), several DSMs showed a trend in elevation due to higher order topographic patterns, such as local slopes. Those slope effects have to be corrected by detrending the data sets. Due to the acquisition design we assume that a spatial trend is only present in the x-direction, while a possible trend in the shorter y-direction (1 m) can be neglected. Therefore the data can be treated

as non-spatial data and the detrending can be carried out by subtracting a trend surface (Z_{mod}) from the original surface (Z). The detrended surface (Z_{res}) is defined as:

$$Z_{res} = Z - Z_{mod} \tag{3}$$

As summarized in 2nd table in Section 3, two detrending models have been defined, which can be described by

$$Z_{mod} \sim mX + b \tag{4}$$

for the linear model and for the polynomial model:

$$Z_{mod} \sim b + m_1X + m_2X^2 + m_3X^3 + ...m_nX^n \tag{5}$$

with m and b representing the regression coefficients slope and intercept and X the x-coordinate of the sample DSM. Figure 6 shows as an example the results of the detrending procedure, with Figure 6(a) the acquired original surface with a present trend in the right part of the DSM. For detrending a surface is fitted (Figure 6(b)) using a fifth order polynomial approach and subtracted from the original surface to represent a residual surface with a removed trend (Figure 6(c)). As can be seen, the row and seedbed structure is preserved using this approach, allowing the random and orientated roughness components to be quantified. Fitting the trend surface (Z_{mod}) to the original heights (Z) by omitting the wheel tracks, a least squares approach using the best fit (R^2) was chosen.

Figure 6. Results of detrending sample plot R13 with (**a**) original surface, (**b**) fitted trend surface using polynomial approach and (**c**) residual surface preserving row structure. Units in cm.

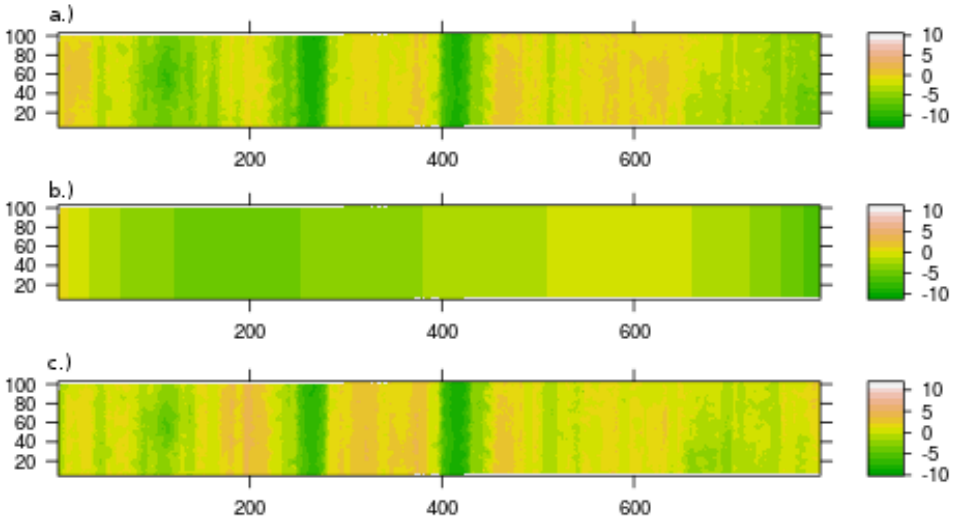

Decomposing the Data into Two Scales

From Figure 4(a) and its corresponding sample variogram (Figure 5(a)) it is obvious that a two scale roughness pattern can be observed on these agriculturally formed soil surfaces. As different roughness scales have an impact on the backscattered signal in microwave remote sensing, it is important to

characterize both scales. Therefore, again variography is used to decompose and characterize the soil surface at different scales. As the variogram of Figure 5(a) shows a surface inherent behaviour with strong similarities at distances in range of 180 cm, which correspond to the wheel tracks in Figure 4(a), a two scale roughness pattern is indicated. Thus, the variogram for the whole sample plot describes the semi-variance of the roughness pattern, which is strongly imposed by the large scale roughness pattern (e.g., wheel tracks of drilling machine). To characterize the small scale roughness pattern (e.g., seedbed rows, soil clod distribution) we defined a distance threshold, based on the findings of the variography, to mask out the wheel tracks and calculated variograms for each surface again. As a result, for each roughness scale a roughness index is calculated (see Figure 7).

2.3. Calculation of Roughness Indices

In order to describe soil surface conditions numerically for remote sensing applications, roughness indices are necessary. In this study, the focus is on the application of the RMS height *s* and the autocorrelation length *l*, since both are roughness indices used by default in radar remote sensing applications for the characterization of soil surface roughness [1,16,29]. While the RMS height describes the vertical roughness component as the standard deviation of the heights (Z) to a reference height $\left(\overline{Z}\right)$,

$$s = \sqrt{\frac{\sum_{i=1}^{n}\left(Z_i - \overline{Z}\right)^2}{n-1}} \tag{6}$$

the autocorrelation length *l* describes the horizontal component of the roughness spectra. While *l* is usually determined along 1d profiles, the derivation of *l* using three dimensional roughness measurements is more complex. For an efficient estimation of *l*, the autocorrelation function (ACF) can be inverted from a sample variogram $(\hat{\gamma})$ (see Equation (2)), where *l* is defined as the distance (*h*) at which the ACF drops under e^{-1} [2]. This implies an exponential fit of the theoretical variogram and therefore of the ACF. Several models were tested, however best fit was always achieved with an exponential model (data not shown). Blaes *et al.* [2] and Davidson *et al.* [17] reported similar observations. A theoretical variogram $(\tilde{\gamma})$ with an exponential shape is fitted to the sample variogram $(\hat{\gamma})$ of Equation (2) and from the theoretical variogram $(\tilde{\gamma})$ the ACF $(\tilde{\rho})$ can be derived as follows:

$$\tilde{\rho}\,(h) = 1 - \frac{\tilde{\gamma}\,(h)}{\tilde{\gamma}\,(\infty)} \tag{7}$$

where $\tilde{\gamma}\,(h)$ is the modelled semi-variance at distance *h* between two points and $\tilde{\gamma}\,(\infty)$ is the modelled semi-variance at distance where the sill of the variogram is reached. For the assumed exponential model, where the sill is asymptomatically approached, $\tilde{\gamma}\,(\infty)$ corresponds to the distance where 95% of the sill is reached.

Due to the high resolution of the DSMs, *l* was calculated using only a random subsample of 15,000 points, while *s* was calculated for the whole DSM. Therefore, four roughness representations are given for each sample plot (see 2nd table in Section 3).

3. Results

Table 6 shows the root mean square error in the Z-direction ($RMSE_Z$) and the planimetric error of the sample plots. The results show a high accuracy of the generated DSMs compared to the manually measured checkpoints installed on the reference frame, thus providing a robust basis for the characterization of soil surface roughness statistics. Except sample plot R30, which has a $RMSE_Z$ of 0.22 cm. From Figure 4 one can clearly identify the seedbed pattern as well as the nearly random distribution of soil clods and aggregates. The wheel tracks of the different tillage machines used are clearly distinguishable. There are no interpolated artifacts visible which indicate a high rate of matched points during photogrammetric image processing.

Thus, due to the highly accurate results of the DSMs, the calculated roughness indices represent the roughness conditions precisely. While for rougher surface the RMS height s increases, the autocorrelation length l decreases (see Table 7). In general the considered surfaces appear smooth, except for sample plots R11 and R30 which represent a freshly prepared seedbed and therefore show the highest values for s and the lowest values for l.

Several studies (e.g., [29]) showed the impact of the sample size on the retrieved roughness values. For the 22 m^2 sample plot R30 we analyzed the dependency of the roughness values in context of the sample size according to [7] for the original and the detrended surface. While for the detrended surface the measurements can be assumed to be representative at a sample size of 1.5 m^2, the original surface of R30 shows a strong dependency of the roughness values from the sample size which reflects the topographic impact.

Table 6. Root mean square error in cm of generated DSM height values compared to the manually measured GCPs.

ESU	R11	R12	R13	R14	R21	R22	R23	R30
$RMSE_Z$	0.17	0.13	0.05	0.07	0.05	0.06	0.02	0.22
$RMSE_{XY}$	0.03	0.04	0.04	0.04	0.11	0.04	0.04	0.04

Table 7. Results of two scale roughness representation and order of fitted detrending surface. In brackets are the results for the non-detrended original surfaces. Units in cm, s_1, l_1 correspond to the small scale roughness pattern, s_2, l_2 to the large scale roughness pattern.

ESU	s_1	s_2	l_1	l_2	**Detrending**
R11	0.88	1.84	11.0	29.5	-
R12	0.85	1.73	71.6	38.27	-
R13	1.15 (1.09)	2.43 (2.84)	38.3 (17.7)	53.04 (69.05)	polynomial 5th order
R14	0.24 (0.86)	2.26 (2.5)	41.01 (96.39)	98.04 (169.14)	polynomial 2nd order
R21	1,24	1.45	31.1	38.52	-
R22	0.77 (0.93)	1.12 (1.51)	20.5 (26.4)	23.47 (55.4)	polynomial 5th order
R23	1.08 (1.31)	2.38 (2.71)	27.3 (25.7)	105.6 (107.5)	linear fit
R30	1.18 (2.84)	1.19 (3.26)	17.2 (145.7)	17.2 (359.52)	polynomial 9th order

3.1. Effect of Detrending

Considering only the raw non-detrended dataset, the roughness indices of several surfaces (see Table 7, bracketed values) are influenced by higher order topographic effects such as general slope effects. Figure 4(b) and the corresponding variogram (Figure 5(b)) show this higher order trend for sample plot R14. Using the non-detrended DSM, the calculated roughness indices for $s = 2.5$ and $l = 169.14$ for the whole dataset are two times the calculated roughness values for the detrended dataset. Thus, the large values, especially for l, represent the higher order general slope effects. Indeed the detrended sample plot, using a second order polynomial model according to Table 7, represents the random and orientated roughness component defined by [9]. Figure 6 shows the output of detrending sample plot R13 using a fifth order polynomial model approach. It is worth highlight that the row structure of the seedbed is preserved by the detrending approach permitting to characterize the periodicity of soil surface roughness as well as the random appearance of single soil aggregates. In Table 7 the roughness indices for the original non-detrended surfaces are provided in brackets. While for the RMS height no significant change is observed due to the detrending procedure, the results for the autocorrelation length l change significantly in the order of several decimetre. Except for R30, the 22 m^2 large sample plot, a significant change in s can be observed, due to the strong topographic influence with a range in heights of 20 cm. To model this strong trend a polynomial approach of 9th order was chosen.

3.2. Two Scale Roughness Representation

Figure 5(a) indicates a significant two-scale roughness pattern for sample plot R12. Different points with a certain distance in range of 200 cm to each other show a strong similarity, thus indicating periodicity in the soil surface roughness pattern with a range of 200 cm. From Figure 4(a) it is obvious that this pattern is clearly related to the wheel tracks of the tillage machines used during seedbed preparation. Thus the sharply bounded wheel tracks with a height difference of 4–6 cm to the surrounding seedbed biases the characterization of the roughness indices. Table 7 shows the results of the decomposing approach for each roughness index and each scale separately. While s_1, l_1 correspond to the small scale roughness pattern (soil clods, soil aggregates and seedbed rows), s_2, l_2 relate to the large scale roughness pattern such as wheel tracks. As the soil surface appeared smooth with only a reduced fraction of the random roughness component (soil clods and aggregates were almost washed out by rain), we decided to comprise the random appearance of soil clods with the seed bed rows in one class separate from the wheel tracks. All sample plots show a two scale roughness representation, due to the availability of a seedbed structure imposed over wheel tracks, at which for the small scale roughness pattern the values for s_1 and l_1 are lower than for the large scale roughness pattern. Figure 7 shows the autocorrelation length for three different sample plots. For sample plot R12 (Figure 7(a)), which represents a smooth crusted onion field, the autocorrelation length for the small scale roughness pattern is higher than the large scale roughness pattern, indicating a very smooth surface with sharply bounded wheel tracks (Figure 4(a)). It should be highlighted that even under the same land use type (e.g., sugar beet) the roughness values indicate different roughness conditions, which are a result of the different tillage machines used and the state of crusting. Figure 7(a,b) illustrates this effect for sample plots R14 and R21 which both represent sugar beet fields at the same crusted stage. In contrast, sample

plot R30 shows no significant two scale roughness process, which is due to the missing presence of wheel tracks or other higher order roughness patterns and thus roughness is only defined by the present seedbed structure. As a result, the values of s and l are equal for both scales.

Figure 7. Decomposed two scale roughness pattern for sample plots R12 (**a**), R14 (**b**) and R21 (**c**). Filled dots show the sample variogram and corresponding fitted theoretical variogram (black solid line). Derived autocorrelation function (ACF) (l_1 fine dashed line; l_2 coarse dashed line) and corresponding autocorrelation length are indicated by hollow dots.

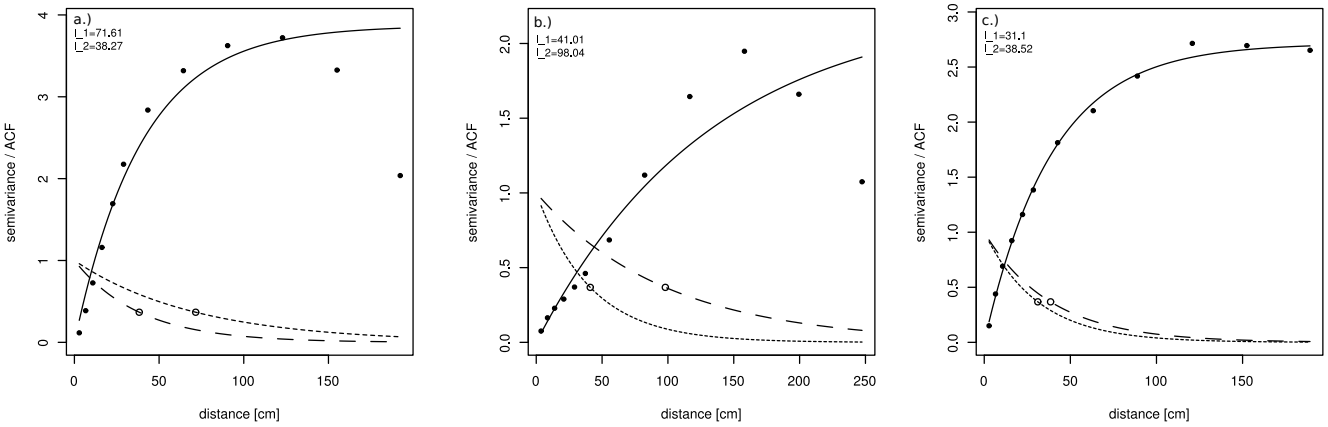

4. Discussion

In this paper we presented an approach to characterize the different scales of soil surface roughness for microwave remote sensing applications. Therefore, we established a method based on photogrammetric roughness acquisitions to decompose roughness into two different scales. While the small scale roughness pattern could be clearly related to the seedbed rows of an agricultural field, the large scale roughness pattern is related in to the occurrence of wheel tracks. Both scales are only dependent on the tillage tools used and on the field conditions during tillage operations.

As in microwave remote sensing, soil surface roughness is treated and parametrized in available backscatter models as a single scale stationary process; this approach enables to describe soil surface roughness in such models more accurate [10]. Shin *et al.* [6,8,30] provide several modelling approaches comprising the roughness scales investigated in this paper. Looking closely to the theoretical study of [8] and comprising the retrieved roughness information into the Modified Shin and Kong Model (MSK) proposed by [8], the findings are in good accordance with our investigations as Figure 8 indicates. Based on our roughness measurements, we used the MSK model to predict the SAR backscattering of several nearly simultaneous acquired ERS-2 datasets. Therefore, we used the derived s1/l1 as the random component of the anisotropic roughness and s2/l2 as the deterministic sinusoidal component of the MSK model (see [4,8]). As first very preliminary results of this approach show (see Figure 8 and [31]), the results reflect very well the obtained ERS-2 backscatter values and even the directional scattering of the fields with a row orientation nearly perpendicular to the incident wave (off-perp = 0°) are modelled accurately. Thus, future studies have to assimilate the output of the proposed method into the available backscatter models of [30] and especially of [8] to verify this first results.

As shown in this study, both roughness scales differ by several decimetres in the calculated roughness indices, which would thus lead to insufficient results in the inversion of soil moisture by using only a single scale roughness descriptor. While soil surface roughness in an agricultural environment can be considered to be multi-scale, the derived roughness indices are biased by several roughness components. For microwave remote sensing applications it is the two characterized components that have a strong impact on the backscattered signal. Several other roughness components such as general slope effects affect the backscatter signal as well as the proposed roughness measurements. Therefore, the generated DSMs have to be detrended to calculate a roughness index for these two roughness scales. In this study it was obvious that for a surface with medium slope effects, a detrending has a higher impact on the autocorrelation length compared to the RMS height. For surfaces with a keen slope effect, even the results for the RMS height vary strongly.

Figure 8. Backscattering [dB] *versus* row direction (0°= rows perpendicular to the incidence wave) for the roughness samples plots and results of the Modified Shin and Kong model ([8]) averaged for sugar beet parametrization and five ERS-2 scenes (dashed line) acquired nearly simultaneous to the roughness measurements.

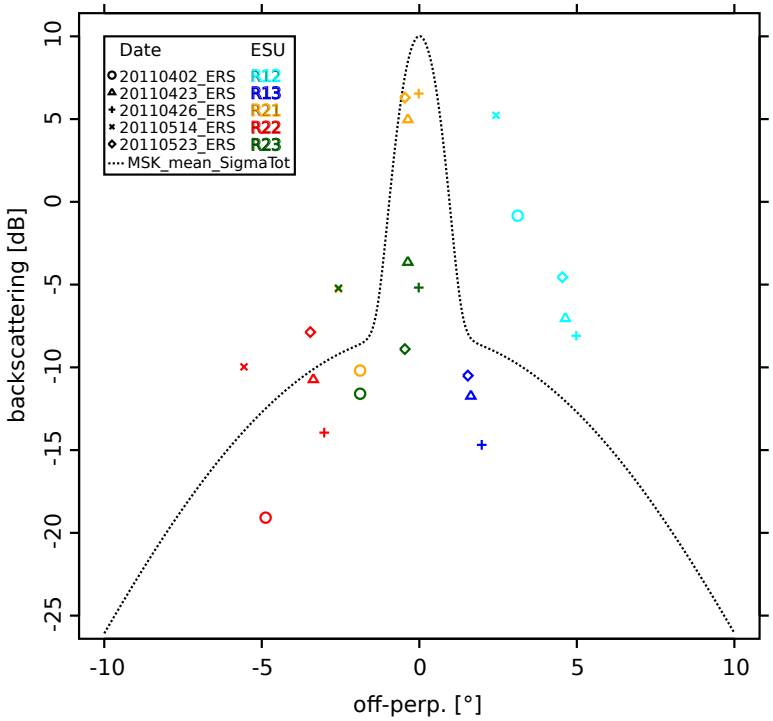

As the findings of this paper are based on highly accurate DSMs, the results are very promising for the parametrization of microwave backscatter models to characterize surface soil moisture. The generated DSMs show a mean RMSE of 0.1 mm in the Z-direction with a maximum $RMSE_Z$ of 2.2 mm and a negligible planimetric error in the sub-pixel region of the imagery. Lievens *et al.* [32] suggested a threshold for the vertical derivation of heights of 0.2 cm at which an impact on soil moisture retrieval from microwave imagery is negligible. Thus the proposed roughness acquisition method is well suited for soil surface roughness measurements for microwave remote sensing applications. Using such a setup, no systematic errors in the generated DSMs could be identified, thus the utilization of the customized

non-metric Canon EOS 5d camera shows a high potential for the measurement of soil surface roughness at reduced costs compared to a metric camera. In the context of field capability, the acquisition time to cover the reference frame is about 15 min, thus outperforming laser devices which need for the same size at same accuracy 2–4 h [14,22]. In addition, as the frame is very portable several roughness measurements can be carried out within a day over several fields.

5. Conclusions

In this paper we presented a unique method for measuring soil surface roughness using a simple photogrammetric acquisition system. A consumer grade Canon EOS 5d was customized by fixing the outer lens tube to increase the accuracy of the interior orientation to fulfill metric needs. In combination with a portable reference frame the developed system produces highly accurate digital surface models in any desired size at low cost. Using the system, several roughness measurements were acquired during different field campaigns to characterize soil surface roughness for microwave remote sensing applications. With a vertical accuracy of $\leq$2.0 mm and a planimetric error smaller than 0.57 mm, the acquired dataset is highly accurate and unique for the characterization of soil surface roughness. Using geostatistical analysis, several roughness scales could be identified, which were decomposed into a large scale roughness pattern (wheel tracks) and a small scale roughness pattern comprising tillage rows and the random appearance of soil clods. Both roughness scales and values were used for the prediction of backscattering using the Modified Shin and Kong model [8] to justify the decomposition of the roughness scales and show its impact on the obtained backscatter values acquired by a SAR sensor. Thus, major progress was achieved in understanding and quantifying the different roughness scales obtained in an agricultural environment leading to a multi-scale roughness parametrization which is mandatory for microwave remote sensing applications.

References

1. Verhoest, N.; Lievens, H.; Wagner, W.; Alvarez-Mozos, J.; Moran, M.; Mattia, F. On the soil roughness parameterization problem in soil moisture retrieval of bare surfaces from Synthetic Aperture Radar. *Sensors* **2008**, *8*, 4213–4248.
2. Blaes, X.; Defourny, P. Characterizing bidimensional roughness of agricultural soil surfaces for SAR modeling. *IEEE Trans. Geosci. Remote Sens.* **2008**, *46*, 4050–4061.
3. Marzahn, P.; Ludwig, R. On the derivation of soil surface roughness from multi parametric PolSAR data and its potential for hydrological modeling. *Hydrol. Earth Syst. Sci.* **2009**, *13*, 381–394.
4. Wegmuller, U.; Santoro, M.; Mattia, F.; Balenzano, A.; Satalino, G.; Marzahn, P.; Ludwig, R.; Floury, N. Progress in the understanding of narrow directional microwave scattering of agricultural fields. *Remote Sens. Environ.* **2011**, *115*, 2423–2433.
5. Ulaby, F.T.; Kouyate, F.; Fung, A.K.; Sieber, A.J. A backscatter model for a randomly perturbed periodic surface. *IEEE Trans. Geosci. Remote Sens.* **1982**, *20*, 518–528.
6. Shin, R.T.; Kong, J.A. Scattering of electromagnetic waves from a randomly perturbed quasiperiodic surface. *J. Appl. Phys.* **1984**, *56*, 10–21.

7. Marzahn, P.; Rieke-Zapp, D.H.; Ludwig, R. Assessment of soil surface roughness statistics for microwave remote sensing applications using a simple photogrammetric acquisition system. *ISPRS J. Photogramm.* **2012**, accepted.
8. Mattia, F. Coherent and incoherent scattering from anisotropic tilled soil surfaces. *Wave. Random Complex* **2011**, *21*, 278–300.
9. Roemkens, M.J.; Wang, J.Y. Effect of tillage on surface roughness. *Trans. ASAE* **1986**, *29*, 429–433.
10. Callens, M.; Verhoest, N.E.C.; Davidson, M.W.J. Parameterization of tillage-induced single-scale soil roughness from 4-m profiles. *IEEE Trans. Geosci. Remote Sens.* **2006**, *44*, 878–888.
11. Davidson, M.; Le Toan, T.; Borgeaud, M.; Manninen, T. Measuring the Roughness Characteristics of Natural Surfaces at Pixel Scales: Moving from 1 Metre to 25 Metre Profiles. In *Proceedings of 1998 IEEE International Geoscience and Remote Sensing Symposium*, Seattle, WA, USA, 6–10 July 1998; Vol. 3, pp. 1200–1202.
12. Alvarez-Mozos, J.; Verhoest, N.; Larranaga, A.; Casalí J.; Gonzáez-Audíana, M. Influence of surface roughness spatial variability and temporal dynamics on the retrieval of soil moisture from SAR observations. *Sensors* **2009**, *9*, 463–489.
13. Warner, W.S. Mapping a three-dimensional soil surface with hand-held 35 mm photography. *Soil Till. Res.* **1995**, *34*, 187–197.
14. Aguilar, M.; Aguilar, F.; Negreiros, J. Off-the-shelf laser scanning and close-range digital photogrammetry for measuring agricultural soils microrelief. *Biosyst. Eng.* **2009**, *103*, 504–517.
15. Taconet, O.; Ciarletti, V. Estimating soil roughness indices on a ridge-and-furrow surface using stereo photogrammetry. *Soil Till. Res.* **2007**, *93*, 64–76.
16. Zribi, M.; Ciarletti, V.; Taconet, O.; Paillé, J.; Boissard, P. Characterisation of the soil structure and microwave backscattering based on numerical three-dimensional surface representation: Analysis with a fractional brownian model. *Remote Sens. Environ.* **2000**, *72*, 159–169.
17. Davidson, M.W.J.; Toan, T.L.; Mattia, F.; Satalino, C.; Manninen, T.; Borgeaud, M. On the characterization of agricultural soil roughness for radar remote sensing studies. *IEEE Trans. Geosci. Remote Sens.* **2000**, *38*, 630–640.
18. Mattia, F.; Davidson, M.W.J.; Le Toan, T.; D'Haese, C.M.F.; Verhoest, N.E.C.; Gatti, A.M.; Borgeaud, M. A comparison between soil roughness statistics used in surface scattering models derived from mechanical and laser profilers. *IEEE Trans. Geosci. Remote Sens.* **2003**, *41*, 1659–1671.
19. Rieke-Zapp, D.; Tecklenburg, W.; Peipe, J.; Hastedt, H.; Haig, C. Evaluation of the geometric stability and the accuracy potential of digital cameras—Comparing mechanical stabilisation versus parameterisation. *ISPRS J. Photogramm.* **2009**, *64*, 248–258.
20. Rieke-Zapp, D.H. A digital medium-format camera for metric applications—Alpa 12 metric. *Photogramm. Rec.* **2010**, *25*, 283–298.
21. Chandler, J.H.; Fryer, J.G.; Jack, A. Metric capabilities of low-cost digital cameras for close range surface measurement. *Photogramm. Rec.* **2005**, *20*, 12–26.
22. Rieke-Zapp, D.; Nearing, M. Digital close range photogrammetry for measurement of soil erosion. *Photogramm. Rec.* **2005**, *20*, 69–87.

23. Aicon 3D Systems. *Aicon 3D Studio—User Manual*; Aicon 3D Systems: Braunschweig, Germany, 2009; [CD-ROM].
24. Ebner, H. Self Calibrating Block Adjustment. In *Proceedings of The XIIIth Congress of the International Society for Photogrammetry*, Helsinki, Finnland, 11–23 July 1976; pp. 1–17.
25. Linder, W. *Digital Photogrammetry A Practical Course*; Springer: Berlin/Heidelberg, Germany, 2009.
26. Heng, P.B.C.; Chandler, .J.H.; Armstrong, A. Applying close range digital photogrammetry in soil erosion studies. *Photogramm. Rec.* **2010**, *25*, 240–265.
27. Schlenz, F.; Dall'Amico, J.T.; Loew, A.; Mauser, W. SMOS Validation in the Upper Danube Catchment (UDC): A Status Report Eigth Month after Launch. In *Proceedings of ESA Living Planet Symposium 2010*, Bergen, Norway, 28 June–2 July 2010.
28. Webster, R.; Oliver, M.A. *Geostatistics for Environmental Scientists*, 2nd ed.; John Wiley and Sons, LTD: Chichester, UK, 2007; p. 315.
29. Davidson, M.W.J.; Mattia, F.; Satalino, G.; Verhoest, N.E.C.; Le Toan, T.; Borgeaud, M.; Louis, J.M.B.; Attema, E. Joint statistical properties of RMS height and correlation length derived from multisite 1-m roughness measurements. *IEEE Trans. Geosci. Remote Sens.* **2003**, *41*, 1651–1658.
30. Zribi, M.; Taconet, O.; Ciarletti, V.; Vidal-Madjar, D. Effect of row structures on radar microwave measurements over soil surface. *Int. J. Remote Sens.* **2002**, *23*, 5211–5224.
31. Marzahn, P.; Wegmueller, U.; Mattia, F.; Ludwig, R. FLASHING FIELDS! and the Impact of Soil Surface Roughness. In *Proceedings of IEEE International Geoscience and Remote Sensing Symposium IGARSS 2012*, Munich, Germany, 22–27 July 2012.
32. Lievens, H.; Vernieuwe, H.; Alvarez-Mozos, J.; De Baets, B.; Verhoest, N. Error in radar-derived soil moisture due to roughness parameterization: An analysis based on synthetical surface profiles. *Sensors* **2009**, *9*, 1067–1093.

2.5 Paper V: JSTARS - Modeling of Directional Scattering from Agricultural Fields in C- and X-Band SAR Imagery using the Modified Shin and Kong Model and Multi-Scale Soil Surface Roughness Representations

Paper V is an extended version of the invited paper to the special session on *Remote Sensing of Terrestrial Environmental Observatories for Ecosystem Research* during the IGARSS2012 conference. It was submitted to a special Issue about IGARSS2012 published in the *Journal of Selected Topics in Applied Earth Observation and Remote Sensing - JSTARS*. It summarizes the findings of Paper IV and offers deep insights into the impact of the different roughness scales on the directional scattering problem described in Paper II. At the Wallerfing test-site located in Bavaria, where several fields showed strong directional scattering, a field campaign was carried out to identify and quantify the impacts of soil surface roughness on the occurring directional scattering. It was shown that besides the row orientation of the agricultural fields, which has a major impact on directional scattering, soil surface roughness can significantly alter the directional scattering.

Marzahn, P., Mattia, F., Wegmueller, U. and Ludwig, R. Modeling of Directional Scattering from Agricultural Fields in C- and X-Band SAR Imagery using the Modified Shin and Kong Model and Multi-Scale Soil Surface Roughness Representations, submitted to the *Journal of Selected Topics in Applied Earth Observation and Remote Sensing*, Special Issue on IGARSS2012, 2013, 6

Modeling of Directional Scattering from Agricultural Fields in C- and X-Band SAR Imagery using the Modified Shin and Kong Model and Multi-Scale Soil Surface Roughness Representations

Philip Marzahn, *Member, IEEE-GRSS,* Francesco Mattia, *Senior Member, IEEE,* Urs Wegmüller, *Senior Member, IEEE,* and Ralf Ludwig,

***Abstract*—This paper presents results of an additional campaign in the context of *Flashing Fields* showing the impact of soil surface roughness on the directional backscattering. For the characterization of soil surface roughness a photogrametric measurement device was chosen and roughness was measured simultaneous to SAR observations made by ERS-2 and TerraSAR-X over the Wallerfing test site. In a rigorous approach, different roughness scales obtained from a single roughness measurement were decomposed in its single contributors. The derived roughness values were further used as input parameters for the modified Shin and Kong model to predict directional backscattering occurring in the acquired SAR images. As this study mainly confirmed and consolidated the findings of the previous *Flashing Fields* studies, major progress was made in the understanding of the impact of soil surface roughness on the flashing phenomenon. It is concluded, that besides row orientation, certain roughness conditions can significantly alter the flashing effect.**

***Index Terms*—SAR, soil surface roughness, directional scattering**

I. Introduction

RECENT studies have revealed a strong directional scattering over several fields in ERS-2 and Envisat ASAR pairs acquired within a short temporal baseline (< 30 min) but with slightly different azimuth aspect angles below 1°[1]. Differences in backscatter in such pairs up to 6 dB and more were observed over test-sites across Europe by several authors [2], [3], [1], [4]. The differences of backscatter values could not be related to a change in environmental conditions due to the short acquisition interval, thus the fine differences in the observing geometries of the two sensors have to be considered. In the recent "Flashing Fields!" study [4], the importance of the field and row orientation of an illuminated agricultural field on the backscattering was investigated and highlighted as one of the main sources for directional scattering. With a row orientation quasi perpendicular, with a deviation of few degrees ($\pm$ 2°), to the look vector of the microwave sensor, a strong backscattering is produced. In addition, as recent studies show [3], [4] the so called *Flashing Fields* occur mainly on bare or even sparsely vegetated fields, and is characterized by a significantly higher backscattering up to 10 dB compared to fields with a row direction quasi parallel to the sensor look vector. In the above mentioned study of [4], it was assumed, that this directional scattering follows a Gaussian distribution showing a peak at a row orientation perpendicular to the sensor look vector and is only widened by infield row deviation (e.g. the linearity of the seed bed rows). This relation was established by a great amount of *in-situ* measurements and modelled by the modified Shin and Kong model developed by [5]. However, due to missing measurements, the impact of soil surface roughness could only be quantified in a qualitative manner and the accuracy of the developed backscatter model could not be definitely assessed.

In this paper, we present results of an add-on study to quantify the impact of soil surface roughness, especially the periodical horizontal component, on the flashing phenomenon respectively the directional scattering. With a rigorous roughness measurement technique, deployed over agricultural fields showing directional scattering in the imagery of ERS-2 and TerraSAR-X, the impact of soil surface roughness is investigated and modelled using the modified Shin and Kong model.

P. Marzahn and R. Ludwig are with the Department of Geography, Ludwig-Maximilians University of Munich, Munich, Germany (p.marzahn@lmu.de; r.ludwig@lmu.de).

F. Mattia is with ISSIA-CNR, Bari, Italy (mattia@ba.issia.cnr.it).

U. Wegmüller is with Gamma Remote Sensing, Gümlingen, Switzerland (wegmuller@gamma-rs.ch).

Manuscript received September 30, 2012; revised XXX XX, XXXX.

II. Methods

A. Field Measurements

According to the previous "Flashing Fields!" study [4], several *in-situ* measurements were made in Spring 2011 over the Wallerfing test site which is part of the Upper Danube SMOS Cal/VAl as well as TanDEM-X test site operated by the Ludwig-Maximilians University and German Aerospace Center (DLR-HR). The test site is located approx. 100 km North East of Munich, Germany in the Isar watershed and is mainly characterized by moderate relief under extensive agricultural use [6]. The main crops are sugar beet, winter wheat, winter barley, maize, cucumber, onions and potato following the typical crop cycle in this area, with sowing of sugar beet, maize and onions in spring and Winter wheat and barley in autumn. The *in-situ* measurements comprised row orientation, row linearity, vegetation height, vegetation cover and soil moisture over 55 fields with 3 repetitions each. In addition soil surface roughness was measured at

ESU	Landuse	surface type	size $[m^2]$
R11	maize	seedbed	6
R12	onion	smooth crusted	6
R13	sugarbeet	crusted seedbed	8
R14	sugarbeet	crusted seedbed	8
R21	sugarbeet	crusted seedbed	6
R22	sugarbeet	crusted seedbed	6
R23	sugarbeet	crusted seedbed	6
R30	winter rape	seedbed	22

TABLE I
CHARACTERISTICS OF ROUGHNESS SAMPLE POINTS (ESU) ACQUIRED WITHIN THIS STUDY

Date	Sensor	Dop. Centroid $[Hz]$	Mode	Pol
20110402	ERS	-2427.0	Image	VV
20110423	ERS	160.0	Image	VV
20110426	ERS	752.0	Image	VV
20110507	TSX	-9.8	Stripmap	VV/HV
20110514	ERS	-3598.0	Image	VV
20110523	ERS	7.0	Image	VV

TABLE II
ACQUIRED SAR IMAGERY AND CORRESPONDING CHARACTERISTICS

seven sample points over fields showing directional scattering as well as fields showing no directional scattering. To consider the anisotropic appearance of soil surface roughness, a photogrametric approach was chosen to describe soil surface roughness as proposed by [7], using a customized Canon EOS 5D at sample sizes of 6-8 m^2. Due to the measurement design of the deployed system, roughness measurements were carried out in two directions: perpendicular and parallel to the tillage direction respectively the seedbed row orientation. The acquisitions perpendicular to the tillage direction were further processed and analysed as it is expected that the in-perpendicular direction has a direct impact on the directional scattering. However, the in-parallel acquisitions were used to calculate the random roughness component as they are not influenced by a periodic pattern such as seedbed rows. To quantify soil surface roughness, digital surface models (DSMs) have been generated from the *in-field* image acquisitions with a horizontal resolution of 2 mm providing the basis for the characterization of soil surface roughness using two roughness values: the autocorrelation length (l) and the RMS-height (s). In order to characterize the multi-scale appearance of soil surface roughness, the roughness values have been calculated for several roughness scales of the perpendicular acquisitions as proposed by [8]. Table I summarizes the main characteristics of the sample points.

B. SAR Data

Five ERS-2 and one TerraSAR-X (TSX) scene (Table II) were acquired in ascending mode simultaneous to the field measurements over the Wallerfing test site in spring 2011. The ERS-2 imagery was acquired in image mode with an incidence angle of approx. 23°. The TerraSAR-X scene was acquired in Stripmap mode, in VV and VH polarization and with an incidence angle of 33°. In context of directional scattering the ERS-2 imagery showed good variations in the Doppler Centroids ranging from -3598.0 Hz to 752.0 Hz. [4] suggested several methods for the detection of directional scattering. As only ascending ERS-2 and TSX imagery were acquired less methods are available. Thus, to eliminate the effect of a potential temporal change (e.g. in soil moisture, vegetation growth), detection of directional scattering was carried out in accordance to [4], using an azimuth sub-look approach for both data sets. In addition for the TerraSAR-X dataset the VH/VV ratio which indicates directional scattering at very low values, due to the vanished directional scattering effects in the cross polarization. Using the sub-look approach, the full azimuth bandwidth of the original SLC image is split into several sub-bands, resulting in several co-registered SLC with slightly different Doppler Centroids [3], [4]. The achieved Doppler Centroid difference is dependent from the initial Doppler Bandwidth of the original SLC image. For the ERS-2 dataset the processed azimuth Doppler Bandwidth is approx. 1500 Hz resulting in a difference in azimuth angle between the first sub-look and last sub-look of 0.6°(1007 Hz). For the TSX dataset a Doppler difference of 827 Hz, which corresponds to an azimuth angle of approx. 0.3°, is calculated. In the presented study, five sub-looks for the ERS-2 dataset and 4 sub-looks for the TSX data take with an overlap of 50 percent were generated.

C. Modified Shin and Kong Model (MSK)

To predict backscatter from anisotropic quasi-periodic surfaces several models have been proposed in the past [9], [10], [2]. Those models were able to predict the large variations in backscatter (10 - 20 dB) for an off-azimuth angle range of 0°to 90°. However they were not able to predict a large change in backscatter for variations of the off-azimuth angle of a few degrees (e.g. 1°- 3°). [5] improved the backscatter model of Shin and Kong by deriving finite expressions of the backscatter terms of a quasi-periodic surface originally introduced by [10]. Therefore two principal changes were made compared to the original Shin and Kong model:
Firstly, an important change was done to derive a more accurate description of the coherent term contributing to the total backscatter. This was introduced by using the Kirchhoff diffraction integral under the Fresnel approximation rather than the Fraunhofer approximation as assumed in the original Shin and Kong model.
Secondly, the systems spatial resolution to characterize the antenna pattern was integrated in the modelling of the scattered field which allows to derive a finite form of all backscatter terms contributing to the total backscatter. In addition, to account for the quasi-periodicity (e.g. linearity) of the seedbed rows, a measure based on the standard deviation of the linearity of the seedbed rows was introduced which results in a widening of the directional pattern (see [4]). Thus the modified Shin an Kong model [5] consists of three terms modelling the total backscatter:

$$\sigma_{0pp} = \sigma^{c}_{pp} + \sigma^{nc_1}_{pp} + \sigma^{nc_2}_{pp} \quad (1)$$

- the first one due to the coherent field related to the scattering of the deterministic periodic function (σ_{pp}^{c});
- the second one representing the incoherent scattering of the combined isotropic and anisotropic random roughness components modulated by the deterministic periodic function ($\sigma_{pp}^{nc_1}$);
- the third one due to the incoherent field scattered only by the anisotropic random component modulated by the deterministic periodic function ($\sigma_{pp}^{nc_2}$).

The roughness model underlying the MSK can be characterized by six terms forming the above mentioned three terms of equation 1 [5]:
- random isotropic roughness; with a vertical standard deviation of heights s [cm] and the correlation length l [cm]
- anisotropic roughness; with a deterministic sinusoidal component described by the amplitude A [cm], the periodicity of the seedbed rows L [cm] and a random component, described by a vertical perturbation standard deviation s_y [cm] and an autocorrelation length l_y [cm]

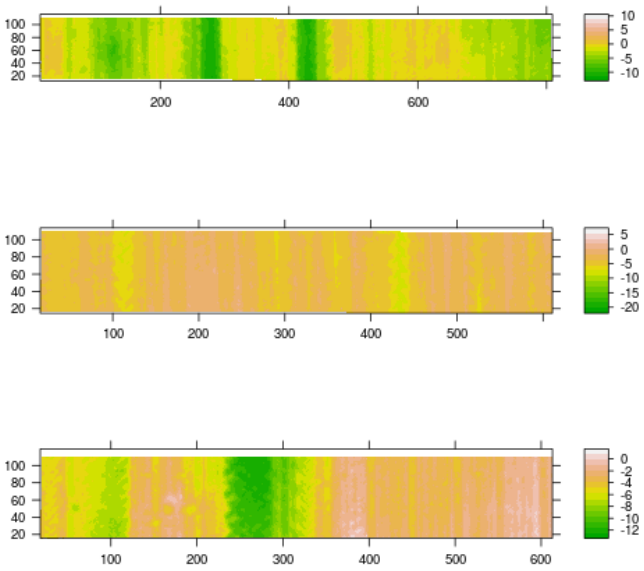

Fig. 1. Examples (top = R13, middle = R21, bottom = R23) of generated Digital Surface Models (DSM) acquired during the campaign in Spring 2011. Acquisition direction is perpendicular to the seedbed rows

III. Results

A. in-situ Measurements

Figure 1 shows as an example three generated DSMs (R13, R21, R23) acquired at the 15th of May 2011. One can easily distinguish the different seedbed rows as well as the small randomly distributed soil clods. With a vertical displacement of $RMSE_z \leq 2$ mm and a planimetric error $\leq$0.57 mm, the technique fits well the needs for the characterization of soil surface roughness for microwave remote sensing studies [11]. The roughness measurements allows to distinguish several roughness scale at some of the acquired roughness samples. Thus, for samples R13, R14, R22 and R23, which were acquired over slightly moderate relief, a significant topographic impact on the roughness measurements can be observed, which can be classified to different roughness scales. For example for R13 and R23 a roughness pattern related to the micro scale (soil aggregates and seedbed rows) with a vertical range of 2-5 cm can be observed. In addition a meso-scale roughness pattern is visible, which is characterized by vertical range of approx. 10-15 cm and comprises small slopes over a horizontal range of 1-2 metres. Finally a macro-scale roughness pattern is visible which can be related to the general slope of the field. For fields R11, R12 and R21, which were more smooth fields compared to the before mentioned, this impact is not visible. Using variogram analysis, the different roughness scales could be quantified and displayed as in Figure 2. Thus, for samples with a topographic impact (in Fig. 2 R13 and R23) the empirical variogram shows a strong increase in semivariance and does not reach a sufficient sill. In addition the variograms of R13 and R23 also show a *hole-effect* which indicates a similarity of adjacent height values at a distance of 150-200 cm indicating a low frequency periodic roughness pattern. For the fields with no significant topographic impact (R11, R12 and R21), a sill is sufficiently reached at a distance of approx. 40 cm. However for theses samples a second roughness scale composed by the wheel tracks of the tillage machines can be determined, indicated by the *hole effect* mentioned above. According to [8], two roughness scales can be quantified which where decomposed in its constituents, were s_{y1},l_{y1} correspond to the seedbed rows and the reduced random roughness fraction of the agricultural field, while s_{y2},l_{y2} also comprises wheel tracks and higher order roughness patterns. As an example, Figure 3 shows the results from the roughness decomposition approach for sample plot R11 and the horizontal periodical roughness component. To correct the above mentioned macro-scale topographic impact a detrending procedure was applied using a polynomial approach. Having a closer look on Table III reveals a significant difference in the obtained values for the samples. While under the same crop (e.g. sugar beet) most of the samples have been prepared with similar tillage tools, the yielded roughness values show a wide range of values. Applying the detrending procedure, the roughness values are more alike. Except for R12, the values obtained for s_{y1},l_{y1} are always lower than the values of s_{y2},l_{y2}. It is to notice, that a Onion field, such as R12, shows, due to tillage and precipitation, mostly a very reduced fraction of the random roughness as well as seedbed rows compared to the deterministic small scale periodic roughness component, such as wheel tracks, which are usually developed very sharp. In context of the roughness model underlying the MSK model, the detected roughness pattern is more complex showing more roughness scales. Thus to match the two roughness scales represented in the MSK model (random and anisotropic roughness), an intermediate roughness value of the estimated roughness scales was used to characterize the random anisotropic roughness component s_y/l_y.

ESU	s	l	s_{y1}	s_{y2}	l_{y1}	l_{y2}
R11	0.12	2.5	0.88	1.84	11.0	29.5
R12	0.1	3.0	0.85	1.73	71.6	38.27
R13	0.04	4.7	1.15 (1.09)	2.43 (2.84)	38.3 (17.7)	53.04 (69.05)
R14	0.14	2.1	0.24 (0.86)	2.26 (2.5)	41.01 (96.39)	98.04 (169.14)
R21	0.01	5.4	1,24	1.45	31.1	38.52
R22	0.23	1.4	0.77 (0.93)	1.12 (1.51)	20.5 (26.4)	23.47 (55.4)
R23	0.2	1.5	1.08 (1.31)	2.38 (2.71)	27.3 (25.7)	105.6 (107.5)

TABLE III
RESULTS OF ROUGHNESS MEASUREMENTS FOR EACH SAMPLE POINT (ESU). IN ROUND BRACKETS THE RESULTS FOR THE NON DETRENDED ORIGINAL SURFACES. UNITS IN CM, s_{y1}, l_{y1} CORRESPOND TO THE SMALL SCALE ROUGHNESS PATTERN (SEEDBED ROWS, SOIL CLODS), s_{y2}, l_{y2} TO THE LARGE SCALE ROUGHNESS PATTERN (WHEEL TRACKS)

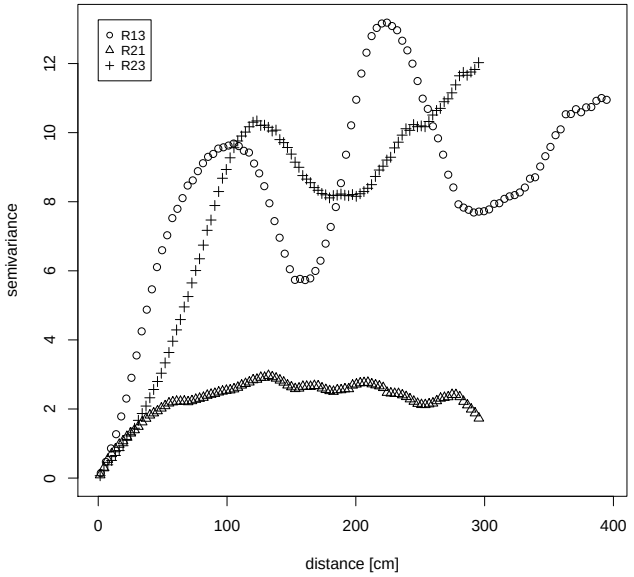

Fig. 2. Semi-variograms of sample plots R13, R21 and R23 indicating the topographic trend in the data for R13 and R23.

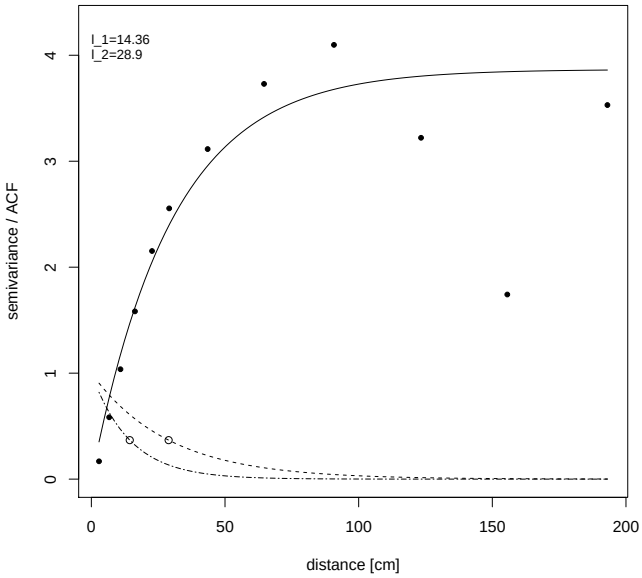

Fig. 3. Example (R11) of roughness decomposition approach showing the semi-variance of the heights in dependency of the distance (lag) of the corresponding heights. In addition the derived autocorrelation function (dashed and dashed-dotted lines) and autocorrelation (hollow dots) is indicated for each roughness scale

B. Evidence of directional scattering

A visual interpretation of the ERS-2 SAR imagery revealed a strong directional scattering at several patches of fields in the North-West of the acquired scenes (see Fig. 4, bright areas). Due to the difference in the Doppler Centroids of the TSX imagery, compared to the ERS-2 Doppler, slightly different fields show in the TSX imagery directional scattering (Fig.: 5). From the field campaign it was clearly observable that the fields showing directional scattering were all bare soil or sparsely vegetated (Fig.: 9) confirming the assumptions of [3], [4]. In addition, all the fields showed a roughness pattern with a strong periodical component (e.g. seedbed rows) and with a reduced random roughness fraction due the ongoing precipitation since sowing. The main crops showing directional scattering were summer crops like maize sugar beet and onions confirming the assumption and findings of [4] that vegetation attenuates the flashing effect.

Results of the sub-look approach (see Fig.: 6) indicate also a significant difference in backscattering between the used sub-

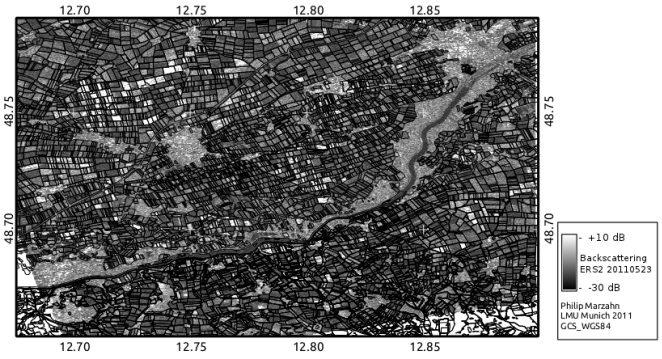

Fig. 4. Backscattering [dB] of an ERS-2 image acquired at the 23 of May 2011 with overlaying field borders. Fields in the North-West showing strong directional backscatter

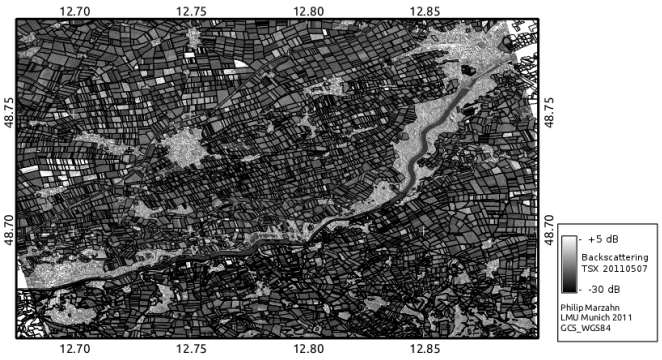

Fig. 5. Backscattering [dB] of a TerraSAR-X image acquired at the 7th of May 2011 with overlaying field borders. Fields in the North-West showing strong directional backscatter

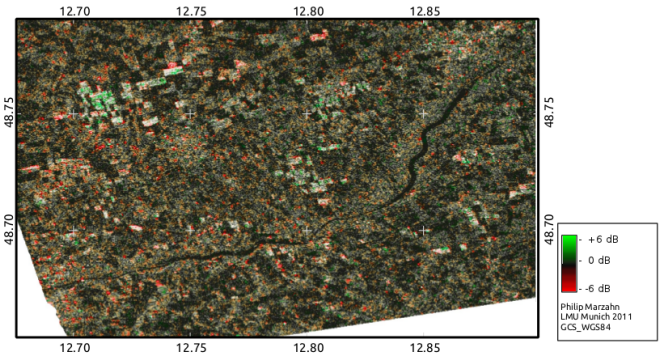

Fig. 6. ERS-2 HSI (HueSaturationIntensity) composite of the backscatter ratio (hue), backscatter change (saturation) and backscattering in the first image of the pair (intensity) over Wallerfing site on 23 of May 2011. Backscatter ratio (hue) ranges from 6 to + 6 dB; mean intensity (intensity) from 22 dB to + 6 dB; absolute backscatter change (saturation) from 0 to + 6 dB. Red indicates higher intensity for the sub look 1, and green higher intensity for sub look 5.

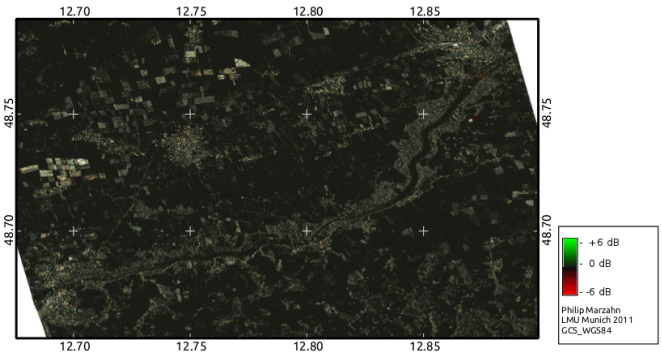

Fig. 7. TerraSAR-X HSI (HueSaturationIntensity) composite of the backscatter ratio (hue), backscatter change (saturation) and backscattering in the first image of the pair (intensity) over Wallerfing site on 07 of May 2011. Backscatter ratio (hue) ranges from 6 to + 6 dB; mean intensity (intensity) from 22 dB to + 6 dB; absolute backscatter change (saturation) from 0 to + 6 dB. Red indicates higher intensity for the sub look 1, and green higher intensity for sub look 4.

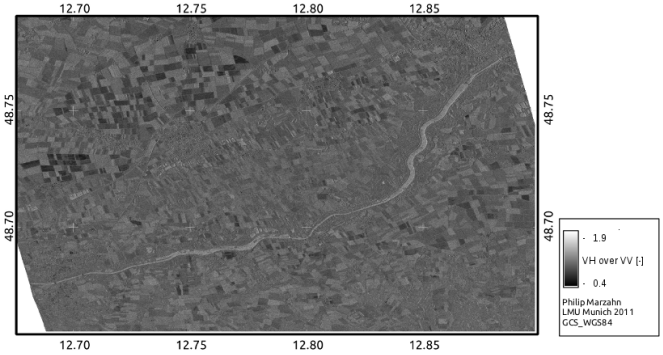

Fig. 8. VH/VV image of the TSX scene acquired at the 7th of May 2011. Dark fields indicate a possible directional scattering.

looks confirming a directional scattering. For the patches of fields showing a directional scattering in the ERS-2 imagery, sub-look 5 showed a significant higher scattering ($\geq$ 6 dB) compared to sub-look 1. It is to notice, that using the sub-look approach for the TSX imagery failed in the detection of directional scattering (see Fig. 7) which could be related to the small Doppler Difference between the used sub-looks in relation to the wavelength dependent roughness conditions. In other words, a change in azimuth angle of 0.3°is not large enough to accomplish a change in backscatter for a X-Band SAR system such as TSX. Indeed, due to the polarization dependent flashing, the VH/VV ratio indicated a strong directional scattering of the fields with very strong backscattering, showing very low values over the fields of interest (Fig.: 8).

C. Impact of soil surface roughness conditions on directional scattering

From Figure 10 one can easily observe a difference in backscattering due to the different roughness conditions of the flashing fields. With a row orientation perfectly perpendicular to the sensors look vector a strong backscatter is produced for every sample point, which is reduced by an increase in azimuth angle (off-perp angle in Fig. 10 and 11). However, for sample points R12 and R21 the backscattering is significantly higher compared to sample points R13 and R23. This could be related to the roughness conditions measured at both sample points, which were acquired over more smooth micro-relief as indicated by the variogram analysis. As a consequence the agricultural seedbed pattern of the imaged fields appears more regular thus producing a stronger flashing. In other words, it is to assume, that such topographic features, even in range of only a few decimetres, alter the directional scattering by reducing its amplitude and attenuate the flashing. Using the mean derived roughness values for the sugar beet fields as inputs for the modified Shin and Kong model, the model predicts quite accurate the directional scattering over the narrow azimuth angle pattern for the ERS-2 dataset (see dashed line in Fig. 10). Same could be state for the model results of the TerraSAR-X scene (Fig. 11). Indeed, with a reduced amount of samples, due to only one acquisition available, the MSK model predicts the flashing at X-Band also accurate. However, it appears that the width of the directional pattern is for the measured backscatter

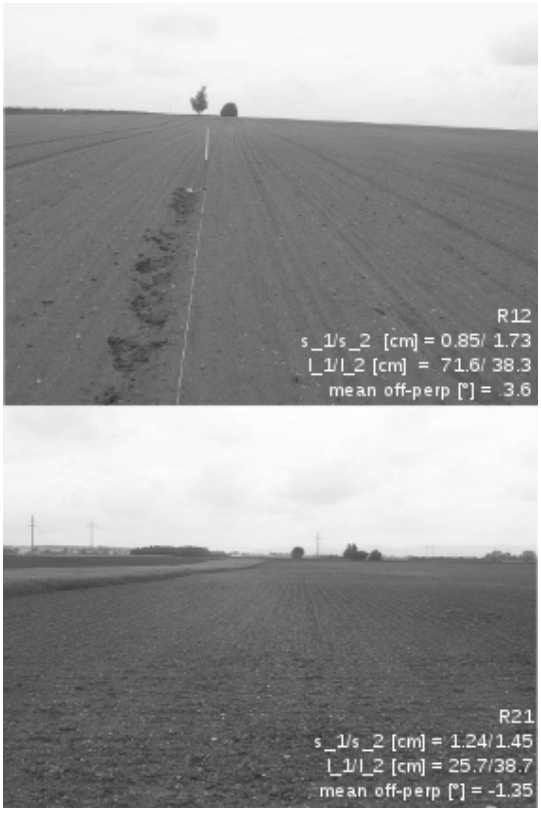

Fig. 9. Examples of fields showing directional scattering and field characteristics. Top: onion field (R12), bottom: sugar beet field (R21). Mean off-perp [°] = row orientation to the mean incident wave

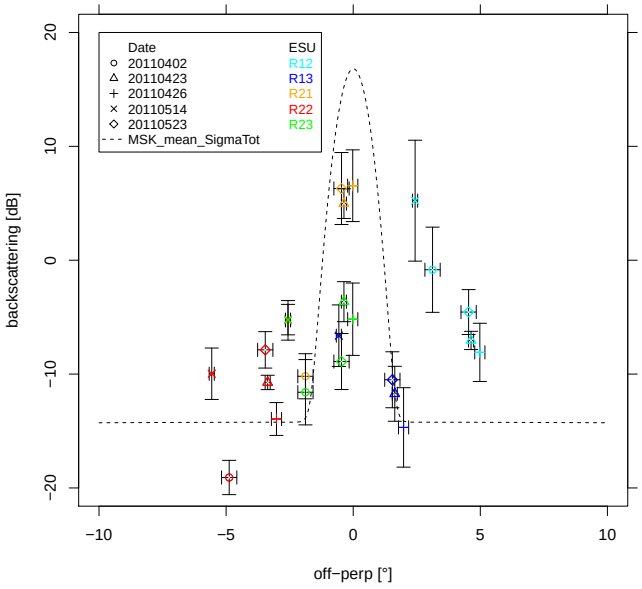

Fig. 10. Backscattering [dB] versus row direction (0°= rows perpendicular to the incidence wave) for the roughness samples plots and modelled mean ERS-2 backscatter values using the *modified Shin and Kong model* (MSK) proposed by [5], [4] (dashed line) parametrized for the averaged sugar beet fields. Roughness parameters: A=1.5cm, L=50cm,s=0.1cm, l=2.5cm, sy=1.4cm, ly=47cm

values wider than the predicted. Assuming a larger deviation of the row linearity as the measured one could mitigate this effect, as indicated by the dotted and dotted-dashed lines in Figure 11. Thus, with an increase in the standard deviation of the row linearity the width of the modelled directional scattering is widened up [5]. In addition it is to notice, that best model output in X-Band was achieved by normalizing the vertical roughness components of the model (*s, A*) by the wavenumber *k* using *ks*, respectively *kA*, as inputs.

IV. Conclusions

In this paper we widely confirmed and consolidated the findings of the previous *Flashing Fields!* study [4]. However, several further findings were be made in this study. As during the previous second *Flashing Fields!* study [4] good progress was made in the understanding and detection of narrow directional scattering, including a backscatter model development [5], the study was mainly based on qualitative measurements assuming an estimation of several roughness parameters based on a visual inspection for example. In this study we extended the understanding of the directional scattering by quantifying the impact of the roughness conditions on the directional scattering. From the acquired roughness samples highly accurate digital surface models were derived to characterize soil surface roughness with an accuracy in the Z-direction of $RMSE_Z$ = 1.6 mm. From the digital surface models roughness values were calculated and decomposed into each roughness scale

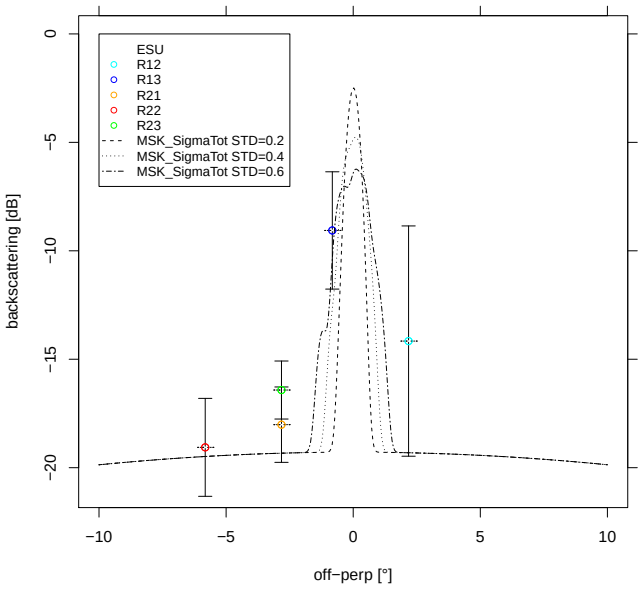

Fig. 11. Backscattering [dB] versus row direction (0°= rows perpendicular to the incidence wave) for the roughness samples plots and modelled TerraSAR-X backscatter values using the *modified Shin and Kong model* (MSK) proposed by [5], [4] (dashed/dottedlines) parametrized for the averaged sugar beet fields. Roughness parameters: A=3.0cm, L=50cm,s=0.2cm, l=2.5cm, sy=1.4cm, ly=47cm. dashed line = row linearity of 0.2°, dotted line = row linearity of 0.4°, dot-dashed line = row linearity of 0.6°. 0.2°corresponds to the measured mean value for all samples.

constituents. Analysing the directional scattering pattern, it could be observed (see Fig. 10 and Fig. 11) that several fields show a stronger directional scattering compared to other fields with directional scattering under the same field conditions (row orientation, soil moisture, landuse and vegetation cover). As there is only a difference in roughness conditions revealing an impact of soil surface roughness on the flashing. It could be observed from variogram analysis that the different scales of soil surface roughness can alter directional scattering significantly. Thus, fields with little micro-topography in range of a 1-2 decimetres (meso-roughness), such as R13 and R23, showed a reduced amplitude in directional scattering compared to fields R12 and R21 which do not show this meso-roughness component. It is to assume, that this detected meso-roughness component, interferes the regular pattern of the seedbed pattern attenuating the directional scattering effect. Thus future studies have to account for this finding and a multi-scale description of soils surface roughness over large sample areas is mandatory. Using the modified Shin and Kong model (MSK), proposed by [5], with the retrieved roughness values from the *in-field* roughness measurements, consolidated the good performance of the MSK model to predict the narrow directional scattering over agricultural fields at C- and X-Band. Even, when the detected roughness pattern was more complex as the one introduced in the MSK model which only accounts for a two scale roughness pattern. However, it is to notice, that predicting directional scattering at X-Band using the MSK model a higher standard deviation of the row linearity has to be considered which can be related to wavelength depending scaling issues. This is also true for the roughness values, especially the values describing the vertical roughness component. Thus, using the MSK at X-Band scaling the mentioned roughness values by the wavenumber k gives best model results. In context of the detection of directional scattering in a single SAR scene, the utilized sub-look approach performed well with the ERS-2 dataset, permitting a detection of directional scattering in a single SAR scene, eliminating potential environmental changes. However, for the TerraSAR-X dataset the sub-look approach failed due to the resulting low Doppler difference between the generated sub-looks and the high roughness values. Thus, at short wavelength sensors such as TerraSAR-X a reliable detection of directional scattering using the sub-look approach is not possible due to the up-scaled roughness at X-Band giving a wider directional scatter pattern. Finally we can conclude, that directional scattering is strong correlated to the fields row orientation towards the sensors look direction and secondary to the in-field roughness conditions as this study has shown.

REFERENCES

[1] U. Wegmuller, R.A. Cordey, C. Werner, and P.J. Meadows, "'Flashing Fields' in nearly simultaneous ENVISAT and ERS-2 C-band SAR images," *Geoscience and Remote Sensing, IEEE Transactions*, vol. 44, no. 4, pp. 801–805, 2006.

[2] A. Beaudoin, T. Le Toan, and Q.H.J. Gwyn, "SAR observations and modeling of the C-Band backscatter variability due to multiscale geometry and soil moisture," *Geoscience and Remote Sensing, IEEE Transactions on*, vol. 28, no. 5, pp. 886–895, 1990.

[3] L. Ferro-Famil, A. Reigber, E. Pottier, and W.-M. Boerner, "Scene characterization using subaperture polarimetric SAR data," *Geoscience and Remote Sensing, IEEE Transactions on*, vol. 41, no. 10, pp. 2264–2276, 2003.

[4] U. Wegmuller, M. Santoro, F. Mattia, A. Balenzano, G. Satalino, P. Marzahn, R. Ludwig, and N. Floury, "Progress in the understanding of narrow directional microwave scattering of agricultural fields," *Remote Sensing of Environment*, vol. 115, no. 10, pp. 2423–2433, 2011.

[5] F. Mattia, "Coherent and incoherent scattering from anisotropic tilled soil surfaces," *Waves in Random and Complex Media*, vol. 21, no. 2, pp. 278300, 2011.

[6] F. Schlenz, J. T. dall'Amico, A. Loew, and W. Mauser, "Uncertainty assessment of the SMOS validation in the upper Danube catchment," *Geoscience and Remote Sensing, IEEE Transactions on*, , no. 99, pp. 1–13, 2011, Early Access.

[7] P. Marzahn, D. H. Rieke-Zapp, and R. Ludwig, "Assessment of soil surface roughness statistics for microwave remote sensing applications using a simple photogrammetric acquisition system," *ISPRS Journal of Photogrammetry and Remote Sensing*, vol. 72, pp. 80–89, 2012.

[8] P. Marzahn, M. Seidel, and R. Ludwig, "Decomposing dual scale soil surface roughness for microwave remote sensing applications," *Remote Sensing*, vol. 4, no. 7, pp. 2016–2032, 2012.

[9] F. T. Ulaby, F. Kouyate, A. K. Fung, and A. J. Sieber, "A backscatter model for a randomly perturbed periodic surface," *Geoscience and Remote Sensing, IEEE Transactions on*, vol. 20, no. 4, pp. 518–528, 1982.

[10] R. T. Shin and J. A. Kong, "Scattering of electromagnetic waves from a randomly perturbed quasiperiodic surface," *J. Appl. Phys.*, vol. 56, no. 1, pp. 10–21, July 1984.

[11] H. Lievens, H. Vernieuwe, J. Alvarez-Mozos, B. De Baets, and N. Verhoest, "Error in radar-derived soil moisture due to roughness parameterization: An analysis based on synthetical surface profiles," *Sensors*, vol. 9, no. 2, pp. 1067–1093, 2009.

Philip Marzahn Philip Marzahn (M'09) received is MS degree from the Christian-Albrechts University of Kiel, Kiel Germany, where he studied geography, soil science, hydrology and landscape ecology from 2001 to 2007. He is currently working at the Department of Geography at the Ludwig-Maximilians University of Munich, Munich, Germany.

His research interests include the retrieval of bio- and geophysical parameters from multi-dimensional SAR data as well as the uncertainty assessment of such variables. He also focuses on the measurement and parametrization of soil surface roughness using photogrametric approaches and geostatistics. He is principle investigator of several spaceborne campaigns such as TerraSAR-X and TanDEM-X and participated in several ESA funded remote sensing campaigns . He is a reviewer of several international journals.

Francesco Mattia Francesco Mattia received the Laurea degree in physics and the M.S. degree in signal processing from the University of Bari, Italy, in 1990 and 1994, respectively, and the Ph.D degree from the University Paul Sabatier, Toulouse, France, in 1999. From 1991 to 1994 he has been grant holder of the Italian National Council of Research (CNR) and of the European Commission at the Institute for Remote Sensing Applications of the Joint Research Centre, Ispra, Italy. From 1995 to 2003 he has been research scientist at the Institute for Information and Space Technology (ITIS) of CNR, Matera, Italy. In 2003 he joined the Institute for Intelligent Systems and Automation (ISSIA) of CNR, Bari, Italy, where he is presently senior research scientist. During 1996, 1997, 1998 and 1999 he has been visiting scientist at the Centre dEtudes Spatiales de la BIOsphere (CESBIO), Toulouse, France. In 2007, he was co-organizer of the 5th International Symposium on Retrieval of Bio-and Geophysical Parameters from SAR Data for Land Applications held in Bari (Italy). His scientific interests include the direct and inverse modeling of microwave scattering from land surfaces and the use of information derived from Earth observation sensors to improve land surface process models. He has been involved as CI or PI in several national and international scientific proposals concerning SAR sensors aboard ERS-1/2, ENVISAT, ALOS and COSMO-SkyMed satellites.

Urs Wegmueller Urs Wegmüller (M94SM03) received the M.S. and Ph.D. degrees in physics from the University of Berne, Berne, Switzerland, in 1986 and 1990, respectively.

Between 1991 and 1992, he was with the Jet Propulsion Laboratory, Pasadena, CA, and between 1993 and 1995, with the University of Zürich, Zürich, Switzerland. Since 1995, he has been with GAMMA Remote Sensing AG (GAMMA), Gümligen, Switzerland, which is a Swiss company active in the development of signal-processing techniques and remote-sensing applications, where he was a Founding Member. Currently, as the Chief Executive Officer of GAMMA, he has overall responsibility for GAMMAs activities. At present, his main involvement is in the development of applications and the definition and implementation of related services in land-surface-deformation, hazard, land-use, and topographic mappings. He is/was the Principal Investigator for projects supported by ESA and the European Commission Framework programs.

Ralf Ludwig Ralf Ludwig was born in Fuerstenfeldbruck, Germany, in 1967. He studied geography, geology, geophysics, and remote sensing at the University of Munich (LMU), Munich, Germany. He received the M.S. degree in geography and the Ph.D. degree from LMU in 1994 and 1999, respectively. From 2005 to 2007, he has been a Full Professor for physical geography and remote sensing at the University of Kiel, Kiel, Germany. He is now with the Ludwig-Maximilians University of Munich, Munich, Germany, where he owns a Full Professor for physical geography and environmental modelling. His research interests include the utilization of remote sensing information for an assimilation in physically based hydrological models and the development of process models for the description of land surface processes and human dimension interactions. He is a member of the European Geophysical Union, Principal Investigator for the Shuttle Radar Topography Mission, the ALOS PALSAR mission, and Co-Investigator for several ENVISAT ASAR studies. He is the project coordinator of the EU-FP7 project CLIMB - Climate Induced Changes on the Hydrology in Mediterranean Basins - Reducing Uncertainty and Quantifying Risk. He is a reviewer for several national and international journals.

3 Conclusions and Outlook

This thesis focused on the characterization of soil surface roughness for microwave remote sensing applications. The major goal is to provide a measurement system which is able to measure soil surface roughness over large samples and to account for its multi-scale and anisotropic appearance. With a customized consumer-grade digital camera, Canon EOS 5D, and a reference frame, a simple and highly-portable photogrammetric acquisition system was introduced which is unique and outstanding in the fields of roughness characterization. As today's conventional roughness measurement devices are mainly stationary devices based on measurements in the two-dimensional space (e.g. laser profilers or mesh boards) the proposed system extends the measurements to the high-resolution three-dimensional space, allowing soil surface roughness to be characterize with new possibilities. Also up to now soil surface roughness was considered as an isotropic single-scale stationary process. In this thesis this assumption was revised by analysing soil surface roughness over several agricultural fields. It was shown that soil surface roughness has to be considered anisotropic as potential roughness values such as the RMS-height s or autocorrelation length l differ significantly depending on the direction of the roughness measurements related to the tillage orientation. The analysed data revealed a significant difference in the roughness values of a ploughed and seedbed surface especially for the autocorrelation length which was in several cases three times higher for the parallel direction compared to the perpendicular measurements to the tillage orientation. For the RMS-height this effect was not significant. Also the assumption of a single-scale process could be disapproved and evidence of the multi-scale appearance of soil surface roughness was given. In a unique approach, geostatistical analysis was used to decompose the different roughness scales into its sub-scales which have a severe impact on the backscattering of microwave remote sensing systems. It was found that the different roughness scales which could be differentiated and quantified for each scale separately have a severe impact on the directional scattering problem occurring in SAR images illuminating agricultural landscapes. As such directional scatter is characterized by a strong anomalous backscatter over bare or sparsely vegetated fields, the different roughness scales can decrease the coherent scattering over such surfaces, thus reducing the received backscattering. Thus, major progress was made in the understanding of the directional scattering problem in microwave remote sensing. Besides the row orientation of the seedbed pattern of an agricultural field, the soil surface roughness conditions and their different scales are what have a severe impact on the directional scattering. A backscatter model, the *Modified Shin and Kong* model (MSK) Mattia (2011) was developed in the framework of this thesis and used to predict SAR backscatter values in the presence of directional scattering. Using the retrieved multi-scale roughness values derived in this thesis, it is possible to predict directional scattering more accurately. Up

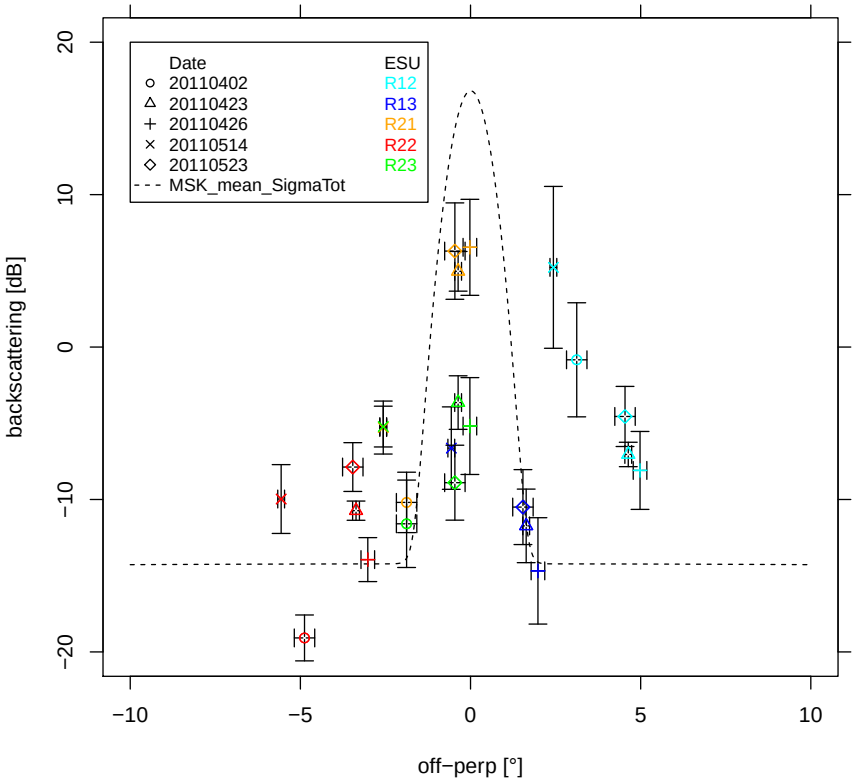

Figure 3.1: Backscattering [dB] versus row direction (0°= rows perpendicular to the incidence wave) for the roughness sample plots and modelled mean ERS-2 backscatter values using the *modified Shin and Kong model* (MSK) proposed by Mattia (2011); Wegmuller et al. (2011) (dashed line) parametrized for the averaged sugar beet fields.

to now, this was not possible and is thus a unique contribution to the scientific community. Analysing the directional scattering pattern, it could be observed (see Fig. 3.1 that several fields show a stronger directional scattering compared to other fields with directional scattering under the same field conditions (row orientation, soil moisture, landuse and vegetation cover). As there is only a difference in roughness conditions revealing an impact of soil surface roughness on the flashing. It could be observed from geostatistical analysis that the different scales of soil surface roughness can significantly alter directional scattering. Thus, fields with little micro-topography in range of a 1-2 decimetres (meso-roughness), such as R13 and R23, showed a reduced amplitude in directional scattering compared to fields R12 and R21 which do not show this meso-roughness component. It is to assume, that this detected meso-roughness component, interferes the regular pattern of the seedbed pattern attenuating the directional scattering effect. Thus future studies have to account for this finding and a multi-scale

description of soils surface roughness over large sample areas is mandatory.
The achievements of this thesis provide a framework for the future analysis and derivation of soil surface roughness information from SAR observations. It is expected that with the proposed in-field roughness characterization approach, soil surface roughness information can now be derived in a more stable way than was proposed by Marzahn and Ludwig (2009a) due to the now more refined scale-dependent descriptions of soil surface roughness. Indeed the database for the AgriSAR2006 study is unique in its SAR acquisitions, acquiring polarimetric SAR data on a weekly basis for a whole growth cycle of vegetation. Thus, with the upcoming new (fully) polarimetric spaceborne SAR sensors operating at an appropriate frequency for the retrieval of soil surface roughness, such as PALSAR-2 (Shimada et al., 2011) or TanDEM-L (Krieger et al., 2010), new opportunities in the continuous acquisition of polarimetric SAR data will exist. The proposed method by Marzahn and Ludwig (2009a) for the retrieval of soil surface roughness can then be verified and further analyzed. In a next step, such derived roughness maps can be, on the one hand, assimilated in high-resolution eco-hydrological models or soil erosion models to better understand the occurring surface processes and their interdependencies. As there is a strong demand for such maps (Morgan and Nearing, 2011), the proposed methods have to be further refined. On the other hand, the availability of an approach to decompose the different roughness scales from *in-situ* measurements allows for a better understanding of the contribution of soil surface roughness to the total backscatter of a resolution cell within a SAR image. Thus, using the proposed approach, new and enhanced backscatter models can and must be developed and applied which account for the different scales of soil surface roughness such as the model provided by Mattia (2011). In the context of directional scattering, the TanDEM-X mission, operated by the German Aerospace Center, offers an interesting possibility to detect and characterize directional scattering in the future. Using the two sensors, acquiring polarimetric SAR images at different azimuth angles, a detection of the seedbed row orientation may be possible. Such characterization could be a useful value in the calculation of overland flow pathways or preferential routing in eco-hydrological models.

4 Bibliography

S. Allain, L. Ferro-Famil, and E. Pottier. Two novel surface model based inversion algorithms using multifrequency polsar data. In *Proc. IEEE International Geoscience and Remote Sensing Symposium IGARSS '04*, volume 2, pages 823–826, 2004.

R. R. Allmaras, R. E. Burwell, W. E. Larson, and R. F Holt. Total porosity and random roughness of the interrow zone as influenced by tillage. USDA Conservation Research Report 7, USDA, 1966.

J. Alvarez-Mozos, N.E.C. Verhoest, A. Larranaga, J. Casal, and M. Gonzlez-Audcana. Influence of surface roughness spatial variability and temporal dynamics on the retrieval of soil moisture from SAR observations. *Sensors*, 9(1):463–489, 2009.

A. Beaudoin, T. Le Toan, and Q.H.J. Gwyn. SAR observations and modeling of the C-Band backscatter variability due to multiscale geometry and soil moisture. *Geoscience and Remote Sensing, IEEE Transactions on*, 28(5):886–895, 1990.

X. Blaes and P. Defourny. Characterizing bidimensional roughness of agricultural soil surfaces for SAR modeling. *Geoscience and Remote Sensing, IEEE Transactions on*, 46(12):4050–4061, 2008. ISSN 0196-2892.

R. Bryant, M. S. Moran, D. P. Thoma, C. D. Holifield Collins, S. Skirvin, M. Rahman, K. Slocum, P. Starks, D. Bosch, and M. P. Gonzalez Dugo. Measuring surface roughness height to parameterize radar backscatter models for retrieval of surface soil moisture. *Geoscience and Remote Sensing Letters, IEEE*, 4(1):137–141, 2007.

N. H. D. T. Cremers, P. M. VAN Dijk, A. P. J. DE Roo, and M. A. Verzandvoort. Spatial and temporal variability of soil surface roughness and the application in hydrological and soil erosion modeling. *Hydrological Processes*, 10(8):1035–1047, 1996.

D. Currence, H. and W. G. Lovely. The analysis of soil surface roughness. *Trans. ASAE*, 13:710–714, 1970.

F. Darboux and C. H. Huang. Does soil surface roughness increase or decrease water and particle transfers? *Soil Sci. Soc. Am. J.*, 69(3):748–756, May 2005.

F. Darboux and C.H. Huang. An instantaneous-profile laser scanner to measure soil surface microtopography. *Soil Sci. Soc. Am. J.*, 67(1):92–99, 2003.

M. W. J. Davidson, T. Le Toan, F. Mattia, C. Satalino, T. Manninen, and M. Borgeaud. On the characterization of agricultural soil roughness for radar remote sensing studies. *Geoscience and Remote Sensing, IEEE Transactions on*, 38(2):630–640, 2000.

M. W. J. Davidson, F. Mattia, G. Satalino, N. E. C. Verhoest, T. Le Toan, M. Borgeaud, J. M. B. Louis, and E. Attema. Joint statistical properties of rms height and correlation length derived from multisite 1-m roughness measurements. *Geoscience and Remote Sensing, IEEE Transactions on*, 41(7):1651–1658, 2003.

A. P. J. De Roo, R. J. E. Offermanns, and N. H. D. T. Cremers. LISEM: A single-event, physically based hydrological and soil erosion model for drainage basins. II: Sensitivity analysis, validation and application. *Hydrological Processes*, 10(8):1119–1126, 1996.

R. Duttman. Partikuläre Stoffverlagerungen in Landschaften. In *Geosynthesis*, number 10. Mosimann, T. and Kuhnt, G., 1999.

P. J. Farres. The dynamics of rainsplash erosion and the role of soil aggregat stability. *CATENA*, 14(1-3):119–130, 1987.

J.C. Fernandez Diaz, J. Judge, K.C. Slatton, R. Shrestha, W.E. Carter, and D. Bloomquist. Characterization of full surface roughness in agricultural soils using groundbased LiDAR. In *Geoscience and Remote Sensing Symposium (IGARSS), 2010 IEEE International*, pages 4442–4445, 2010.

L. Ferro-Famil, A. Reigber, E. Pottier, and W.-M. Boerner. Scene characterization using subaperture polarimetric SAR data. *Geoscience and Remote Sensing, IEEE Transactions on*, 41(10):2264–2276, 2003. ISSN 0196-2892.

N. Fohrer, J. Berkenhagen, J. M. Hecker, and A. Rudolph. Changing soil and surface conditions during rainfall: Single rainstorm/subsequent rainstorms. *CATENA*, 37 (3-4):355–375, 1999.

A.K. Fung, Z. Li, and K.S. Chen. Backscattering from a randomly rough dielectric surface. *Geoscience and Remote Sensing, IEEE Transactions on*, 30(2):356–369, 1992.

I. Hajnsek and P. Prats. Soil moisture estimation in time with D-InSAR. In *Proc. IEEE International Geoscience and Remote Sensing Symposium IGARSS 2008*, volume 3, pages III–546–III–549, 7–11 July 2008.

I. Hajnsek, K.P. Papathanassiou, A. Moreira, and S.R. Cloude. Surface parameter estimation using interferometric and polarimetric SAR. In *Geoscience and Remote Sensing Symposium, 2002. IGARSS '02. 2002 IEEE International*, volume 1, pages 420–422 vol.1, 2002.

I. Hajnsek, E. Pottier, and S. R. Cloude. Inversion of surface parameters from polarimetric SAR. *Geoscience and Remote Sensing, IEEE Transactions on*, 41(4):727–744, 2003.

I. Hajnsek, T. Jagdhuber, H. Schoen, and K. P. Papathanassiou. Potential of estimating soil moisture under vegetation cover by means of PolSAR. *Geoscience and Remote Sensing, IEEE Transactions on*, 47(2):442–454, 2009.

K. H. Hartge and R. Horn. *Einführung in die Bodenphysik*. Ferdinand Enke Verlag, Stuttgart, Germany, 3 edition, 1999.

K. Helming. *Die Bedeutung des Mikroreliefs für die Regentropfenerosion*. PhD thesis, TU Berlin, 1992.

T. Jagdhuber. *Soil parameter retrieval under vegetation cover using SAR polarimetry*. PhD thesis, Ph.D.-Thesis University of Potsdam, Germany, 2012.

W. Jester and A. Klik. Soil surface roughness measurement–methods, applicability, and surface representation. *CATENA*, 64(2-3):174–192, December 2005.

C. B. Johnson, J. V. Mannering, and W. C. Moldenhauer. Influence of surface roughness and clod size and stability on soil and water losses. *Soil Sci. Soc. Am. J.*, 43(4):772–777, 1979.

E.C. Kamphorst, V. Jetten, J. Guerif, J. Pitkanen, B.V. Iversen, J.T. Douglas, and A. Paz. Predicting depressional storage from soil surface roughness. *Soil Sci. Soc. Am. J.*, 64(5):1749–1758, September 2000.

G. Krieger, I. Hajnsek, K. Papathanassiou, M. Eineder, M. Younis, F. De Zan, S. Huber, P. Lopez-Dekker, P. Prats, M. Werner, Y. Shen, A. Freeman, P. Rosen, S. Hensley, W. Johnson, L. Veilleux, B. Grafmueller, R. Werninghaus, R. Bamler, and A. Moreira. Tandem-L: And innovative interferometric and polarimetric SAR mission to monitor earth system dynamics with high resolution. In *Geoscience and Remote Sensing Symposium (IGARSS), 2010 IEEE International*, pages 253–256, 2010.

B. Lascelles, D. Favis-Mortlock, T. Parsons, and J. Boardman. Automated digital photogrammetry: A valuable tool for small-scale geomorphological research for the non-photogrammetrist? *Transactions in GIS*, 6(1):5–15, 2002. ISSN 13611682.

Y. Le Bissonnais, H. Benkhadra, V. Chaplot, D. Fox, D. King, and J. Daroussin. Crusting, runoff and sheet erosion on silty loamy soils at various scales and upscaling from m^2 to small catchments. *Soil and Tillage Research*, 46(1-2):69–80, 1998.

J.-S. Lee, D. L. Schuler, and T. L. Ainsworth. Polarimetric SAR data compensation for terrain azimuth slope variation. *Geoscience and Remote Sensing, IEEE Transactions on*, 38(5):2153–2163, 2000.

J.-S. Lee, D. L. Schuler, T. L. Ainsworth, E. Krogager, D. Kasilingam, and W. M. Boerner. On the estimation of radar polarization orientation shifts induced by terrain slopes. *Geoscience and Remote Sensing, IEEE Transactions on*, 40(1):30–41, 2002.

W. Linder. *Digital Photogrammetry A Practical Course*. Springer Berlin / Heidelberg, 2009.

T. Luhmann. *Nahbereichsphotogrammetrie - Grundlagen, Methoden und Anwendungen*, volume 2. Springer Berlin / Heidelberg, 2003.

B. Mandelbrot, Benoait. *Les Objetcs Fractals*. Champs, Flammarion, Paris, 1995.

A.T. Manninen. Multiscale surface roughness description for scattering modelling of bare soil. *Physica A: Statistical Mechanics and its Applications*, 319(0):535–551, 2003.

P. Marzahn and R. Ludwig. On the derivation of soil surface roughness from multi-parametric PolSAR data and its potential for hydrological modeling. *Hydrology and Earth System Sciences*, 13:381–394, 2009a.

P. Marzahn and R. Ludwig. Using fully polarimetric SAR data for the retrieval of soil surface roughness: potentials and limitations for an operational use. In *Proceedings of the ESA PolInSAR Workshop, Frascati, Italy, on CD-ROM*, 2009b.

P. Marzahn, D. Rieke-Zapp, U. Wegmuller, and R. Ludwig. Multidimensional roughness characterization for microwave remote sensing applications using a simple photogrammetric acquisition system. *Int. Arch. Photogramm. Remote Sens. Spatial Inf. Sci.*, XXXIX-B5:423–428, 2012a.

P. Marzahn, D. H. Rieke-Zapp, and R. Ludwig. Assessment of soil surface roughness statistics for microwave remote sensing applications using a simple photogrammetric acquisition system. *ISPRS Journal of Photogrammetry and Remote Sensing*, 72:80–89, 2012b.

P. Marzahn, M. Seidel, and R. Ludwig. Decomposing dual-scale soil surface roughness for microwave remote sensing applications. *Remote Sensing*, 4(7):2016–2032, 2012c.

P. Marzahn, U. Wegmueller, F. Mattia, and R. Ludwig. FLASHING FIELDS! and the impact of soil surface roughness. In *Proc. IEEE International Geoscience and Remote Sensing Symposium IGARSS 2012*, 2012d.

F. Mattia. Coherent and incoherent scattering from anisotropic tilled soil surfaces. *Waves in Random and Complex Media*, 21(2):278300, 2011.

F. Mattia, T. Le Toan, J. C. Souyris, C. De Carolis, N. Floury, F. Posa, and N. G. Pasquariello. The effect of surface roughness on multifrequency polarimetric SAR data. *Geoscience and Remote Sensing, IEEE Transactions on*, 35(4):954–966, 1997.

F. Mattia, M. W. J. Davidson, T. Le Toan, C. M. F. D'Haese, N. E. C. Verhoest, A. M. Gatti, and M. Borgeaud. A comparison between soil roughness statistics used in surface scattering models derived from mechanical and laser profilers. *Geoscience and Remote Sensing, IEEE Transactions on*, 41(7):1659–1671, July 2003.

I. D. Moore and C. L. Larson. Estimating microrelief surface storage from point data. *Transactions of the ASABE*, 22(5):1073–1077, 1979.

R. P. C. Morgan and M. A. Nearing, editors. *Handbook of erosion modelling*. Wiley-Blackwell, Chichester, UK, 2011.

R. P. C. Morgan, J. N. Quinton, R. E. Smith, G. Govers, J. W. A. Poesen, K. Auerswald, G. Chisci, D. Torri, and M. E. Styczen. The european soil erosion model (EUROSEM): a dynamic approach for predicting sediment transport from fields and small catchments. *Earth Surf. Process. Landforms*, 23(6):527–544, 1998.

L. Oelze, M., M. Sabatier, J., and R. Raspet. Roughness measurements of soil surfaces by acoustic backscatter. *Soil Sci. Soc. Am. J.*, 67(1):241–250, 2003.

Y. Oh, K. Sarabandi, and F. T. Ulaby. An empirical model and an inversion technique for radar scattering from bare soil surfaces. *Geoscience and Remote Sensing, IEEE Transactions on*, 30(2):370–381, 1992.

D. Rieke-Zapp and A. Nearing, M. Digital close range photogrammetry for measurement of soil erosion. *Photogrammetric Record*, 20(109):69–87, 2005.

D. Rieke-Zapp, W. Tecklenburg, J. Peipe, H. Hastedt, and C. Haig. Evaluation of the geometric stability and the accuracy potential of digital cameras – comparing mechanical stabilisation versus parameterisation. *ISPRS Journal of Photogrammetry and Remote Sensing*, 64(3):248–258, 2009.

M. J. Römkens and J. Y Wang. Effect of tillage on surface roughness. *Trans. ASAE*, 29:429 433, 1986.

M. J. M. Römkens, K. Helming, and S. N. Prasad. Soil erosion under different rainfall intensities, surface roughness, and soil water regimes. *CATENA*, 46(2-3):103–123, 2001.

J. Schmidt. A mathematical model to simulate rainfall erosion. *CATENA*, 19:101–109, 1991.

D. L. Schuler, J.-S. Lee, D. Kasilingam, and G. Nesti. Surface roughness and slope measurements using polarimetric SAR data. *Geoscience and Remote Sensing, IEEE Transactions on*, 40(3):687–698, 2002.

M. Shimada, Y. Kankaku, M. Watanabe, and T. Motooka. Current status of the ALOS-2/PALSAR-2 and the cal/val program. In *Proceedings of CEOS SAR Calibration and Validation Workshop 2011*, 2011.

R. T. Shin and J. A. Kong. Scattering of electromagnetic waves from a randomly perturbed quasiperiodic surface. *J. Appl. Phys.*, 56(1):10–21, July 1984.

H. Sommer. Quantifizierung der Rauigkeit von Bodenoberflaechen und Simulation hydromechanischer Prozesse anhand von Oberflaechenmodellen. FAM-Bericht 18, Forschungsverbund Agraroekosysteme Muenchen, 1997.

Y. Sun, J. Lin, P. Schulze-Lammers, and L. Damerow. Estimating surface porosity by roughness measurement in a silt-loam field. *J. Plant Nutr. Soil Sci.*, 169(5):630–632, 2006.

O. Taconet and V. Ciarletti. Estimating soil roughness indices on a ridge-and-furrow surface using stereo photogrammetry. *Soil and Tillage Research*, 93(1):64–76, March 2007.

C. Thiel. Measuring surface roughness on base of the circular polarization coherence as an input for a simple inversion of the IEM model. In *Proc. ESA Workshop on Applications of SAR Polarimetry and Polarimetric Interferometry, PolInSAR 2003, Frascati*, 2003.

F. T. Ulaby, F. Kouyate, A. K. Fung, and A. J. Sieber. A backscatter model for a randomly perturbed periodic surface. *Geoscience and Remote Sensing, IEEE Transactions on*, 20(4):518–528, 1982.

F. T. Ulaby, R. K. Moore, and A. K. Fung. *Microwave Remote Sensing: Active and Passive, Vol. II Radar Remote Sesning and Surface Scattering and Emission Theory*, volume II. The Artech House Remote Sesning Library, 1986.

N. Verhoest, H. Lievens, W. Wagner, J. Alvarez-Mozos, M. Moran, and F. Mattia. On the soil roughness parameterization problem in soil moisture retrieval of bare surfaces from synthetic aperture radar. *Sensors*, 8(7):4213–4248, 2008.

M. von Werner. *GIS- orientierte Methoden der digitalen Reliefanalyse zur Modellierung von Bodenerosion in kleinen Einzugsgebieten.* PhD thesis, Freie Universität Berlin, 1995.

R. Wackrow and J. H. Chandler. A convergent image configuration for DEM extraction that minimises the systematic effects caused by an inaccurate lens model. *The Photogrammetric Record*, 23(121):6–18, 2008. ISSN 1477-9730.

W. S. Warner. Mapping a three-dimensional soil surface with hand-held 35 mm photography. *Soil and Tillage Research*, 34(3):187–197, 1995. ISSN 0167-1987.

U. Wegmuller, R.A. Cordey, C. Werner, and P.J. Meadows. 'Flashing Fields' in nearly simultaneous ENVISAT and ERS-2 C-band SAR images. *Geoscience and Remote Sensing, IEEE Transactions*, 44(4):801–805, 2006.

U. Wegmuller, M. Santoro, F. Mattia, A. Balenzano, G. Satalino, P Marzahn, G. Fischer, R. Ludwig, and N. Floury. Progress in the understanding of narrow directional scattering over agricultural fields. In *Proceedings of ESA Living Planet Symposium 2010 Bergen, Norway*, 2010.

U. Wegmuller, M. Santoro, F. Mattia, A. Balenzano, G. Satalino, P. Marzahn, R. Ludwig, and N. Floury. Progress in the understanding of narrow directional microwave scattering of agricultural fields. *Remote Sensing of Environment*, 115(10):2423–2433, 2011.

I. H. Woodhouse. *Introduction to microwave remote sensing.* CRC Press Taylor & Francis, Boca Raton, New York, US, 2006.

M. Zeiger. *Assessment of dynamic biotic and abiotic processes at the soil surface affected by different management systems*. PhD thesis, Christian Albrechts University Kiel, 2007.

M. Zribi, V. Ciarletti, O. Taconet, J. Paill, and P. Boissard. Characterisation of the soil structure and microwave backscattering based on numerical three-dimensional surface representation: Analysis with a fractional brownian model. *Remote Sensing of Environment*, 72(2):159–169, 2000.